Re-modelling buildings Data-efficient models to evaluate energy efficiency in operative buildings

Palmer Real, Jaume

Publication date:
2022

Document Version
Publisher's PDF, also known as Version of record

DTU Compute
Department of Applied Mathematics and Computer Science

Re-modelling buildings

Data-efficient models to evaluate energy efficiency in operative buildings

PhD Thesis

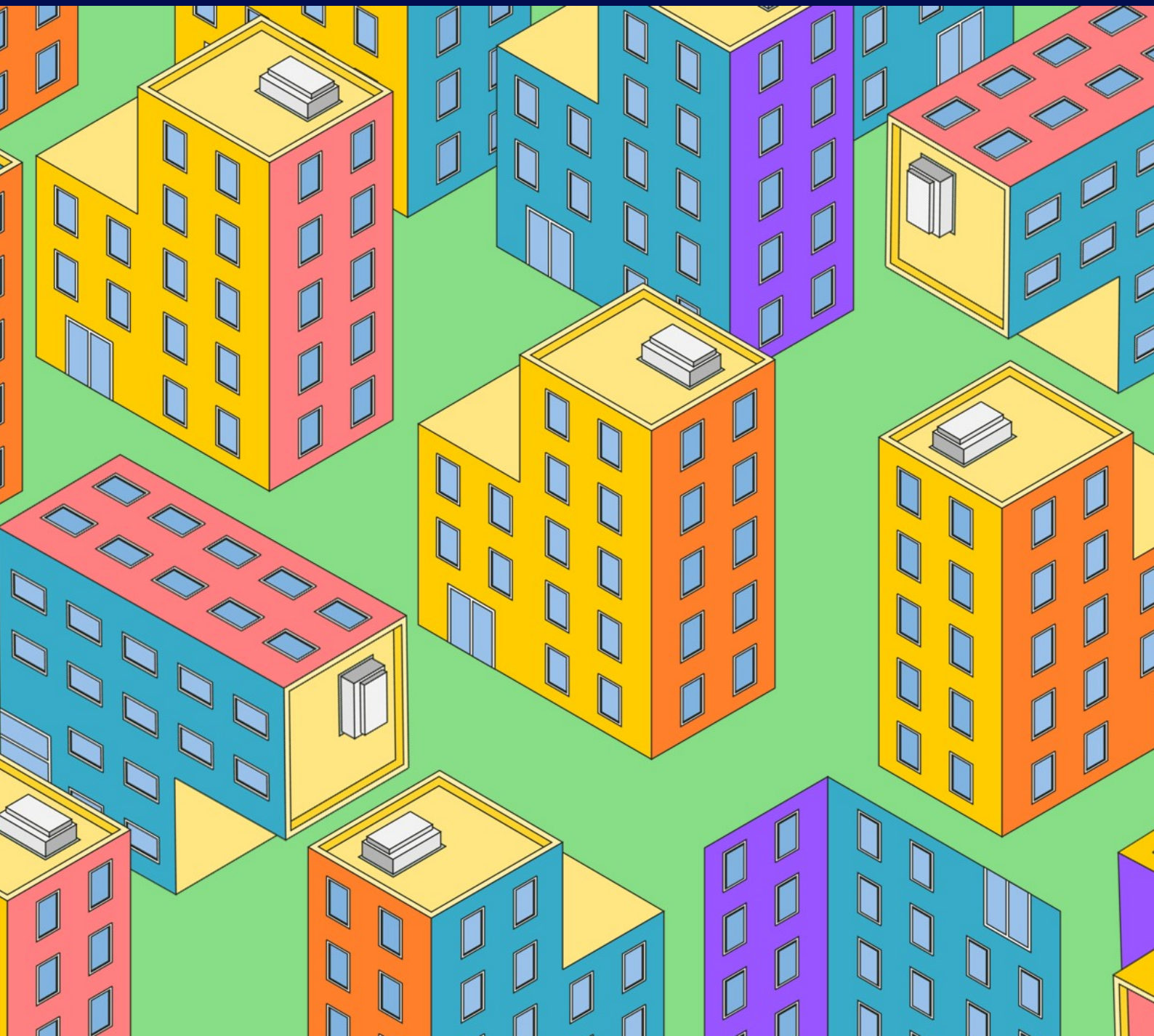

Re-modelling buildings

PhD Thesis
May, 2022

By: Jaume Palmer Real
Supervisor: Henrik Madsen
Co-supervisors: Rongling Li, Jan Kloppenborg Møller

Cover photo: Jaume Palmer, 2020
Published by: DTU, Department of Applied Mathematics and Computer Science, Richard Petersens Plads, Building 324, 2800 Kgs. Lyngby Denmark
www.compute.dtu.dk
ISSN: [0000-0000] (electronic version)

Preface

This PhD thesis was prepared at the Department of Applied Mathematics and Computer Science at the Technical University of Denmark in fulfilment of the requirements for acquiring a PhD degree in Applied Mathematics and Computer Science.

This PhD study is supported financially by the partnership with the following projects: Smart Energi i Hjemmet, IFD CITIES, Norforsk FlexBuild, IFD SEM4Cities, EUDP IEA EBC Annex 71, and IFD Flexibility Energy Denmark.

Jaume Palmer Real

.....

Signature

.....

Date

Summary (English)

More than half of the world's population lives in cities, and the number is expected to rise in the coming decades. Given the current population growth rate, it is necessary to optimise how energy is used in the building stock to ensure sustainable urban development.

The building sector is being digitalised due to the appearance of cheaper monitoring devices and an increase in computational power. The access to these data has caused a rise of data-driven models to study how energy is used in buildings. These models aim to disentangle the numerous processes governing energy flow to develop strategies to increase energy efficiency.

Despite the advance in data-collecting methods, it is often challenging to use building models that require numerous variables since relying on many sensors increases complexity fast, and potential issues during installation and maintenance may occur. In addition, data is collected by different stakeholders, so access to consolidated databases is scarce. Moreover, extensive monitoring of occupied buildings might raise privacy concerns. Thus, we are in a transition period where on the one hand, we acknowledge the need to take measurements from buildings, but, on the other hand, the available data do not match the expectations.

This work explores modelling techniques to develop data-efficient building models that are flexible, computationally light, and easy to interpret. We study traditional building models based on physics principles and propose simpler model structures that hold physical interpretation. In addition, we investigate statistical methods so our models can assimilate complex phenomena that are often impossible to incorporate using traditional heat transfer principles.

The results are two-fold: i) we see that the proposed methods are flexible and can enhance current building models to work with limited resources; ii) the modelling methods discussed in this thesis serve as a foundation to tailor specific models to describe concrete processes that occur in occupied buildings. Thus, the outcomes of this thesis are useful for researchers and practitioners that want to study building energy use on a large scale. In particular, we discuss different applications such as characterising the building stock, quantifying building energy flexibility, and simulation tools for urban planning.

Resumé (Danish)

Acknowledgements

It has been a long journey, and I could have not done it alone.

I would like to thank my main supervisor, Henrik Madsen, for giving me the opportunity to be a part of his team. Also, thanks to him and my co-supervisors, Rongling Li and Jan Kloppenborg Møller, for their support over the last three years.

Special thanks to my office colleagues Christoffer Rasmussen, Dominik Dominikov, Hjörleifur Bergsteinsson and Rune Junker; I learned so much being in the ”CITIES” office and I owe many good memories to the time we spent together.

Finally, I want to thank my partner Silvia for the energy, the patience and for making tough times easier and good times better.

List of Works

Peer-reviewed publications

Published

A Jaume Palmer Real, Christoffer Rasmussen, Rongling Li, Kenneth Leerbeck, Ole M Jensen, Kim B Wittchen and Henrik Madsen."Characterisation of thermal energy dynamics of residential buildings with scarce data". *Energy and Buildings*, Volume 230, January 2021.

B Jaume Palmer Real, Jan Kloppenborg Møller, Christoffer Rasmussen, Karen B Lindberg, Igor Sartori and Henrik Madsen."Simulating heat load profiles in buildings using mixed effects models". *Journal of Physics: Conference Series*, Volume 2069, December 2021.

Accepted

C Jaume Palmer Real, Christoffer Rasmussen, Davide Cali, Henrik Madsen. "Revealing the hidden dynamics of the energy signature model". *Building Simulation Conference proceedings 2021*.

D Jaume Palmer Real, Jan Kloppenborg Møller, Rongling Li and Henrik Madsen. "A data-driven framework for characterising building archetypes: a mixed effects modelling approach". *Energy*, May 2022.

Other media

Not-included publications

E Rune Grønborg Junker, Carsten Skovmose Kallesø, Jaume Palmer Real, Bianca Howard, Rui Amaral Lopes and Henrik Madsen. "Stochastic nonlinear modelling and application of price-based energy flexibility". *Applied Energy*, Volume 275, October 2020.

F Julien Leprince, Henrik Madsen, Clayton Miller Jaume Palmer Real, Rik der Vlist van, Kaustav Vasu and Wim Zeiler. "Fifty shades of grey: Automated stochastic model identification of building heat dynamics". *Energy and Buildings*, Volume 266, July 2022.

Presentations

G Jaume Palmer Real. "Simulating heat load profiles in buildings using mixed effects models". *NTNU Energy transition week workshop*, April 2021.

H Jaume Palmer Real. "Simulating heat load profiles in buildings using mixed effects models". *8th International Buildings Physics Conference*, August 2021.

I Jaume Palmer Real. "Revealing the hidden dynamics of the building energy signature model". *Building simulation conference*, September 2021.

Posters

J Jaume Palmer Real. "Charging homes: models for thermal characterisation of buildings". *DTU Compute's PhD bazaar*, May 2019.

Videos

K Jaume Palmer Real. "Modelling buildings using stochastic differential equations". *DTU Compute's PhD bazaar*, August 2021.

Reports

L Kim B Wittchen, Ole M Jensen, Jaume Palmer Real and Henrik Madsen. “Analyses of thermal storage capacity and smart grid flexibility in Danish single-family houses”. *Buildsim-nordic Vol. 5*, October 2020.

M Ole M Jensen, Kim B Wittchen, Jaume Palmer Real and Henrik Madsen. “Bygninger som energilager i et smart-grid”. *Aalborg Universitet*, May 2020.

Contents

List of Figures

Part I

Summary Report

1 Introduction

This thesis focuses on combining building domain knowledge, physics and statistical methods to introduce practical, interpretable and computationally light building models to help accelerate the much needed green transition.

1.1 Scope and motivation

The built environment is a significant contributor to the total energy consumption in developed countries [1]. This fact highlights the importance of increasing the share of clean energy sources and improving the energy efficiency of the building sector. For this reason, the European Commission set numerous decarbonisation targets to be climate-neutral by 2050 [2]. However, these targets are tight, and some indicators show that additional effort is needed to accelerate the green transition and minimise irreversible climatic damage [3]. This situation puts pressure on researchers and practitioners to overcome the energy sector's main challenges.

There are multiple approaches to study energy management in buildings, though the fundamental idea remains: decoupling the numerous processes that govern the heat transfer in buildings. To achieve this goal, the usage of data collected in-situ in operative buildings has gained popularity in the past years due to the appearance of affordable data-collection devices. This resource gives an insider's perspective of how the energy is used in buildings.

A clear example of the faith put in data can be seen in Europe's roll-out of electric smart meters surpassing the 50% milestone by 2020; it is expected to increase a 7.2% each year until 2026 [4]. Similarly, the number of gas smart meter installations will approach 70 million by 2026 [5].

The grown interest in research about data-driven building models can be easily seen in Figure 1.1, which shows the yearly number of publications over the past 20 years focusing on data-driven methods for building energy modelling.

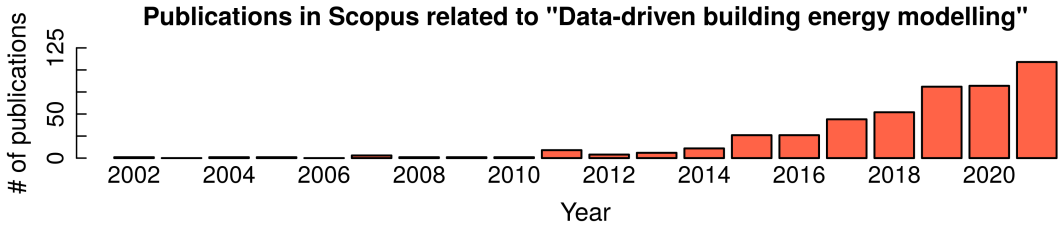

Figure 1.1: Trend of annual publications that contain the following terms: ”building”, ”energy”, ”data-driven”, and ”modelling” (Source: Scopus).

The data collected in buildings is used to develop models that can describe the most important features of buildings, clusters of buildings, and the building stock. Yet, the collection of data is not straightforward. Numerous agents intervene in building management, making it challenging to access consolidated data sources with complete building information [6]. Moreover, setting up the sensors and ensuring good maintenance can be costly. In

addition, over-relying on an abundance of data can lead to models that are difficult to generalise, given that the data used for one building might not be available for another.

Researchers might opt for using simulated data from buildings to bypass the problem of data inconsistency. Traditional building simulation models rely on physics first principles to describe the heating flow in buildings. However, since buildings are complex systems with numerous interacting elements, this traditional approach leads to cumbersome models that are computationally demanding. Still, this modelling approach is often used during the building design phase and numerous authors have pointed out a gap between the expected building performance and the measured performance during operation [7].

Thus, the issues mentioned above present a dilemma: on the one hand, we want to use data from operative buildings, so our findings represent reality; on the other hand, we want to keep the number of measured variables low to develop methods that can be implemented easily. Moreover, we are interested in working with models that hold physical interpretation, so they help understand better the fundamental processes that impact the energy flow.

This thesis explores statistical methods that can reduce the data requirements in building models to maximise their applicability in occupied buildings. Given the breadth of the subject, this work reduces the problem into two main questions: *how can we benefit from current building physics knowledge to reduce model complexity? How can we generalise building models efficiently?*

We believe that answering these questions can accelerate the transition to a digitalised building sector and help deploy energy-efficient strategies that positively impact the current and future urban landscape.

1.2 Research Objectives

This thesis presents data-driven models to study the energy flow in buildings; the focus is on data-efficient models that are scalable and easy to interpret. The research goals of this thesis can be summarised as follows:

- Exploring tools to develop *simplified grey-box models*, i.e. low order models that benefit from fundamental principles of energy dynamics in buildings. Thus, these models should be easy to interpret and not require extensive data and information from the building side.
- Identifying key parameters to characterise the energy use in buildings. The features should be accessible using minimal non-intrusive data so the building stock can be investigated on a broad scale.
- Introducing statistical methods to generalise current building models to be able to study larger populations of buildings without sharply increasing the computational requirements. These methods should be flexible and not be bound to a particular modelling framework.

1.3 Thesis Structure

This work is divided into six chapters, followed by the Appendix. Figure 1.2 gives a schematic representation of the flow of this thesis. It can be seen that Chapter 3 and Chapter 4 contain the relevant content discussed in Chapter 5. The content chapters give the basis for the presented publications as shown in Figure 1.2; the three tracks presented in Section 1.2 intersect both content chapters.

The content of each chapter is introduced below:

- Chapter 2 introduces the background of the work. First, the chapter gives an overview of how data is currently captured and used to develop building models. Then, the chapter presents basic principles of heating dynamics to introduce an exhaustive model used in commercial software to describe the energy flow in buildings.
- Chapter 3 is dedicated to describing models that combine physics first principles and statistical methods. This approach is often referred to as *grey-box* modelling; the chapter describes an array of known modelling structures presented as *simplified grey-box* models. Instead of delving into the technical details, the chapter highlights the link between the different proposed methods to understand the physical assumptions behind each approach. For this reason, most of the mathematical details are either formulated in the Appendix or cited from other sources. The methods introduced in this chapter are most relevant in **Paper A** and **Paper C**.
- Chapter 4 proposes mathematical methods to quantify the impact of phenomena that affect the building energy use and either cannot be explained by physical principles or require numerous variables that might not be measured. The chapter is divided into two parts: first, we focus on mixed-effects modelling, a general framework to refine the quantification of model uncertainty; second, we propose different methods to bypass data scarcity and lack of information in buildings. Mixed-effects models are used in **Paper B** and **Paper D**. The presented support methods have been used in all the publications that constitute this thesis.
- Chapter 5 contains the discussion of the main results obtained during this thesis. Thus, the content presented in Chapter 3 and Chapter 4 is directly linked to the presented publications.
- Chapter 6 concludes the work and summarises the primary outcomes of the thesis.

Although there are cross-references present, Chapter 3 and Chapter 4 can be read independently. Each chapter represents one approach to address the same question: *How to develop data-efficient models to study energy efficiency in buildings*.

(!) Concepts

The results of this thesis are transversal and combine different branches of building physics, time series analysis and dynamical systems. For this reason, the discussion is intertwined with fundamental concepts explained in text boxes; the reader can skip these if already familiar with the subject.

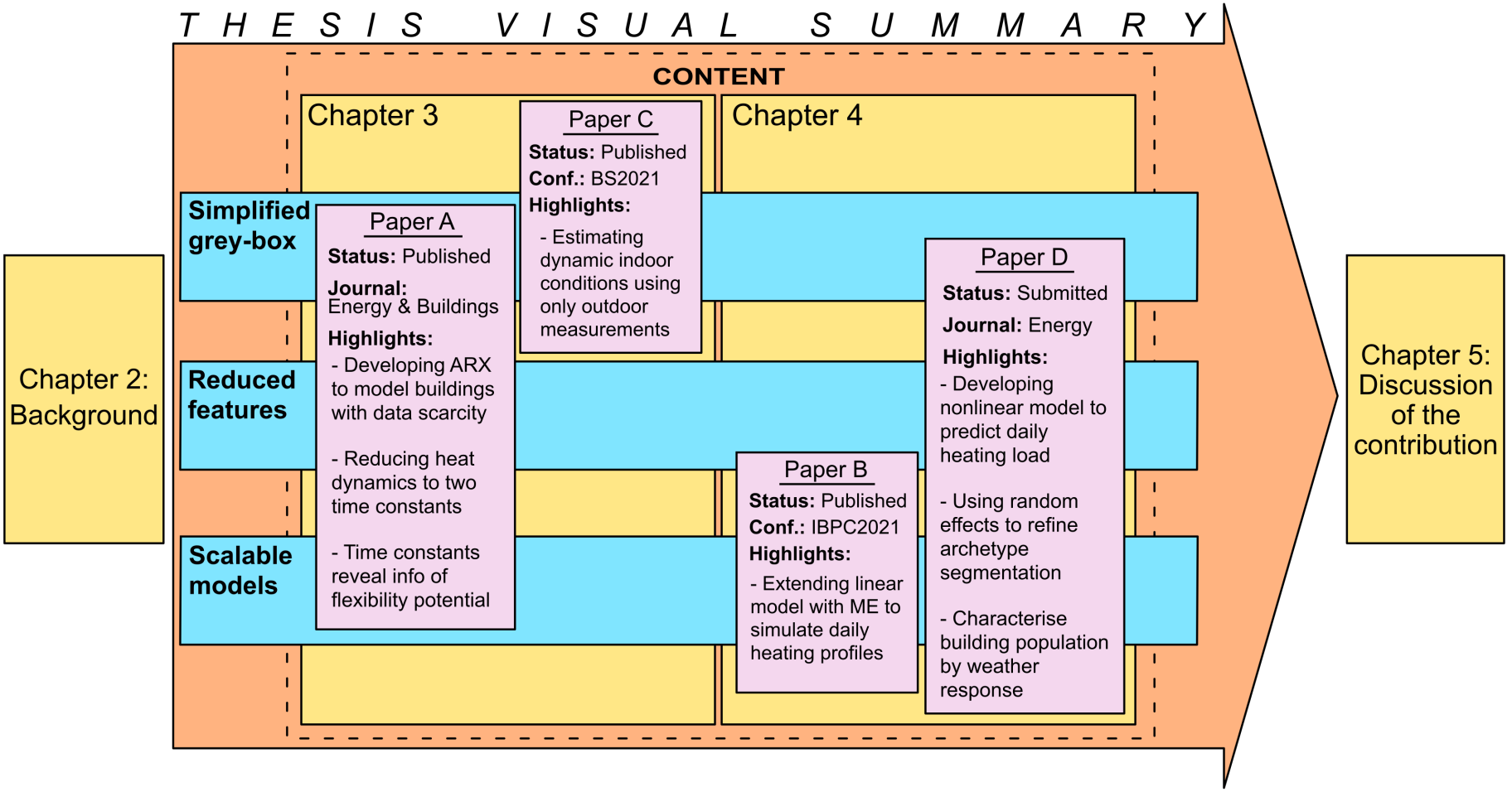

Figure 1.2: Schematic representation of the thesis content.

2 Background on data and building modelling

This thesis suggests statistical methods that, combined with building physics fundamentals, reduce the data requirements to develop models to study the building energy flow. To introduce the subject, this section discusses different types of measurements that can be gathered in buildings and their typical sources; in addition, we discuss the potential limitations of the information that can be extracted from operational buildings.

Then, the section gives a brief introduction of fundamental processes that govern the heat flow in buildings. These principles will be the foundation to develop reduced data-efficient models in the following chapter.

2.1 Data availability for data-driven modelling

Over the recent years, the use of data to model building energy use has been rising. This has caused numerous authors to investigate the best methods to use data from buildings. Collected data are to be used in numerous applications: from the development of smart demand-side strategies [8], investigating the energy performance of building components, identifying retrofitting opportunities [9] or urban energy planning [10].

Numerous authors have identified a *performance gap* between the expected building consumption during the design phase of buildings and the measured consumption during operation [11]. This difference suggests that simulation software is not able to reflect reality completely. Moreover, measured data provides more information about a building's energy use than typical engineering audits [12].

Given the diverse nature of energy use in buildings, using data raises the question of which variables should be measured. Even though some authors have suggested application-independent building models [13], in general, the required variables will depend on the application of the model.

Category	Examples
Energy use	Electric power, heating load, heat load, domestic hot water,...
Indoor conditions	Temperature, humidity, CO2 concentration,...
Climatic conditions	Temperature, humidity, solar radiation,...
Occupancy	# of occupants, activity logs, comfort status, appliance use...
Architectural	Blueprint of building, heating system, renovation,...
Socio-economic	Personal details of occupants, socio-demographic details of the region,...

Table 2.1: Types of data from buildings.

Table 2.1 shows different categories of data found in literature. Notice that the type of data ranges from qualitative concepts, e.g. comfort, to specific numeric variables, such as indoor temperature readings. There are additional factors to take into account, like the spatial and temporal resolution of the measurements, as well as, when dealing with user activity, the reliability of the data; for instance, there exist region/nation-wide registries of architectural details of the building stock, but it is not guaranteed that they are kept updated [14].

Given the numerous services that keep track of climatic conditions, weather data might be regarded as easier to capture. Yet, the available weather stations might not be placed in suitable locations rendering the data useless for our purposes [15].

Furthermore, when using data to describe the building energy flow, it is necessary to assess how representative the measured data is of the variable that we want to capture. For instance, the measured air temperature of a room might vary significantly due to potential temperature stratification. Hence, it is not only necessary to measure the appropriate variables but locate the sensors correctly.

For this reason, numerous authors opt for using simulated data; a systematic review on building models for energy flexibility by Li et al. [8] found that less than 15% of the evaluated studies had measurements from field or experiments. On the other hand, Amasyali and El-Gohary [16] found that 67% of the literature on prediction heating/cooling load used real data; however, their review shows that normally prediction work uses external data, i.e. climatic data, calendar data and consumption, which are often more accessible than indoor variables.

Another option is to extract data from buildings built in research facilities that are devoted to be laboratories [17]. This way, sensors can be deployed which gives researches and practitioners freedom to complete specific experiments to fulfill a scientific purpose. Alternatively, data-driven models have focused on using measurements from buildings from university campus [18, 19]; however, this represent a clear limitation since these studies can only focus on one building typology. Finally, best case scenario is to be able to study fully functioning occupied buildings, since they have the complete information of how energy is being used, however they tend to present data limitations due to privacy and comfort concerns [20].

Moreover, the cases discussed so far focus on single buildings. Yet, the models being developed should be scalable to maximise the positive impact of current research. Studies that manage to gather data from numerous buildings at urban or region level rely on utilities and other stakeholders that can only share limited information [21].

The above-mentioned examples suggest that there is a gap between the data that we can access easily at large scale and the information we want to retrieve. Thus, it is necessary to investigate non-intrusive methods that are data-efficient so the building stock can be investigated reliably.

2.2 Physics based multi-zone model

Multi-zone models are the foundation of many commercial building simulation software [22]. These models reduce a building into a network of nodes that resembles an electric circuit where heat is transferred. Each node represents a different heat-accumulating element inside the building and has its thermal capacity; if heat transfer exists between two parts, they are connected by thermal resistance. For this reason, this type of modelling is also referred to as Resistance-Capacity (RC) models.

For every node, a heat balance equation is solved such that, for the j_{th} node.

$$\dot{q}_{\text{in}} = \dot{q}_{\text{out}} + \dot{q}_{\text{acc}} \tag{2.1}$$

where $\dot{q}_x$ is the heat flux going in the node, going out the node and being accumulated in the medium, respectively. Thus, a node x is described by the following differential equation

$$C_x \frac{\mathrm{d}T_x}{\mathrm{d}t} = \dot{q}_{\text{in}} - \dot{q}_{\text{out}} \tag{2.2}$$

where T_x is the temperature of an element x.

Each of the heat flux terms q_x in Equation (2.1) is a combination of the three main heat transfer processes: convection, conduction and radiation. These terms are described as,

- Conduction is the process of transferring heating energy through solid materials. Mathematically it is described as

$$\dot{q}_{\text{cond}} = A(T_1 - T_2)/R \tag{2.3}$$

  where A is the area orthogonal to the heat flow direction, R is the thermal resistance, and $T_i \ \ \forall i \in [1, 2]$ are the temperatures at both sides of the material.

- Convection is the propagation of heat through a liquid or gas. The convection through a surface that is in contact with a mass of air is

$$\dot{q}_{\text{conv}} = hA(T_1 - T_s)\,, \tag{2.4}$$

  with A being the area of the surface, h is the convective heat transfer, T_1 the mean air temperature and T_s the surface temperature. If the heat transfer occurs through a stream of air, the appropriate model is

$$\dot{q}_{\text{conv}} = \dot{m} c_p \rho (T_{\text{sys}} - T_1) \tag{2.5}$$

  where $\dot{m}$, c_p, ρ, T_{sys} are the mass flow-rate, specific heat, density and temperature of the fluid, respectively.

- Radiation is the heat transfer through electromagnetic waves. The heat transfer between two bodies follows

$$\dot{q}_{\text{rad}} = \frac{\sigma(T_1^4 - T_2^4)}{\frac{1-\epsilon_1}{A_1\epsilon_1} + \frac{1}{A_1 F_{1-2}} + \frac{1-\epsilon_2}{A_2\epsilon_2}} \tag{2.6}$$

  where σ is the Stefan-Boltzmann constant, T_1 and T_2 are the surface temperatures, ϵ_1, ϵ_2 are emitances and F_{1-2} is the *view factor*– a coefficient that quantifies the proportion of radiation that departs from surface 1 and hits surface 2, and vice versa.

When using the multi-zone framework, the modeller has the role of setting up the network of building elements, so it represents the building of interest. A combination of Equations (2.3)-(2.6) will be used to match the complexity of the building. This scheme already introduces simplifications, such as the one-dimensional nature of heat transfer or the omission of heating gradients in each element; the reader can find a complete description of the method in Hensen and Lamberts [23]. Nevertheless, the multi-zone model potentially allows the modeller to set a complex network to represent the heat transfer.

The multi-zone scheme is primarily used for the purpose of building design and it requires a significant level of detail from the building components. For example, it is necessary to know the materials, properties and spatial configuration of the different elements that are part of the building.

2.2.1 An example using ordinary differential equations

Next chapter introduces model assumptions to develop reduced-order models based on data. Similar to the work of Rouchier [24], we use the example depicted in the Figure 2.1 to showcase the necessary assumptions.

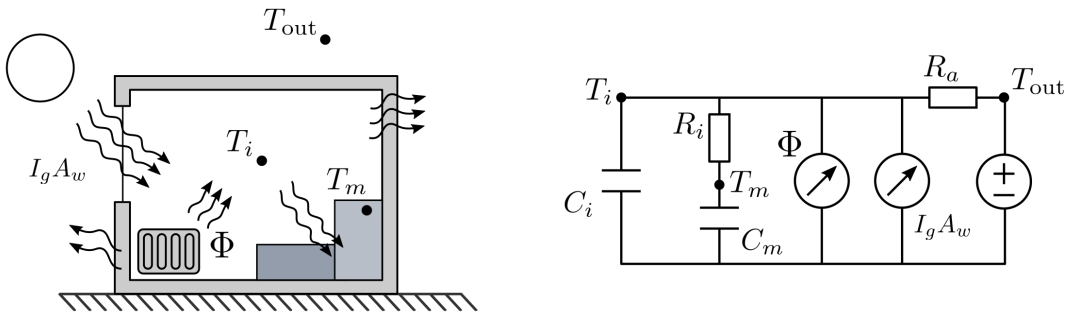

Figure 2.1: Representation of the differential equation building model in Equation (2.7) with its equivalent RC network.

The model in Figure 2.1 assumes that a building is well described as a single space with two primary heat accumulative elements: the indoor air and a *thermal mass* which, in this case, represents an aggregation of other building elements such as walls and furniture. The solar irradiation comes directly through the window, which has no resistance; similarly, the building has a heater with a direct heat transfer to the indoor air. Since surface temperatures are disregarded, no radiative effects are taken into account. Finally, notice that this model only considers a space-aggregated representative temperature, omitting the inner flows inside a single element.

The system in Figure 2.1 can be expressed as the follows

$$\begin{cases} C_i \dfrac{\mathrm{d}T_\mathsf{i}}{\mathrm{d}t} = \dfrac{1}{R_i}\left(T_\mathsf{m} - T_\mathsf{i}\right) + \dfrac{1}{R_a}\left(T_\mathsf{out} - T_\mathsf{i}\right) + \Phi + I_g A_w \\ C_m \dfrac{\mathrm{d}T_m}{\mathrm{d}t} = \dfrac{1}{R_i}\left(T_\mathsf{i} - T_\mathsf{m}\right) \, . \end{cases} \tag{2.7}$$

where T_i and T_m are the system variables that represent the indoor air temperature, respectively. The system has three different inputs: the outdoor air temperature T_out, the solar irradiation I_g and the heating load Φ. The parameters of the system are given by the thermal resistances R_i and R_a, the thermal capacities C_i and C_m and the effective window area A_w.

Equation (2.7) is a second order differential equation system. Defining $\boldsymbol{x}_t = (T_\mathsf{i} \;\; T_\mathsf{m})^\top$, it can be written compactly as

$$\frac{\mathrm{d}\boldsymbol{x}}{\mathrm{d}t} = \boldsymbol{A}\boldsymbol{x} + \boldsymbol{B}\boldsymbol{u} \, , \tag{2.8}$$

where $\boldsymbol{A}$ and $\boldsymbol{B}$ are constant matrices defined as

$$\boldsymbol{A} = \begin{pmatrix} \frac{1}{R_i C_i} & -\left(\frac{1}{R_a C_i} + \frac{1}{R_i C_i}\right) \\ \frac{-1}{R_i C_m} & \frac{1}{R_i C_m} \end{pmatrix}; \quad \boldsymbol{B} = \begin{pmatrix} \frac{1}{R_a C_i} & \frac{1}{C_i} & \frac{A_w}{C_m} \\ 0 & 0 & 0 \end{pmatrix}, \tag{2.9}$$

and $\boldsymbol{u} = (T_{\text{out}}\ \Phi\ I_g)^\top$ is the vector of deterministic inputs. The matrix $\boldsymbol{A}$ is called the *design matrix* and it describes the internal dependencies of the system; $\boldsymbol{B}$ is often called the *input matrix* and describes how the inputs are introduced in the system. The system in Equation (2.8) is deterministic, meaning that, given the initial conditions $\boldsymbol{x}_0$, the future values of the inputs and the matrices $\boldsymbol{A}$ and $\boldsymbol{B}$, it is possible to track the state of the system at any time. The state of the system is characterised by $\boldsymbol{x}_t$; for this reason, $\boldsymbol{x}_t$ is called the *state vector*.

The natural question is how well the model in Equation (2.7) represents an actual building. It is clear that buildings may contain numerous phenomena that affect the indoor air temperature which are not accounted for in Equation (2.7). Similarly, the defined state is a simplification of a more complex system as the defined thermal mass bundles multiple unknown elements. When comparing real data to the model in Equation (2.7), these omissions and assumptions will introduce noise and uncertainty.

Given the numerous factors that affect building energy modelling, even working with a much more thorough building multi-zone model will still contain simplifications which will cause differences between the predicted behaviour and the measured data. In addition, a very detailed deterministic model of a single building will not be robust and will not scale properly. Hence, instead of pursuing a detailed model like the multi-zone model, one can go in the opposite direction and introduce uncertainty in the model. This is the base idea of modelling buildings with stochastic differential equations and is the departing point of the next chapter.

3 Grey matter: leveraging physics to develop simplified building models

Building energy modelling is a thoroughly studied and multi-faceted field. Numerous building components play an essential role in the energy flow: building materials, geometry, climatic conditions, or building usage will affect the energy flow differently, which has motivated years of research. The scientific output has caused an increase in modelling options to consider all phenomena that affect building energy use.

This chapter outlines relevant assumptions and transformations to reduce the complex building model described in Section 2.2 into more accessible and practical models. These models are meant to be fit using measurements, so we introduce the necessary statistical foundation for understanding and facilitating the model estimation. Given the physical nature of the subject, special attention is put to the usage of modelling structures that will hold physical interpretation.

The label *grey-box* describes building models that combine physical knowledge and statistics. However, in practice, building-physics literature most often uses the term *grey-box modelling* to refer to lumped RC models based on stochastic differential equations. This section proposes a looser interpretation of the term since it is argued that other modelling methods may still carry physical meaning.

The methods discussed in this chapter have been discussed in other sources like the work by Jimenez and Madsen [25] and Madsen et al. [26]; yet, this chapter highlights the links that bridge the different modelling options as described by Figure 3.1. We intend to give the modeller the necessary tools to deduce practical information about the building with limited data and resources by unveiling the latent hypotheses that render each model structure relevant.

3.1 Stochastic differential equations

Setting up a deterministic building model that captures all phenomena that affect the energy flow is virtually impossible. Likewise, installing the necessary sensors to estimate the model parameters is not feasible because such a complex model is not structural identifiable, especially when using data from the buildings' regular operation [27]. This section introduces stochastic differential equations (SDE) as a framework to develop more compact and robust building models that leverage physical knowledge and statistics.

Stochastic differential equations are a natural continuation of ordinary differential equations, where a term is added to account for model uncertainty. This new term works two-fold: i) it bundles together numerous processes that cause noise, which reduces the model structure to only the necessary variables; ii) it allows the formulation of statistical methods to estimate the model parameters and characterise the measured system. In general, they present two terms

$$\mathrm{d}\boldsymbol{x} = \underbrace{f(\boldsymbol{x};\boldsymbol{u};t)\mathrm{d}t}_{\text{Drift}} + \overbrace{g(\boldsymbol{x};\boldsymbol{u};t)\mathrm{d}\omega}^{\text{Diffusion}}, \tag{3.1}$$

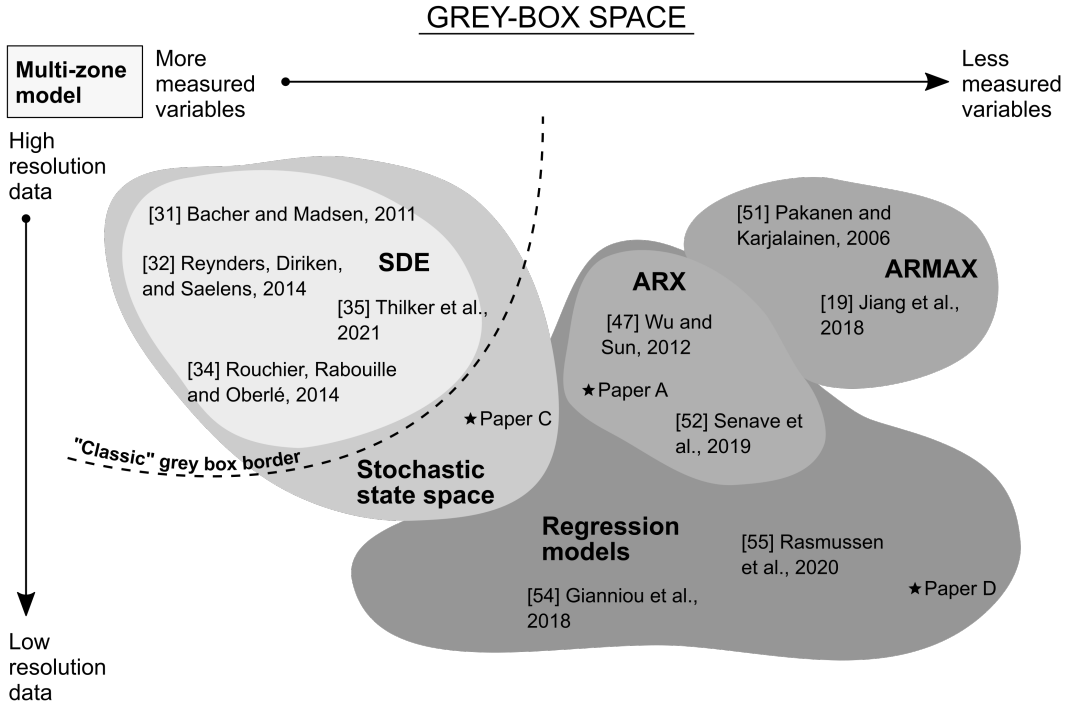

Figure 3.1: Map of extended grey-box space with relevant references.

where $\boldsymbol{w}$ is a stochastic process. Normally, $\boldsymbol{w}$ is defined as a Wiener process, since it has numerous computational benefits given that the process has independent increments.

White noise

A process $\{\varepsilon_1, \varepsilon_2, \varepsilon_3, \cdots, \varepsilon_N\}$ is defined as white noise if it represents a series of mutually uncorrelated and identically distributed random variables with mean value equal to 0 and constant variance σ_ε^2.

The drift term from Equation 3.1 describes the known dynamics of the system. In contrast, the diffusion term captures the uncertainty of $\boldsymbol{x}$ given by model approximations and noise present in the input measurements. This SDE structure is general and widely used to describe, among others, financial markets, marine ecosystems, and pharmacokinetics; hence, both $f(\cdot)$ and $g(\cdot)$ can be complex non-linear functions [28].

In this thesis, the focus is on linear SDEs since buildings are often considered linear time-invariant systems [26]. It is known that non-linearities are found in the energy flow of buildings, but in this work, the impact of non-linear phenomena is assumed to be negligible or captured by the diffusion term.

Thus, the linear ODE system described in Equation (2.8) is transformed into an SDE by the addition of the diffusion term such that

$$\mathrm{d}\boldsymbol{x} = (\boldsymbol{A}\boldsymbol{x} + \boldsymbol{B}\boldsymbol{u})\,\mathrm{d}t + \boldsymbol{G}\mathrm{d}\boldsymbol{w} \tag{3.2}$$

where $\boldsymbol{G}$ is a constant matrix describing how the noise enters the system. Equation (3.2) describes the inner dynamics of the system of interest, for this reason it is often referred to as the *system equation*.

In the ODE presented in Section 2.2.1, the state of the system, x, is described by a vector of temperatures. Yet, the temperatures may or may not be measured directly since any measurement will include noise. The uncertainty present during the process of measuring the states is incorporated into the model by adding the *observation equation*, which describes the interaction between the state, the inputs and what is measurable in the system, $\boldsymbol{Y}_t$. The inclusion of this equation leaves the final SDE model as

$$\begin{cases} \mathrm{d}\boldsymbol{x} = (\boldsymbol{A}\boldsymbol{x} + \boldsymbol{B}\boldsymbol{u})\,\mathrm{d}t + \boldsymbol{G}\mathrm{d}\boldsymbol{w} \\ \boldsymbol{Y}_t = \boldsymbol{C}\boldsymbol{x}_t + \boldsymbol{D}\boldsymbol{u}_t + \boldsymbol{e}_t\,, \end{cases} \tag{3.3}$$

where $\boldsymbol{e}_t$ is a stochastic variable, typically white noise. Matrix $\boldsymbol{C}$ and $\boldsymbol{D}$ give the linear relationship between the observations and the state and input vector, respectively. Notice that the observation equation is written in discrete-time; hence, the subscript t has been added to denote the measurement of $\boldsymbol{x}$ and $\boldsymbol{u}$ at time t.

Equation (3.3) is called *stochastic state-space* formulation, since it describes the evolution of a state variable, $\boldsymbol{x}$, and its observations, $\boldsymbol{Y}_t$, over a space of probabilities (defined by $\boldsymbol{w}$ and $\boldsymbol{e}_t$). The state-space formulation will be further developed in Section 3.2, when focusing on discrete dynamical systems.

Continuing with the example in Equation (2.7), notice that the matrices $\boldsymbol{A}$ and $\boldsymbol{B}$ are the same as the deterministic model since the diffusion term is introduced additively. Assuming that the system noise is independent, $\boldsymbol{G} = \boldsymbol{I}$; where $\boldsymbol{I}$ is the identity matrix. Furthermore, let's assume that only the indoor temperature is measured and none of the inputs influences the sensor; in such case, $\boldsymbol{Y}_t$ represents the temperature of the sensor, and the arrays of the observation equation are

$$\boldsymbol{C} = \begin{pmatrix} 1 & 0 \\ 0 & 0 \end{pmatrix}; \quad \boldsymbol{D} = \begin{pmatrix} 0 & 0 & 0 \\ 0 & 0 & 0 \end{pmatrix}. \tag{3.4}$$

In recent years, the use of SDEs to model building energy flow has been rising [29]. They offer a flexible framework that allows a thorough analysis of a building's dynamic behaviour. In addition, they are computationally efficient and give reliable parameter estimations that are easy to interpret, which is advantageous when modelling physical systems. For this reason, they have been used in numerous applications that can be summarised in three categories: characterisation, control and simulation.

A second-order SDE such as the one described by $\{\boldsymbol{A}, \boldsymbol{B}, \boldsymbol{C}, \boldsymbol{D}\}$ was studied by Madsen and Holst [30] as a sufficient model structure to model heat dynamics in buildings. Bacher and Madsen [31] fit multiple SDE structures using real measurements from a test house; they suggested that even a complex building model is well-represented with a third-order SDE. Furthermore, their work gives an overview of the building's main components that influence the energy flow.

Reynders, Diriken, and Saelens [32] studied the ability of SDE systems to cope with uncertainty and different types of data. They proposed a fourth-order model as a good representative of a single zone dwelling and argue that this model structure is robust and a good choice to simulate and control buildings. Similarly, Himpe and Janssens [33] used a fourth-order model to characterise the heat loss of a test house. These findings are in line with the work of Rouchier, Rabouille, and Oberlé [34], who compared the estimation

results of a deterministic and stochastic third-order RC model. They confirmed that the stochastic structure increases the robustness of the parameter estimates and suggest that this type of model will adapt better to changes in input weather variables. Finally, given the uncertain nature of climatic conditions, Thilker, Madsen, and Jørgensen [35] proposed an SDE model with embedded forecasts of weather variables for control applications.

Thus, numerous authors have proposed different SDE models using typical model building element combinations. To facilitate the model choice, Leprince et al. [36] proposed an automated method for system identification based on CTSM-R [37]. Their selection algorithm departs from a first-order model and tests different RC models up to the seventh-order; the quality of the fit is based on the distribution of residuals in the frequency domain. This methodology was tested in 247 buildings, and 188 resulted in a good model fit.

Lastly, it is important to remark that the general formulation of SDEs makes it possible to incorporate other relevant processes and building components as state variables, i.e. other than indoor temperature states. For example, Thilker et al. [38] included the flow rate as a state vector to model the heating system of a school; the model was then used to control the indoor climate in different classrooms. Jiménez et al. [39] and Friling et al. [40] used a first-order a SDE system to model the heat transfer in a photovoltaic module. Junker et al. [41] developed a general model to characterise the energy flexibility of a system to participate in smart demand-response strategies; their proposed model was tested using measurements from a water tower.

This section has presented SDEs as a flexible method to model physical systems using measured data. The following section will show how, given their compact formulation and clarity, SDEs represent a good departure point for developing simplified models that can be used in case of data scarcity.

3.2 Discrete-time series models

By definition, data are discrete, making discrete-time series an appropriate option to study measured phenomena. Furthermore, these models are easy to formulate and fit, representing an accessible and computationally light option to investigate dynamical systems.

Discrete-time models can be obtained as a simplification of known physical processes, so understanding the latent dynamics of such systems will help identify suitable model structures. This section departs from the stochastic continuous formulation described in Section 3.1 and introduces the necessary tools to transform an SDE system into a physically-interpretable discrete model. The examples presented are based on the RC model in Section 2.2.1; thus, the methods are focused on linear time-invariant systems.

3.2.1 Stochastic sate-space modelling

A system governed by a known stochastic differential equation is discretised by integrating over its sampling interval $[t, t+s)$, where s represents the sampling time [42]. For simplicity, in this work, we will assume the sampling time is constant $s = 1$. This makes it possible to transform the continuous system equation of Equation (3.3) to its discrete-time equivalent

$$\boldsymbol{X}_{t+1} = \boldsymbol{A}^* \boldsymbol{X}_t + \boldsymbol{B}^* \boldsymbol{U}_t + \boldsymbol{\varepsilon}_t \,, \tag{3.5}$$

with

$$\boldsymbol{A}^* = e^{\boldsymbol{A}}; \;\; \boldsymbol{B}^* = \int_t^{t+1} e^{\boldsymbol{A}(t+1-s)} \boldsymbol{B} ds; \;\; \boldsymbol{\varepsilon}_t = \int_t^{t+1} e^{\boldsymbol{A}(t+1-s)} d\boldsymbol{\omega}(s) \,. \tag{3.6}$$

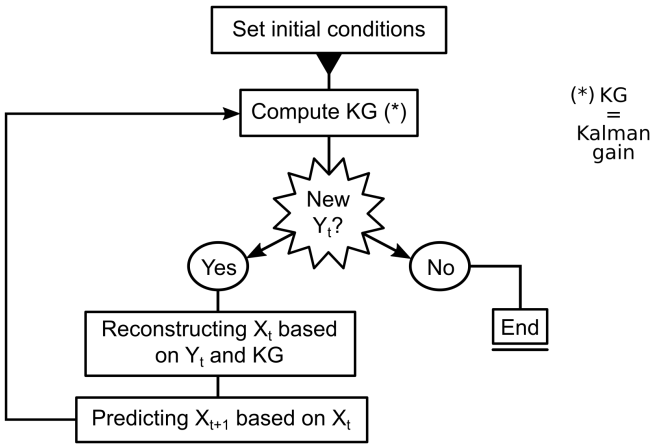

Figure 3.2: Schematic representation of the Kalman filter.

Notice the change in notation, where the superscript $*$ has been added to denote discrete time. In addition, it is important to remark that, to arrive at Equation (3.5), it has been assumed that the inputs are constant between the sampling time.

Recall that $\boldsymbol{x}$ characterised the system in continuous time, and so does $\boldsymbol{X}_t$ in discrete time. As done in the continuous case, to complete the state-space formulation, the observation equation is added to describe the relationship between the state and the variable that we can measure, $\boldsymbol{Y}_t$,

$$\boldsymbol{Y}_t = \boldsymbol{C}\boldsymbol{X}_t + \boldsymbol{D}\boldsymbol{U}_t + \boldsymbol{e}_t\,. \tag{3.7}$$

The residual term ε_t is, again, considered white noise. Similarly, $\boldsymbol{e}_t$ is also white noise and it is independent of ε_t.

The Kalman filter

State-space models are well suited to cope with missing and corrupt data since they can be *filtered*. Filtering is a statistical method that reconstructs a process by leveraging model predictions, observations and inputs. The filtering process uses measurements, $\boldsymbol{Y}_t$, of a dynamic system, $\boldsymbol{X}_t$, to reconstruct states simultaneously based on the relation between variables described by Equations (3.5) and (3.7).

A notable filter for discrete linear time-invariant state-space models is the Kalman Filter (KF), a filtering algorithm that was developed during the 1950s and 1960s, which primary use was tracking spaceflight vessels during the space race [43].

The Kalman filter is based on the mathematical principle of linear projection and provides the optimal reconstruction and prediction of the state variable, $\boldsymbol{X}_t$, using observations $\boldsymbol{Y}_t$. The idea behind the KF is to predict one step ahead and recursively compare the available observations with the prediction. During the process, the uncertainty of the model prediction is compared to the uncertainty of the observations to evaluate which of the two is more reliable. This comparison is encapsulated in a ratio called the Kalman Gain. The filtering process is schematically presented in Figure (3.2) and a more detailed mathematical description can be found in Madsen [44].

Given that the Kalman filter provides the optimal reconstruction of $\boldsymbol{X}_t$, it is often used to estimate the model's characteristic parameters. This is done by wrapping the Kalman

Filter in an optimisation routine aimed at maximising the likelihood of the proposed model; the likelihood function is used as the cost function since it describes how well a model fits the available observations as a function of the model parameters.

Fitting a model by maximising the likelihood function is known as the Maximum Likelihood Estimation (MLE) method. If the model noise is Gaussian and the system is in steady-state, as shown in Appendix I, the parameter estimator that maximises the likelihood minimises the sum of squared residuals.

Likelihood

The likelihood of a model represents the joint probability of having observed a series of measurements $\boldsymbol{Y} = \{y_1, \cdots, y_N\}$ given a parameter vector, $\boldsymbol{\theta}$.

Example: Given the model $Y = \mu + \epsilon_t$ where $\epsilon_t \sim N(0, \sigma_\epsilon^2)$, the distribution f_Y can be defined as

$$f_Y(y_t, \mu, \sigma_\epsilon^2) = \frac{1}{\sigma_\epsilon \sqrt{2\pi}} \exp\left(-(y_t - \mu)^2 / 2\sigma_\epsilon^2\right) \tag{3.8}$$

Given the N observations of $\boldsymbol{Y}$, the likelihood function of the model is

$$L(\boldsymbol{Y}; \mu, \sigma_\epsilon^2) = \prod_{t=1}^{N} f_Y\left(y_t, \mu, \sigma_\epsilon^2\right) . \tag{3.9}$$

Often, for model estimation, the logarithm of Equation (3.8) is used to ease the computational requirements.

As above-mentioned, state-space models can be built directly by discretising an SDE system, which leaves a linear model with no derivative terms that is easier to operate with. This is easily seen writing explicitly the discrete state-space version of the model in Equation (2.7),

$$\boldsymbol{X}_t = \begin{pmatrix} T_{\mathsf{i},t} \\ T_{\mathsf{m},t} \end{pmatrix} = \begin{pmatrix} a_{11} & a_{12} \\ a_{21} & a_{22} \end{pmatrix} \begin{pmatrix} T_{\mathsf{i},t-1} \\ T_{\mathsf{m},t-1} \end{pmatrix} + \begin{pmatrix} b_{11} & b_{12} & b_{13} \\ b_{21} & b_{22} & b_{23} \end{pmatrix} \begin{pmatrix} T_{\mathsf{out},t} \\ \Phi_{h,t} \\ I_{g,t} \end{pmatrix} + \begin{pmatrix} \epsilon_{1,t} \\ \epsilon_{2,t} \end{pmatrix} , \tag{3.10}$$

where a_{ij} and b_{ij} $\forall i, j \in [1, 2, 3]$ are the coefficients of matrices $\boldsymbol{A}^*$ and $\boldsymbol{B}^*$ respectively. Given $\boldsymbol{C}$ and $\boldsymbol{D}$ described in Equation (3.4), the observation equation simply becomes

$$Y_t = \begin{pmatrix} 1 & 0 \end{pmatrix} \begin{pmatrix} T_{\mathsf{i},t} \\ T_{\mathsf{m},t} \end{pmatrix} + e_{2,t} \, . \tag{3.11}$$

The resulting state-space model serves as a foundation for modelling related processes using discrete systems, as shown in **Paper A** where a state-space system was reduced into a univariate linear dynamic model. However, depending on the data availability, it might not be necessary to use a discrete system that is a direct transformation of an SDE model; instead, it might be sufficient to build a proxy model to fulfil the required application. An example of this can be found in **Paper C**, where a discrete state-space was used to reconstruct the indoor conditions of a building using only outdoor measurements and consumption data.

Often, it will be interesting to model the evolution of one variable, e.g. the room temperature or the heating consumption of a building. Next section presents popular model structures used to model univariate time series—as above-mentioned, acknowledging the latent physical processes that govern the variables of interest will be highly beneficial in developing any dynamic model.

3.2.2 The ARMAX model

This section introduces a general framework to model linear discrete-time dynamical systems known as the ARMAX model. ARMAX stands for Auto-Regressive model with Moving Average and eXogenous inputs, in general, this model category has the following structure

$$\begin{aligned} X_t = &\phi_1 X_{t-1} + \cdots + \phi_p X_{t-p} + && \rightarrow \text{AR term} \\ &\omega_1 U_{1,t} + \omega_2 U_{2,t} + \cdots + \omega_m U_{m,t} + && \rightarrow \text{Inputs} \\ &\varepsilon_t + \theta_1 \varepsilon_{t-1} + \cdots + \theta_q \varepsilon_{t-q}\,, && \rightarrow \text{MA term} \end{aligned} \tag{3.12}$$

where X_t is the measured dependent variable, $U_{j,t}\ \forall j \in [1, \cdots, m]$ are measured inputs and $\varepsilon_t \sim N(0, \sigma_\varepsilon^2)$ represents the residuals. As indicated in Equation (3.12), this model structure has three different components:

- An auto-regressive part (AR), which contains the lagged values of the output variable. The parameter p is known as the *order* of the AR term and gives the maximum lagged value of X_t.
- A moving-average term (MA) that contains the residuals and its lagged values. The order of the MA term is characterised by the parameter q.
- Measured external inputs which are considered to be deterministic, i.e. their observations do not contain any source of noise. It is important to remark that Equation (3.12) may contain lagged input variables; for the sake of brevity, these terms have been omitted.

The ARMAX structure describes a linear time-invariant system; this model is highly adaptable and variations of the ARMAX can be found by slicing the general Equation (3.12) into its essential components. Table 3.1 summarises some of the most well-known submodels; for an extended description of the different variants, the reader can check Madsen [44].

Given N observations of X_t and $U_{j,t}$, Box and Jenkins proposed an iterative procedure to fit an ARMAX [45]. Before describing each step, let's write the ARMAX model in compact form as

$$\boldsymbol{X} = \boldsymbol{Z}\boldsymbol{\beta} + \boldsymbol{\varepsilon} \tag{3.13}$$

with

$$
\begin{aligned}
\boldsymbol{X} =& (X_{d+1} \ \cdots \ X_N)^\top \\
\boldsymbol{Z} =& \begin{pmatrix} X_d & \cdots & X_{d-p+1} & U_{1,d} & \cdots & U_{m,d} & 1 & \varepsilon_d & \cdots & \varepsilon_{d-q+1} \\ \vdots & & & \vdots & & \vdots & & & & \vdots \\ X_{N-1} & \cdots & X_{N-p+1} & U_{1,N} & \cdots & U_{m,N} & 1 & \varepsilon_{N-1} & \cdots & \varepsilon_{N-q+1} \end{pmatrix} \\
\boldsymbol{\beta} =& (\phi_1 \ \cdots \ \phi_p \ \ \omega_1 \ \ \cdots \ \omega_n \ \ 1 \ \ \theta_1 \ \cdots \ \theta_q)^\top
\end{aligned}
\tag{3.14}
$$

where $d = \max(p, q)$. Now, to find an appropriate model structure that describes our data, the following scheme is proposed:

1. **Identification**: exploring the available data and prior information of the system behaviour can be used to propose an initial model candidate, e.g. having knowledge of a preceding state-space model that describes the variable of interest. To illustrate this idea, we can use model in Equation (2.7) and its equivalent state-space formulation in Equation (3.10). Let's assume that we can take reliable measurements of the thermal mass T_{m} so it can be considered an input; in that case, it is possible to write a univariate time series model for the indoor temperature as

$$
\begin{aligned}
T_{\mathsf{i},t} =& a_{11} T_{\mathsf{i},t-1} + a_{12} \overbrace{\left(a_{21} T_{\mathsf{i},t-2} + a_{22} T_{\mathsf{m},t-2} + \cdots \right)}^{T_{\mathsf{m},t-1}} + \\
& b_{11} T_{a,t} + b_{12} \Phi_{h,t} + b_{13} I_{g,t} + \epsilon_{1,t} \, .
\end{aligned}
\tag{3.15}
$$

   Equation (3.15) has an ARX structure where $p = 2$; this model will have weather variables, heating load and lagged values of the thermal mass as inputs. Moreover, as detailed in Appendix II, any linear and time-invariant state-space formulation can be translated into ARMAX formulation.

2. **Estimation**: we propose three different methods to estimate the parameters of the linear model from Equation (3.13): least squares (LS), prediction error method (PEM), and maximum likelihood estimation (MLE). When the model noise is Gaussian and the system is in steady state, these three methods return the estimator, $\widehat{\boldsymbol{\beta}}$, defined as

$$
\widehat{\boldsymbol{\beta}} = \arg\min_{\beta} \left\{ S(\boldsymbol{\beta}) = (\boldsymbol{X} - \boldsymbol{Z}\boldsymbol{\beta})^\top (\boldsymbol{X} - \boldsymbol{Z}\boldsymbol{\beta}) = \sum_{t=p+1}^{N} \varepsilon_t^2(\boldsymbol{\beta}) \right\} . \tag{3.16}
$$

   As shown in Table 3.1, the choice of estimation method depends mainly on the model structure that is being used. In the absence of an MA(q) term, $\boldsymbol{\beta}$ is estimated using the LS method. However, including an MA(q) term introduces residuals that have not been computed yet in the matrix $\boldsymbol{Z}$. For this reason, the PEM represents a generalised version of the LS. MLE is the most general estimation method and it will be discussed in more detail in the following chapter. Appendix I gives a more detailed mathematical description of LS, PEM and MLE.

3. **Validation**: a model is considered adequate when $\boldsymbol{\varepsilon}_t(\widehat{\boldsymbol{\beta}})$ behaves like white noise, since it suggests that the model has captured all observed system dynamics. There are numerous tests to check whether a collection of observations behave like white

noise; the reader is invited to check Madsen [44] for a detailed description of such methods. In this thesis, we focus on two methods:

- Plotting the estimated residuals to visually inspect their behaviour. This includes studying the temporal evolution of the residual and their dependence on other related variables.
- Comparing the residuals' estimated autocorrelation function (ACF) to the expected ACF of a white noise process.

Auto-correlation function (ACF)

The ACF evaluates the correlation between present and past observations of a random variable. Assuming N available observations of a time-series $\boldsymbol{X} = \{x_1, \cdots, x_N\}$, the ACF is estimated by

$$\widehat{\rho}_X(k) = \frac{C(k)}{C(0)} \tag{3.17}$$

where

$$C(k) = \frac{1}{N} \sum_{t=1}^{N-|k|} (x_t - \overline{x})(x_{t+|k|} - \overline{x}) \,. \tag{3.18}$$

The variable k represents the k_{th} lag and $\overline{x} = \sum_{t=1}^{N} x_t / N$.

Notice that $-1 \leq \widehat{\rho}_x(k) \leq 1$ and $\widehat{\rho}_X(0) = 1$.

If X_t behaves like Gaussian distributed white noise, $C(k) \approx 0 \; \forall k > 0$.

As depicted in Figure 3.3, in case the results of the validation are not adequate, it is necessary to return to step 1 and repeat the procedure iteratively until the results are satisfactory.

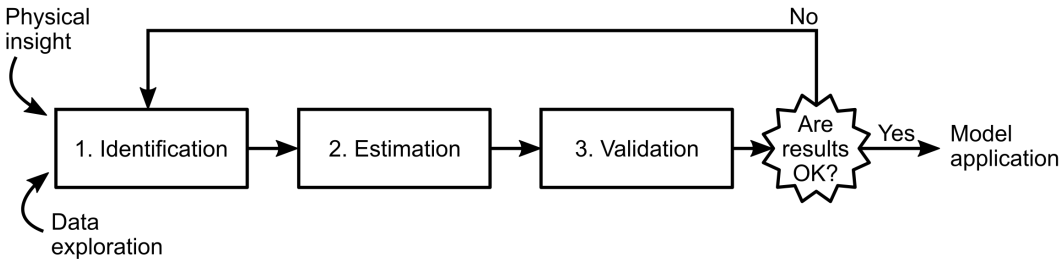

Figure 3.3: Schematic of the model-building procedure

Numerous authors have used ARMAX models to study the energy use in buildings. Ríos-Moreno et al. [46] tried different ARX and ARMAX structures to develop a model to predict the indoor temperature in a school from Mexico. Their work already suggests that ARX and ARMAX can be made simpler and more robust by incorporating physical knowledge. As proposed in this section, Wu and Sun [47] departed from the continuous heat transfer equations for a control volume, and reduced it to an ARX for predicting the indoor temperature and suggest this type of model could be used for control. Lastly, Deconinck and Roels [48] compared the reliability of different auto-regressive models and stochastic differential equation systems to characterise the dynamical elements of a building.

	Model contains			
	AR term ($p > 0$)	MA term ($q > 0$)	Inputs ($U_{j,t} \neq 0$)	Estimation method
ARMAX(p,q)	✓	✓	✓	PEM, MLE
ARMA(p,q)	✓	✓	×	PEM, MLE
ARX(p)	✓	×	✓	LS, MLE
AR(p)	✓	×	×	LS, MLE
MA(q)	×	✓	×	PEM, MLE

Table 3.1: Some of the model variations of the ARMAX model

Other authors opt for less physically-inspired models; similarly, instead of the proposed scheme from Figure 3.3, they use automatised identification routines Piltan, Tayebi-Haghighi, and Sulaiman [49]. Shakouri G, Kazemi, et al. [50] designed a fuzzy decision-making algorithm to identify an ARMAX model to forecast the energy demand in Iran. Jiang et al. [19] used climatic variables to develop a model for indoor comfort and indoor temperature prediction.

Still, as previously discussed, basing a model on physical principles will aid and enhance our interpretation of the results. Pakanen and Karjalainen [51] were able to estimate the static heat loss of a building after fitting an ARMAX model. Senave et al. [52] studied the accuracy of static characteristics obtained through an ARX model. Using minimal data, they concluded that the model gives reasonably good results, of the overall heat loss of a building.

Both **Paper A** and **Paper C** presented models that follow an ARX structure. The former was used to describe the dynamics of the indoor air in absence of other inputs. The results of this model were used as a departure point to develop the model in **Paper C**. The latter was a proof-of-concept aimed at developing a dynamic model that was able to reconstruct the trend of the indoor temperature of a building using only heating measurements and weather data.

Input-Output formulation

In many cases, it might be relevant to study the direct dynamic effect that a particular input has over the output. For instance, if we are modelling the indoor temperature of a building, we might want to analyse how a particular weather variable affects it. This is the principle behind the input-output formulation.

First, it is necessary to introduce the backshift operator B, defined as $B^n X_t = X_{t-n}$. Depending on the field, other operators might be used. In control applications, the operator $B = z^{-1}$ is used, hinting a connection between the input-output formulation and the Z-transform.

The backshift operator makes it possible to write the ARMAX model in Equation (3.12) as

$$\phi(B)X_t = \omega_1(B)U_{1,t} + \cdots + \omega_m(B)U_{m,t} + \theta(B)\varepsilon_t\,, \tag{3.19}$$

where $\phi(B)$, $\omega_j(B)$ and $\theta(B)$ are now polynomials in the backshift operator. Notice that, $\phi(B)$ is a polynomial of order p and $\theta(B)$ has order q. Given that, Equation (3.12) did not contain lagged inputs, $\omega_j(B)$ are zeroth-order polynomials; still, pursuing generality they are written as $\omega_j(B)$.

The input-output formulation is found by simply dividing both sides of Equation (3.19) by $\phi(B)$ such that

$$X_t = \underbrace{\frac{\omega_1(B)}{\phi(B)}}_{H_1(B)} U_{1,t} + \cdots + \underbrace{\frac{\omega_m(B)}{\phi(B)}}_{H_m(B)} U_{m,t} + \frac{\theta(B)}{\phi(B)}\varepsilon_t \,. \tag{3.20}$$

In Equation (3.20), every term $H_j(B)$ represents the *transfer function* of $U_{j,t}$, which describes the dynamic response of X_t given an impulse of $U_{j,t}$. To study this response, it is necessary to introduce the *zeros* and *poles* of the transfer function, defined as the roots of the numerator and denominator of $H_j(B)$, respectively.

Studying the poles and zeros unveils the system's stability: a system is considered stable if all its poles $q_k \ \forall k \in [1, \cdots, p]$ fall inside the unit circle. In addition, by computing the poles, it is possible to compute the *time constants* of a system.

Notice that, a transfer function has as many poles as the order of $\phi(B)$, p. Moreover, it can be shown that the number of poles is equal to the order of an equivalent state-space system. This was already hinted in the example in Equation (3.15), where it can be seen that $T_{\mathrm{i},t}$ depends on $T_{\mathrm{i},t-1}$ and $T_{\mathrm{i},t-2}$; i.e. the polynomial $\phi(B)$ has order 2.

In **Paper A** and ARX model was transformed to input-output to characterise the heat transfer between the indoor and outdoor air using two time constants. It was shown that they contained information about the flexibility potential of the buildings.

Time constants

The time constants are a dynamic parameter that characterises the time it takes for X_t to reach stationary conditions after a step increase of $U_{j,t}$. As represented in Figure 3.4, the larger a time constant is, the slower their associated process is.

For positive real poles, the time constants are computed by

$$\tau_k = \left| \frac{s}{\log\left(q_k\right)} \right| \quad \forall k \in [1, \cdots, p] \,, \tag{3.21}$$

where s is the sampling time.

The time constants are recurrent parameters in different fields that study dynamical systems, and they can be retrieved using other methods; Appendix III gives an overview of the interpretation of the time constants in state-space.

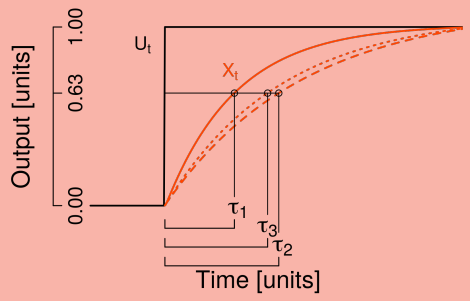

Figure 3.4: Step response for three different first-order dynamical system with three different time constants τ_1, τ_2 and τ_3.

3.3 Dynamic to static linear regression

This section connects the dynamical methods discussed previously in the chapter to one of the most widespread model structures: the linear regression. In general, given N observations of a random variable X and a series of m regressors, $U_j \ \ \forall j \in [1, \cdots, m]$, we can define a linear model such that

$$X_i = \beta_1 U_{1,i} + \cdots + \beta_m U_{m,i} + \varepsilon_i \,, \tag{3.22}$$

where $\varepsilon \sim N(0, \sigma_\varepsilon^2)$ is defined as white noise. In this case, the subscript i denotes the ith observation of the variable X; the subscript has been changed from t to i to emphasise that Equation (3.22) is not considered a time series.

Static linear models are easy to interpret since the effects of the regressors over the output are straightforward. In addition, they are computationally light, and the parameters can be estimated in closed form using the LS method. For these reasons, the linear regression has been abundantly used to model the energy usage in buildings. In addition, access to high-resolution data-gathering devices has been scarce, so models used to be static.

Static characteristics can be computed directly from dynamic models since a dynamic model includes the information of the system behaviour in a stationary state. Notice the similarities between Equation (3.22) and (3.20): the transfer functions from Equation (3.20) describe the response of X_t after a step increase of $U_{m,t}$; after enough time has passed, the effects of $U_{m,t}$ will converge to the stationary parameter multiplying $U_{m,i}$ in Equation (3.22). Thus, developing dynamic models provides a complete understanding of the energy usage inside a building. In addition, the ability to deduce static model characteristics through dynamic models reduces the period for data collection.

A fundamental model used to evaluate a building's energy performance is the energy signature (ES), which is based on linear regression. As described by Hammarsten [53], in its simplest form, the ES describes the linear dependence between the heating load of a building and the outdoor temperature. The ES is based on multiple assumptions based on the stationary heat transfer equations. **Paper C** proposed a dynamic version of the ES model, and showed that energy performance characteristics of the classic ES and the proposed dynamic model matched. Another example of a physics-driven regression model can be found in the work by Gianniou et al. [54], who developed a static linear regression model to characterise the set-point temperatures in a population of Danish residential buildings. Finally, Rasmussen et al. [55] proposed a nonlinear model to describe the heat load of a building; their model was based on the classic ES model and used wind speed and solar irradiation measures. In addition, Rasmussen et al. [55] identified that dynamical effects were still present despite using daily-aggregated data, and suggest that these effects are likely caused by the thermal inertia of the building. This result matched the findings in **Paper D**, which will be discussed in the following chapter.

Final words on grey-box

It is worth mentioning that it was remarked in the work by Hammarsten [53] that if the dynamic effects of a building could not be omitted, the expression for the energy signature follows

$$\Phi_t = \phi_{x,t} + \beta_0 (T_{\mathsf{out},t} - T_{\mathsf{i},t}) + C_i \frac{\mathrm{d}T_{\mathsf{i}}}{\mathrm{d}t} + \varepsilon_t \,, \tag{3.23}$$

where Φ_t represents the heating load of a building and the variable $\phi_{x,t}$ represents unmodelled heat gains and losses, e.g. solar gains, ventilation losses, occupant activity.

Equation (3.23) emphasises that, at any given time, the necessary heating load in a building needs to match the losses to the outdoor air and take into account other factors that are bundled in $\phi_{x,t}$.

The inclusion of the derivative term echoes Equation (2.2) from Section 2.2. It is straightforward to rearrange Equation (3.23) such that,

$$C_i \frac{\mathrm{d}T_{\mathrm{i}}}{\mathrm{d}t} = \phi_{x,t} + \beta_0(T_{\mathrm{out},t} - T_{\mathrm{i},t}) + \Phi_t + \varepsilon_t \tag{3.24}$$

and notice indeed that Hammarsten [53] already suggested a SDE to study the building energy dynamics. Moreover, the parameter $\phi_{x,t}$ becomes more transparent: according to the model in Equation (2.7), $\phi_{x,t}$ would contain the heat transferred to the thermal mass and the solar gains.

This example underlines the importance of acknowledging the assumptions behind well-known building models. Despite having numerous mathematical tools to study the energy use in buildings, the fundamental processes that describe the energy flow are the same. Understanding this will allow the modeller to adapt the above-mentioned model structures to numerous ”real-world” circumstances and develop new models that are compact, reliable and efficient.

4 Out of the grey box: methods for building model generalisation

The previous chapter was dedicated to describing models that can incorporate the thermophysical laws that govern energy use in buildings. This knowledge, coupled with crucial assumptions, maximises the amount of information that can be extracted from limited measurements from buildings. The presented methods were dedicated to individual buildings; however, to deploy impactful strategies to mitigate the effects of buildings energy over climate change, we must have tools that allow us to scale up our building models to study the entire building stock.

There are already large-scale studies dedicated to planning energy demand [56], estimating the needs for retrofit [57], or characterising the building stock [58]. These studies rely on gathering data from numerous buildings to draw unified conclusions, complicating the modelling task. A significant challenge of working with measurements from multiple occupied buildings is that the differences in living habits and user needs will cause a considerable amount of noise in the data. In addition, the concrete phenomena behind this noise might be virtually impossible to model explicitly.

This chapter proposes methods to account for phenomena that affect the heat flow in buildings, but we can not capture explicitly due to their randomness or complexity. The chapter is divided into two main sections. First, the concept of *mixed effects* is introduced, a modelling framework that can be used to refine the analysis of the uncertainty of building models; then, an array of different support methods are presented that can be adapted to bypass typical challenges met when modelling a building's energy flow. All methods discussed are flexible and can be included in the models discussed in Chapter 3. Thus, this chapter intends to work as an upgrade to a modeller's toolbox to study how the energy is used in occupied buildings.

4.1 Mixed effects models

This section presents the framework of mixed effects (ME) modelling. This modelling approach makes it possible to expand individual building models and study a population of buildings.

Section 4.1.1 gives a short conceptual description of ME models and their interpretation. Then, Section 4.1.2 provides a more detailed mathematical description.

4.1.1 A conceptual introduction

The models presented in Chapter 3 depart from the assumption that all measured variables belong to the same building. Thus, a set of parameters, β, is unique and characterises our proposed model. **Paper A** and **Paper C** are examples of such an approach since, in both cases, we treated the buildings as a single unit, and we were interested in deducing building-specific properties. In the rest of this chapter, we may refer to β as the *fixed effects* of the model.

In a model that only contains fixed effects, the only source of uncertainty is the model noise, ε, which quantifies the difference between the measured variable and the proposed model.

However, instead of focusing on one particular building, it might be interesting to study and formulate a model for a population of buildings. This requires collecting data from multiple buildings to fit a model for the entire population. It is reasonable to expect that there will be differences in their energy consumption profiles caused by random phenomena even though the buildings might be similar. Examples of such phenomena include arbitrary circumstances, like the heating habits of the occupants or other effects, which are not realistic to be included in large scale modelling due to e.g. complicated geometry and furniture in a building. Thus, taking measures from multiple buildings introduces a new layer of uncertainty to the model, given the variation observed in the entire population of buildings. Ultimately, we want to account for differences between buildings during the modelling process.

Since we assume the causes behind the intrinsic differences between buildings can not be measured, their impact is modelled as a random variable, $\boldsymbol{U}$, which represents the *random effects*.

We consider that the random effects are consistent throughout measurements from the same building, so the collected data is grouped by building. Given measurements from M buildings, we will use the parameter $\boldsymbol{\beta}$ to describe building characteristics that are common to all measurements; in addition, the jth individual building is characterised by a realisation of $\boldsymbol{U}$, denoted by $\boldsymbol{u}_j$. Hence, we say that the fixed effects describe mean value characteristics of the group of buildings, and the random effects quantify the difference between one building from the mean. Since the model contains both fixed effects and random effects, the model is called a *mixed effects* model.

In this work, we only group data by building since we want to account for differences at the building level. However, depending on the system being modelled and the available data, we could assign random effects to different rooms, cities, or climate zones.

Figure 4.1 represents a schematic of a ME model. Notice that, according to this model, each available observation, X_{ij}, is described by a function of the fixed effects $\boldsymbol{\beta}$, the random effects of one building $\boldsymbol{u}_j$, and the residual noise of that particular observation, ε_{ij}. Thus, this model structure assumes that there is an underlying random variable (other than the residuals) that affects the output of our model.

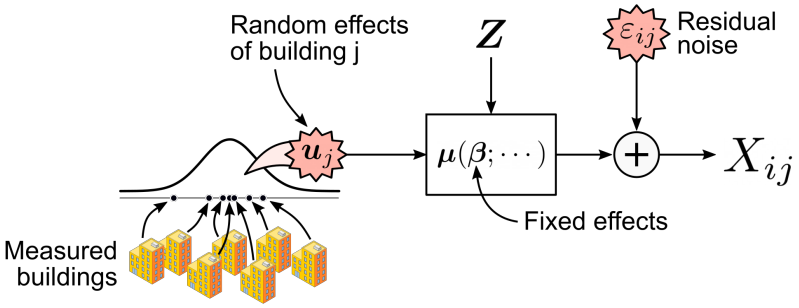

Figure 4.1: Schematic representation of a mixed effects model.

Since $\boldsymbol{U}$ is a random variable, the objective is to estimate its latent distribution. Having access to this distribution quantifies the uncertainty introduced in the model by random phenomena that are building-specific.

4.1.2 The formal introduction

This section provides a mathematical description of ME modelling. As done in Chapter 3, model noise is assumed to be Gaussian distributed. For a more general description, the

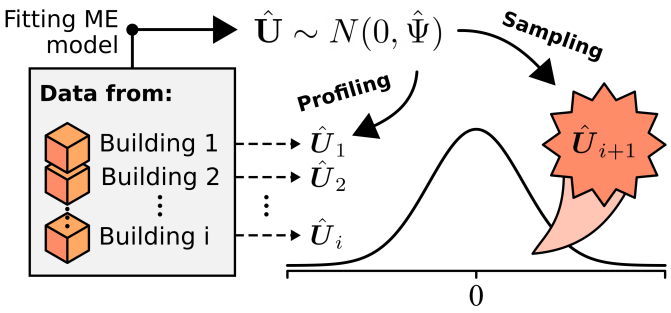

Figure 4.2: Schematic representation of sampling and profiling procedures resulting from mixed effects model estimation.

reader may refer to Thyregod and Madsen [59].

In its most general form, a Gaussian mixed effects model follows the structure

$$\begin{aligned} \boldsymbol{X}|\boldsymbol{U} = \boldsymbol{u} &\sim N(\boldsymbol{\mu}(\boldsymbol{\beta}, \boldsymbol{u}), \boldsymbol{\Sigma}(\boldsymbol{\lambda})) \\ \boldsymbol{U} &\sim N(\boldsymbol{0}, \boldsymbol{\Psi}(\boldsymbol{\psi})) \end{aligned} \tag{4.1}$$

where $\boldsymbol{\mu}(\beta, \boldsymbol{u})$ represents an arbitrary function. The parameter vectors $\boldsymbol{\lambda}$ and ψ are constant and characterise the covariance matrices $\boldsymbol{\Sigma}$ and $\boldsymbol{\Psi}$. As above-mentioned, given that $\boldsymbol{U}$ is distributed around 0, the random effects characterise the differences with respect to the mean $\boldsymbol{\mu}(\boldsymbol{\beta}, \boldsymbol{u} = \boldsymbol{0})$. Inspecting Equation (4.1), it can be noticed that ME models follow a hierarchical structure: the random effects characterise a lower level which describes the variability of observations between buildings; then, given $\boldsymbol{u}_j$, the upper level uncertainty is characterised by the residuals that describe the uncertainty between observations of the same building.

As mentioned in the previous chapter, given a set of N observations, $\boldsymbol{x}$, we assess the model using the likelihood function. However, in this case, the observations come from M different buildings; thus, we write $\boldsymbol{x} = \{x_{1,1}, x_{2,1}, \cdots, x_{N-1,M}, x_{N,M}\}$. To estimate the model in Equation (4.1), we introduce the *hierarchical likelihood* defined as

$$L(\boldsymbol{\theta}; \boldsymbol{u}, \boldsymbol{x}) = f_{X|u}\left(\boldsymbol{x}, \boldsymbol{u}; \boldsymbol{\beta}, \boldsymbol{\lambda}\right) f_U\left(\boldsymbol{u}; \boldsymbol{\psi}\right) . \tag{4.2}$$

Notice that the hierarchical likelihood depends on constant parameters, $\boldsymbol{\theta} = (\boldsymbol{\beta}, \boldsymbol{\lambda}, \boldsymbol{\psi})$, the measured vector, $\boldsymbol{x}$, and random effects, $\boldsymbol{u}$; however, the random effects are, a priori, unobserved since they are ”embedded” in the measurements vector. Hence, to estimate $\boldsymbol{\theta}$ we integrate out the random effects by introducing the *marginal likelihood* defined as

$$L_M(\boldsymbol{\theta}; \boldsymbol{x}) = \int_{\mathbf{R}^q} L(\boldsymbol{\theta}; \boldsymbol{u}, \boldsymbol{x}) \mathrm{d}\boldsymbol{u} \,, \tag{4.3}$$

where q is the dimension of $\boldsymbol{U}$. In order to reduce the computational complexity during the estimation, often the log-likelihood $l(\cdot) = \log(L(\cdot))$ is used instead.

The parameter vector $\boldsymbol{\theta}$ is estimated by maximising the likelihood function; i.e. using the MLE method. Recall that the estimated $\widehat{\boldsymbol{\theta}}$ includes the fixed effects, $\widehat{\boldsymbol{\beta}}$, and the parameters $\widehat{\boldsymbol{\lambda}}$ and $\widehat{\boldsymbol{\psi}}$ that characterise the distribution of $\boldsymbol{U}$ and $\boldsymbol{X}|\boldsymbol{U}$, respectively. The estimation of $\widehat{\boldsymbol{\theta}}$ has two major outcomes:

- Sampling: given $\widehat{\psi}$, we are able to *sample* values, $\boldsymbol{u}_k \, \forall k > M$, from $\boldsymbol{U} \sim N(\boldsymbol{0}, \boldsymbol{\Psi}(\widehat{\psi}))$. Then, using $\boldsymbol{\mu}(\widehat{\beta}, \boldsymbol{u}_k)$ it is possible to simulate buildings that behave similarly to the M buildings that we have measurements from.
- Profiling: given the data from the M observed buildings, it is possible to estimate what are the random effects of those buildings. Mathematically, this is written as

$$\widehat{\boldsymbol{u}} = E[\boldsymbol{U}|\boldsymbol{X} = \{x_{1,1}, x_{2,1}, \cdots, x_{N-1,M}, x_{N,M}\}] \,. \tag{4.4}$$

Sampling and profiling are schematically presented in Figure 4.2. The methods used for estimation, sampling and profiling depend on the complexity of the model structure $\boldsymbol{\mu}(\cdot)$.

Linear mixed effects

When the function $\boldsymbol{\mu}(\cdot)$ is a linear function, we may write the linear mixed effects model as

$$X_{ij} = \boldsymbol{Z}_i\boldsymbol{\beta} + \boldsymbol{R}\boldsymbol{U}_j + \varepsilon_{ij} \,. \tag{4.5}$$

where the sub-index i denotes the ith observation and the sub-index j denotes the observation comes from the jth building. The vector $\boldsymbol{Z}_i$ contains the ith observation of the external variables.

The model in Equation (4.5) can be written in compact form as

$$\boldsymbol{X} = \boldsymbol{Z}\boldsymbol{\beta} + \boldsymbol{R}\boldsymbol{U} + \boldsymbol{\varepsilon} \,, \tag{4.6}$$

where $\boldsymbol{Z}$ and $\boldsymbol{U}$ now are constant matrices. It is easily seen that Equation (4.6) is a straightforward extension of the classic linear model from Equation (3.13). As explained in Thyregod and Madsen [59], the linear structure simplifies the model estimation since it is possible to find a closed form solution to Equation (4.3) and obtain $\widehat{\boldsymbol{\beta}}$. Lastly, $\widehat{\boldsymbol{\beta}}$ can be used to estimate $\widehat{\boldsymbol{u}}$.

Non-linear mixed effects

Random effects can be used in more complex model formulations; in that case, it is often necessary to use mathematical tools to reduce the computational requirements during the estimation.

A popular method to reduce the computational requirements is to compute the Laplace approximation of the log-likelihood of $l_M(\cdot)$. The Laplace approximation uses the Taylor expansion of the log-likelihood with respect to the unobserved random effects $\boldsymbol{u}$. The Taylor expansion is truncated at second-order and centred around the optimum $\widehat{\boldsymbol{u}}$. Thus, the marginal likelihood in Equation (4.3) can be simplified as

$$l_{\text{M,LA}}(\boldsymbol{\theta}, \boldsymbol{u}, \boldsymbol{y}) = l(\boldsymbol{\theta}, \widetilde{\boldsymbol{u}}, \boldsymbol{x}) - \frac{1}{2} \log \left| \frac{\boldsymbol{H}(\widehat{\boldsymbol{u}})}{2\pi} \right| \,, \tag{4.7}$$

where $\boldsymbol{H}(\widehat{\boldsymbol{u}}) = -\partial^2 l / \partial \boldsymbol{u}^2|_{\boldsymbol{u}=\widehat{\boldsymbol{u}}}$. Notice that, as opposed to the linear case, since the Laplace approximation of the likelihood is defined around $\widehat{\boldsymbol{u}}$, the estimation of the fixed effects, the variance parameters and random effects occurs simultaneously; hence, it is necessary to use an efficient optimiser.

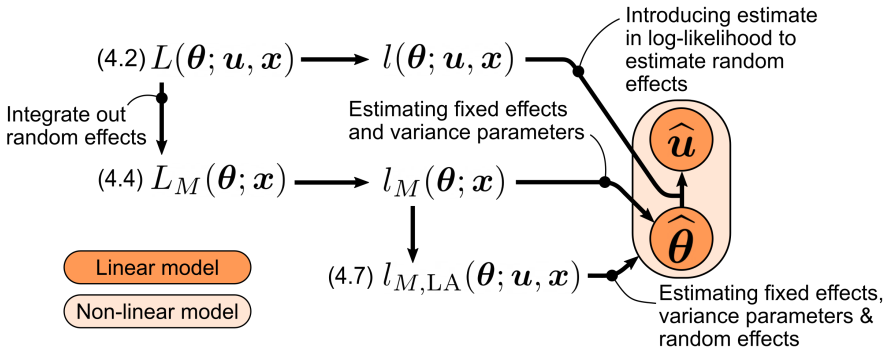

Figure 4.3: Map representing different variants of the likelihood function

Figure 4.3 shows a schematic map of the different estimation methods that can be used depending on the model structure. Additional details of the estimation process of mixed effects models can be found in Thyregod and Madsen [59].

A linear mixed effects model was used in **Paper B** to simulate daily heating load profiles of office buildings; the model was a direct expansion of a fixed-effects linear model developed by Lindberg, Bakker, and Sartori [60]. **Paper D** introduced a non-linear mixed effects model to characterise the daily heating load of a population of buildings. Moreover, given the estimated random effects, in **Paper D** it was possible to refine the characterisation of the initial population of buildings by estimating the random effects of the measured schools. This was used as an alternative to more classic characterisation approach that relies on qualitative data.

4.2 Support methods

This thesis has shown different model structures that can be used to develop data-driven models which do not require extensive measurements and building information. So far, the chapter has focused on mixed effects, which helps evaluating the impact of unobserved phenomena on a particular model. Similarly, this section introduces different modelling techniques to enhance the discussed models.

The tools presented here are not sorted in any specific order; they are independent and can be used regardless of the modelling choice. These tools have been selected so a modeller may incorporate them to improve a model's ability to cope with events that are challenging to capture.

Weighted least squares

Chapter 3 introduced the method of least squares (LS) to estimate the model parameters for the linear model in Equation (3.13). The LS method implicitly assumes that the model residuals are independently and identically distributed (iid); i.e, the residuals are distributed by $\varepsilon \sim N(\mathbf{0}, \boldsymbol{\Sigma} = \sigma^2 \boldsymbol{I})$. This is known as the ordinary least squares (OLS).

However, unmodelled phenomena might affect the correlation of residuals, so the assumption of independence is no longer reasonable. In that case, the residuals are going to be correlated, and the correlation can be described by the matrix $\boldsymbol{\Sigma}$. Then, given N observations of $\boldsymbol{X}$ and $\boldsymbol{Z}$, to estimate $\widehat{\boldsymbol{\beta}}$ we are interested in minimising

$$S(\boldsymbol{\beta}) = (\boldsymbol{x} - \boldsymbol{Z}\boldsymbol{\beta})^\top \boldsymbol{\Sigma}^{-1} (\boldsymbol{x} - \boldsymbol{Z}\boldsymbol{\beta})\,. \tag{4.8}$$

Notice the difference with Equation (3.16). Then, the parameter estimator is found by solving

$$\left(\boldsymbol{Z}^\top \boldsymbol{\Sigma}^{-1} \boldsymbol{Z}\right) \boldsymbol{\beta} = \boldsymbol{Z}^\top \boldsymbol{\Sigma}^{-1} \boldsymbol{X}\,, \tag{4.9}$$

where $\boldsymbol{\Sigma}$ weights the influence of the different N residuals and includes the correlation structure. For this reason this method is known as the weighted least squares method (WLS); other source call this method *generalised least squares*.

In **Paper A**, the WLS method was used to minimise the effects caused by measurement noise that the model could not capture. The paper compares the results obtained with OLS and WLS, and it is seen that the latter provides a better fit.

Non-parametric methods: B-spline curves

B-splines are a family of n piecewise polynomial curves that are continuously differentiable to a certain order. The n curves are defined over a given range and connected through multiple particular points called *knots*. Given these curves' smooth and continuous properties, they can be used for interpolation and function smoothing.

It is important to remark that these curves are generated directly given a range $\boldsymbol{x}$, n, the number of knots and their position. Thus, they do not follow an explicit polynomial formula. For this reason, the use of splines is often labelled as a non-parametric method; more details about splines and other non-parametric methods can be found in Hastie, Tibshirani, and Friedman [61].

The properties mentioned above make splines a good candidate for estimating variable dependencies that are too complex to formulate explicitly. An example of using splines to model is depicted in Figure 4.4; the left-most sub-figure shows arbitrary measurements of a variable, y compared to measurements of another variable x; it can be seen that the dependency between variables is clearly non-linear. Given the range x, we define a family of $n = 5$ spline curves, B_i (solid black lines). Then, by fitting a simple linear model, using the curves as input variables, it is possible to model the relationship between x and y.

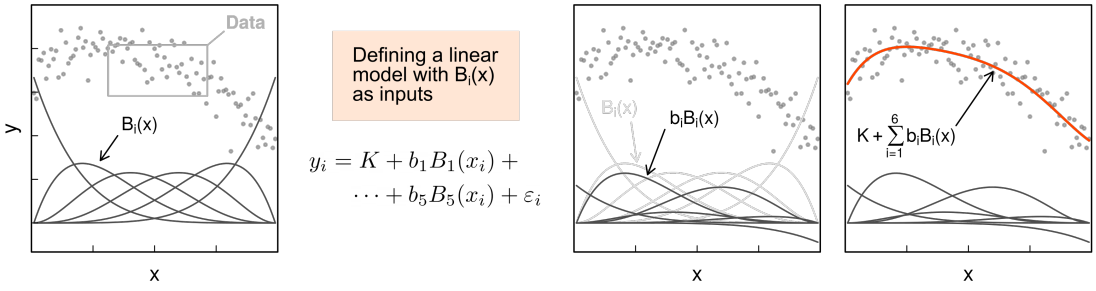

Figure 4.4: Figure representing the fitting of non-linear relationship using spline curves.

In a building context, B-spline curves have been suggested to incorporate the effects of solar irradiation in grey-box building models [62, 63] since solar gains change during the day given the incidence angle potential shading, among other causes. In **Paper D**, B-splines were used to model the effects of solar irradiation over the daily heating load.

Data selection and transformation

It is possible to maximise the information extracted from the available measurements through careful selection. Similarly, data can be transformed to ease the estimation pro-

cess. This section provides notable examples of literature that used selection and transformation to improve their results.

A straightforward approach is to perform a data-oriented selection of the measurements. Ghiaus [64] suggested selecting only data from the inner quantiles for using the energy signature (ES) to predict the heating load of buildings; their method ensured more robust results when applied to different data sets. Kamel, Sheikh, and Huang [65] confirmed that the importance of different input variables changes when modelling heating and cooling load and highlighted the importance of selecting the appropriate features to model a system.

On the other hand, we can use domain knowledge to select data correctly. Since buildings are known physical systems, it is possible to foresee potential biases in the data and try to remove them through data selection. A clear example is the work of Vesterberg, Andersson, and Olofsson [66], who paired data symmetrically around the winter solstice to remove the effects of the solar gains in their model. Paudel et al. [67] used a dynamic time warping (DTW) method to identify similar climatic days and improve their prediction of the consumption of low energy buildings. Eriksson, Akander, and Moshfegh [68] developed a variant of the ES method that included an estimate of the domestic hot water consumption; they selected only measurements from 00:00-5:00 to reduce the noise caused by the occupants.

Paper A used a hidden Markov model to select decaying indoor temperature data from night periods. Thus, the chosen data belonged to periods where typical variables that could affect the indoor conditions, such as solar irradiation and heating load, were negligible.

Buildings are dynamic systems that contain multiple processes that evolve at different frequencies; thus, choosing the correct temporal resolution may significantly impact the results. Working with coarse-resolution data is beneficial for smoothing out disturbances caused by events that only happen at higher frequencies: intra-day heating patterns and dynamic effects of the building elements are omitted when data is logged or aggregated coarsely enough [26]. Typically, if the resolution is daily or lower, one can consider the measurements to be static, even though buildings with high inertia can still present dynamic effects that are longer than a day, as discussed in Rasmussen et al. [55] and **Paper D**. Moreover, the potential importance of long-lasting dynamic effects had been already hinted in **Paper A**, where the long time constants that characterised the heat loss to the outdoor air were significantly larger than 24 hours.

5 Discussion of contribution

This section presents the main findings of this thesis. As explained in Figure 1.2, the results are split into three transversal tracks: simplified grey-box, reduced features and scalable models.

5.1 Simplified grey-box

Paper A illustrates the benefits of acknowledging the fundamental processes that govern the energy flow in buildings. The available data set contained only measurements of the indoor air temperature of a population of Danish single-family houses. In addition, the outdoor air temperature was measured. However, it was possible to retrieve valuable insight into the energy performance of the buildings by developing a physics-based ARX model.

Figure 5.1 shows one week of measured indoor temperature for one building. Notice that it shows a continuous decay pattern during the night, matching the behaviour of buildings with *night setback*s.

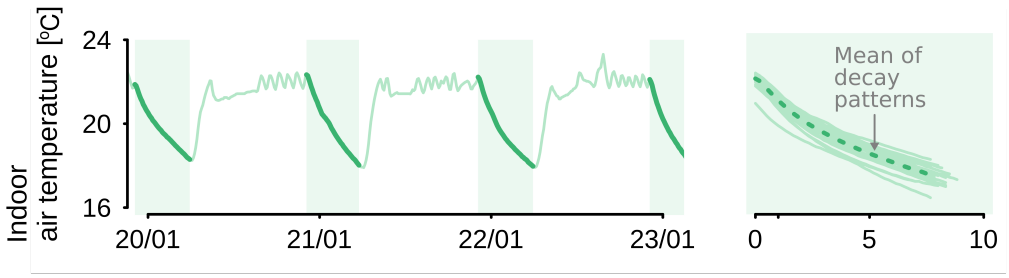

Figure 5.1: Decays for three example buildings

During the night, it is expected that the noise in the data caused by occupants is minimal. In addition, the solar gain is zero, and the outdoor air temperature is relatively stable. The trend in Figure 5.1 suggests that the heating load is turned off during night hours. In these conditions, the primary process governing the decay pattern in Figure 5.1 is the heat loss to the outdoor air.

Departing from the SDE building model introduced in Figure 2.1, it was possible to develop the following ARX model

$$T_{\mathrm{i},t} = \theta_1 T_{\mathrm{i},t-1} + \theta_2 T_{\mathrm{i},t-2} + \omega T_{\mathrm{out},t-1} + \varepsilon_t \tag{5.1}$$

that only relied on variables that we had measures from. The model was computationally light and easy to interpret, so it was possible to use the outcome of the model to characterise the potential of the different buildings as a thermal storage units.

To fulfil the above-mentioned assumptions, it was necessary to only select measurements from continuous decaying periods. As explained in **Paper A**, a series of temperature increments was computed using the time-series of indoor temperature measurements to appropriately select the data; the increments that belonged to a period of continuous temperature decay had a different distribution from the rest of the increments. This difference

was used to identify and select only the data points that fulfilled our needs. The method was inspired by the work of Wolf et al. [69], which detected the presence of occupants by monitoring CO2 concentration.

The data used did not include occupancy data; yet, it was assumed that occupant related activity was more likely to concentrate during the early hours of the night, causing more noise in the indoor air measurements. This was introduced to the model by the means of the weighted least squares (WLS) method so earlier measures had less weight in the estimation.

The results showed that the proposed ARX models captured the main dynamics that govern the heat loss of the building, which, since the model was physics-based, made it possible to evaluate the potential of the studied population of buildings to be used as heat-storing units. Furthermore, it is seen that the model fit obtained using WLS is better than using OLS.

The results of **Paper A** showed that, in the absence of other influential variables, the energy dynamics of a building were well approximated by a second-order ARX system. This outcome was a crucial assumption in **Paper C**, where, instead of using only indoor air measurements, the main variable was the heating load.

The building used in **Paper C** was not occupied as it is part of a research facility. Thus, the data set resulted from a series of experiments where the building heating system was excited to simulate occupants' activity. There were numerous sensor measurements available in different rooms of the building; however, the building was treated as a single unit for simplicity.

The ARX model used was

$$\Phi_t = \alpha_t + \beta_1 T_{\text{out},t} + \varphi_1 T_{\text{out},t-1} + \varphi_2 T_{\text{out},t-2} + \varepsilon_i \tag{5.2}$$

where Φ_t is the heating load of a building and T_{out} is the outdoor air temperature. As explained in **Paper C**, the variable α_t is a function of passive gains and losses of the building and the indoor air temperature value.

The main challenge of using Equation (5.2) was the inclusion of the variable α_t since it is a proxy dynamic variable that is not being observed. The ARX model was transformed into a state-space formulation to have an estimation of the variable; where α_t was defined as a random walk. This made it possible to use the Kalman filter to reconstruct the variable based on the given model structure using only weather data and consumption data.

Figure 7 in **Paper C** shows the reconstructed α_t, compared to the distribution of indoor temperatures from different sensors in the building. It can be noticed that the proxy variable resembles the distribution of temperatures, which suggests that, with the appropriate building model, it is possible to gather insights into the indoor conditions using only outdoor measurements.

The model in **Paper C** was conceived to be a dynamic version of the energy signature (ES). Thus, the results obtained with the model in Equation (5.2) were compared with the classic ES estimates. Figure 5.2 extends the comparison shown in Table 1 in **Paper C**, and visualises the estimated energy signature computed with the static and dynamic method; it is shown that the dynamic model provides a good representative of the studied building.

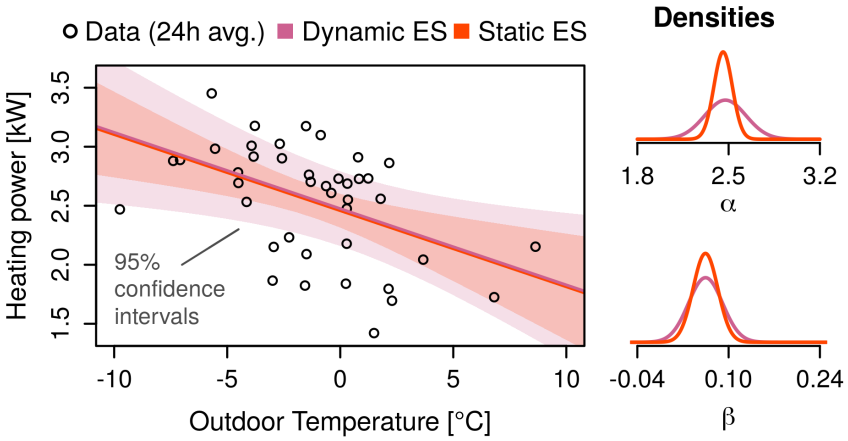

Figure 5.2: Comparison of dynamic and static ES results

Still, it can be noticed that the data points in Figure 5.2 show considerable noise around the estimated trends. Since the data comes from an experimental set-up from the test building, the typical drivers of the heating load are mixed with the experiment purposes. Moreover, notice that the uncertainty of the estimated parameters is larger for the dynamic case, which suggests that the dynamic model is a better representative of the thermal behaviour present in the data.

The current EU annual renovation rate is around 1%, and it should increase to about 2%-3% [70] to meet EU 2050 policy goals. However, identifying retrofitting opportunities is not easy since the building databases are often either incomplete or not up to date. The results shown in this section suggest that buildings can be studied at a large scale using limited data resources. The proposed methodologies represent low-cost methods to obtain insights into the energy performance of buildings in the operation phase. In addition, reducing the required variable to a minimum will help ensure that the users' privacy is respected.

5.2 Reduced features

In **Paper A**, a second-order ARX was proposed to model the heat loss of a population of single-family houses. The linear second-order model structure made it possible to describe the heat loss of each building using two time constants.

One of the time constants, the smallest, characterises the fast heat loss between the indoor air and its surroundings, represented by the thermal mass. The largest time constant describes the time it takes for the heat to be transferred to the ambient air.

It was shown that the two time constants describe the heat loss trend of the indoor air temperature. Thus, reducing buildings to these two parameters presents the opportunity to map populations of buildings, as shown in Figure 5.3. The map gives an easy-to-interpret overview of the thermal behaviour of a population of buildings and could be used by grid operators to select appropriate clusters to deploy a particular demand-response strategy.

This was validated by developing a simulation framework where different building types were simulated to follow different penalty signals and evaluate their flexibility. It was shown that the buildings with the largest time constants could supply more flexibility.

In **Paper D**, the Gompertz curve was proposed to model the heating load of a building.

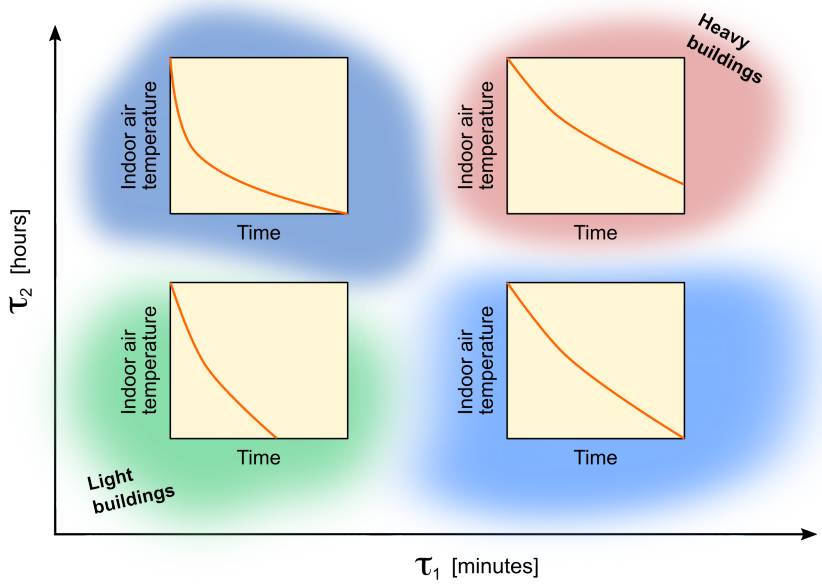

Figure 5.3: map of time constants.

The curve is a monotonic function described as

$$y(x) = A \exp(C \exp(x - Q)), \tag{5.3}$$

and it is characterised by three parameters $\{A, C, Q\}$. Using the non-linear curve to model the heating load allowed: i) transitioning smoothly from heating regime to non-heating regime, and ii) estimating the capacity of the heating system.

As described in Figure 2 in **Paper D**, each parameter in the Gompertz function characterises a very distinct aspect of the curve, and it was possible to link them to known weather variables that impact the heating load. Figure 7 in **Paper D** shows the fit of the model for an arbitrary apartment block and the value of the parameters $\{A, C, Q\}$. Figure 5 in **Paper D** confirms that the three parameters completely describe the weather dependence of a building, as the residuals do not show significant dependency. It is seen that there is still auto-correlation in the residuals, which is likely caused by the thermal intertia of the building. Given the purposes of the model in **Paper D**, this auto-correlation was small enough to be disregarded.

Working with a low order model made it possible to include random effects in each of the main parameters. Consequently, the estimated random effects were estimated for a population of 45 Norwegian buildings. The random effects were clustered and two sub-categories were identified in the initial training population. As shown in Figure 14 in **Paper D**, one of the sub-categories contained low energy buildings.

The dataset used in **Paper D** had been carefully cleaned and presented good quality data; it contained numerous hourly measurements and technical details of the measured buildings. Yet, the qualitative information about the buildings was incomplete and insufficient to categorise all buildings in the training set. On the other hand, reducing the weather response to a reduced number of characteristic parameters made it possible to study effi-

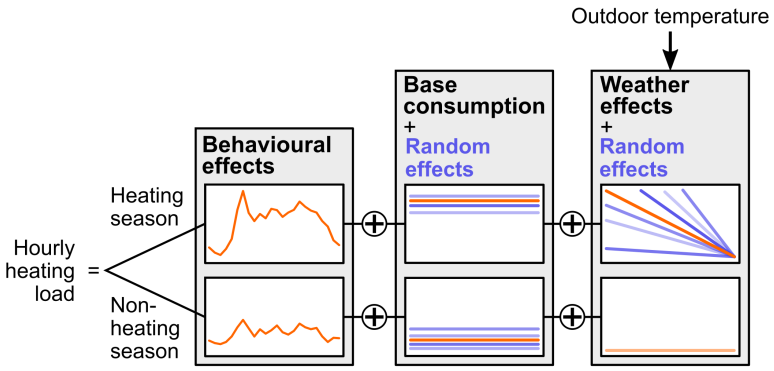

Figure 5.4: Schematic of the model in **Paper B**

ciently the weather response of every building in the training population and improve the initial categorisation.

5.3 Scalable models

All models discussed in this thesis have been developed aiming to overcome data limitations using domain knowledge and statistical methods. Models that use fewer variables will be easier to scale up because they do not require any complex installation of sensors. In particular **Paper C**, **Paper B** and **Paper D** used heating consumption, which is, by default, stored by utility companies and weather measurements, which are often accessible as there exist numerous weather services that provide weather-related data.

Even though **Paper A** requires indoor measurements, the estimation method only requires measurements from night time, allowing the user to use the building as preferred during the day. Buildings already use a night setback strategy to reduce energy use and increase economic savings, so taking measurements during these periods and estimate the heat loss behaviour is proposed as a less intrusive than other alternatives such as the QUB method [71].

The ME framework was presented to overcome the data limitations of buildings. Occupant preferences, complex geometries or poor craftmanship will impact the energy use in buildings, but it is not realistic to measure these effects at a large scale.

Paper B used ME models to directly expand the work from Lindberg, Bakker, and Sartori [60], who proposed a linear model to simulate hourly heat load profiles for building categories. The initial model was a linear fixed effects model, and it was necessary to create an extensive data set containing around 300 variables. The model was solved using STATA, and it was deterministic. The ME alternative in **Paper B** reduced the model structure considerably, requiring 52 variables.

The proposed model was divided into three main blocks, as depicted in Figure 5.4; one block contained the hourly schedule of the heating system, another block contained the seasonal base consumption, and the third block contained weather effects. Random effects were added to the seasonal base consumption and the effects of the weather; i.e., the model was built under the assumption that different buildings would have different baseline consumption and would react differently to changes in climatic conditions.

The hierarchical characterisation of the model uncertainty worked two-fold: i) it provided a stochastic simulation tool to generate realistic heat load profiles, and ii) allowed to draw a confidence region for the heating load all year round. This refinement of the uncertainty

of the model rendered the model as a more robust simulation tool to generate heating load profiles.

Figure 5.5 shows a stochastic simulation using the model from **Paper B** of the hourly heating load of an office building. The figure includes the confidence region and the actual consumption of one test building. Including the uncertainty around the simulation is key for planning possible consumption scenarios of the building stock. Notice that the trend of the test building is captured. In addition, on the days the consumption deviated from the simulated mean, it still falls inside the 90% confidence region.

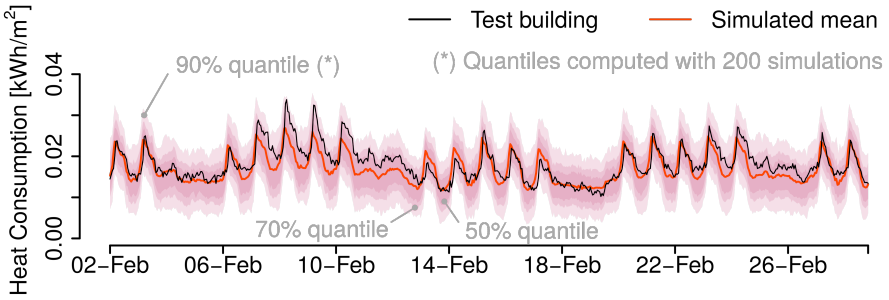

Figure 5.5: Simulation hourly heating load profile

One of the main objectives of **Paper D** was to allow the uncertainty to change throughout the year and adapt to the heating regime change since a symmetric uncertainty like depicted in Figure 5.5 is not realistic. Especially during warm periods, when the heating is low, symmetric uncertainty would contain the possibility of predicting a negative heating load.

Paper D used the logarithm of the heating load as the main output variable to work only with a positive heating load and keep computational complexity as low as possible. Given the exponential structure from Equation (5.3), the model used was

$$\tilde{y} = \log y(x) = \log A + C \exp(x - Q)\,. \tag{5.4}$$

In **Paper D**, y represented the heat consumption and x the outdoor temperature. Gaussian-distributed random effects were added to Equation (5.4) which, when transforming back, $\tilde{y} \to y$, guaranteed positive-skewed uncertainty that adapts to the heating regime change, as can be seen in Figure 10 from **Paper D**. Moreover, the non-linear model structure ensures that the uncertainty region narrows during the warmest periods, adapting to the heating regime change.

The parameter Q describes the horizontal offset of the curve; hence, it is a proxy of passive heat gains and losses. For this reason, in **Paper D**, it was assumed that Q was a function of the solar irradiation. The structure of this function was not known since this would require a detailed description of relevant factors like the building orientation or potential shading. For this reason, **Paper D** uses spline curves to model the dependence between Q and solar irradiation. Figure 10 in **Paper D** shows the fitted non-linear effect of the solar irradiation; the inclusion of splines improved the quality of the fit and provided valuable insight into the solar gains without burdening the computation.

Given the non-linear structure described in **Paper D**, it was necessary to use the Laplace approximation to estimate the model. The fitted model was tested with a set of out-of-

sample buildings, and it was shown that the model was robust and the estimated model captured most of the test data.

6 Conclusion and final words

Measured data in buildings is a crucial resource for investigating how energy is used in operative, fully-functioning buildings. Monitoring devices and computational power have become cheaper and more accessible, so the usage of data-driven methods to study buildings has increased in recent years. Still, buildings are complex systems, and numerous processes impact energy use, which poses the question of which variables need to be measured and how.

Data collection is not homogeneous since many different stakeholders participate in the energy management of buildings. Therefore, measuring a particular variable will require the involvement of specific parties, which might cause challenges in collecting the necessary information. Often, data collection campaigns can only gather partial details, making it challenging to have a consolidated database of real buildings.

Furthermore, data-driven models based on classic building models often use abundant data to try to capture the numerous processes that intervene in the heat transfer in buildings. Given the complexity of the heat flow in buildings, this classic approach leads to building models that require measuring many processes.

The issues mentioned above represent a challenge for the application of data-intensive models. Data scarcity is a recurrent problem which influences the potential developments of new technologies. Thus, it is necessary to find methods to overcome these limitations.

A traditional alternative to data scarcity is to use building simulation tools to generate artificial data. On the other hand, many authors have identified differences between the predicted consumption during the design phase and the actual consumption during operation. This *performance gap* suggests that using simulated data to develop data-driven building models may not provide reliable results.

Buildings physics is a developed field, and there exists a solid understanding of the fundamental processes that govern the energy use in buildings. This domain knowledge can be combined with statistical methods to overcome data limitations. This concept is often referred to as *grey-box* modelling. In practice, the term is used to describe lumped resistance-capacity models based on stochastic differential equations (SDE). However, this thesis suggests that the description of grey-box modelling may fit other model structures; e.g. linear auto-regressive models are often treated as black-box, but they can be derived from the typical classic SDE structure and hold physical interpretation.

Paper A proposed a model to describe the indoor air temperature decay of a population of Danish houses. Since the underlying physical equations that describe the heat flow are known, it was possible to describe the temperature decay with a second-order ARX model that needed only indoor air and outdoor air temperature measurements. Moreover, prior physical knowledge was necessary to select the appropriate data and fulfilled our modelling goals.

The results of **Paper A** were used in **Paper C** to develop a dynamic model to estimate the indoor conditions of a building. The proposed method was used to reconstruct a proxy variable that contained information of the indoor conditions of the building. Given the prior knowledge on building energy dynamics, it was possible to link the proxy variable to the indoor temperature of the buildings, even though indoor air temperature measurements were not used during its reconstruction.

Preserving the physical interpretation of the models was crucial to reduce complex systems into simpler structures that could be characterised using a reduced number of features. **Paper A** reduced the dynamics of residential buildings to two parameters that characterised the potential of the buildings to participate in demand-response strategies. **Paper D** proposed a non-linear structure to model the heating load of a building as a function of climatic conditions. Even though the model was not directly derived from thermodynamic equations, given the prior knowledge of the main drivers of the heating load, it was possible to reduce the weather response of a building to three parameters that were easy to interpret.

Expanding the study of energy use to larger populations of buildings adds a layer of uncertainty since energy will be used differently in different buildings. Thus, it is necessary to quantify the diversity of the building stock to develop adequate strategies that optimise the building energy use.

In particular, we proposed a mixed effects (ME) modelling framework, which proved to be a flexible method to efficiently capture random differences in the building stock.

In **Paper B**, a model was proposed to describe heating profiles for a given building typology. It was shown that, since ME captured the uncertainty caused by building differences, the model is a more robust stochastic simulation tool than its deterministic counterpart. **Paper D** presented a non-linear model structure that adapted to the heating regime changes throughout the year.

In addition, the ME modelling framework was used to extend the knowledge of a measured population of buildings. Traditionally, buildings are categorised based on archetypes and qualitative information. For example, literature uses the building typology, the year of construction, and other static characteristics to divide the building stock into clusters of buildings with similar energy use. However, this qualitative approach relies on data that is easily missing or outdated. Moreover, using only qualitative characteristics overlooks intrinsic differences between buildings, such as the occupants' preferences and built quality. Yet, trying to assess the amount of detail necessary to describe the building stock completely is not feasible at a large scale due to technical factors and privacy concerns.

In **Paper D**, the ME framework was used to evaluate the differences between individual buildings and the mean of the population. These differences were clustered and two subgroups were identified in the initial training population. This outcome suggested that the initial categorisation was not accurate due to incomplete data from the building side.

Building energy modelling combines multiple study areas, which requires a partnership between many different parties. Still, the end goals are shared among the participants, namely, reducing energy waste, minimising the negative impact on climate and bringing societal value.

In an effort to find the right solutions, we may aim as far as possible, assuming that, since our scientific goals are so big, the answer shall be distant. However, progress can still happen by focusing inwards. This thesis re-framed different modelling approaches that benefit from well-known fundamentals to strengthen our insight into how we use energy in buildings. The results were obtained without abundant resources and keeping the model complexity low. The presented outcome may help future research determine what is needed to develop the building stock that ensures sustainable growth and living conditions.

Appendix

I LS, PEM and MLE

This section gives more complete description of the least squares method (LS), the prediction error method (PEM) the maximum likelihood method (MLE).

First let's introduce a series of N observations

$$(y_1, \boldsymbol{x}_1)(y_2, \boldsymbol{x}_2) \cdots (y_N, \boldsymbol{x}_N)\,,$$

where y_i is the output variable and $\boldsymbol{x}_i$ a vector of input variables; with $i \in [1, ..., N]$.

To model this series of observations, we want to find a function $\mu(\cdot)$ such that

$$y_i = \mu(\boldsymbol{\theta}; \boldsymbol{x}_i) + \varepsilon_i\,, \tag{I.1}$$

where $\boldsymbol{\theta}$ is the parameter vector that characterises $\mu(\cdot)$ and $\varepsilon_i \sim N(\mathbf{0}, \sigma_\varepsilon^2)$. To reduce notation, we introduce

$$\boldsymbol{y} = \{y_1, y_2, \cdots, y_N\} \tag{I.2}$$
$$\boldsymbol{x} = \{\boldsymbol{x}_1, \boldsymbol{x}_2, \cdots, \boldsymbol{x}_N\} \tag{I.3}$$

I.i Least squares (continued)

The LS method uses the sum of squared errors (SSE) as a measure of how close the model, $\mu(\cdot)$, is to the observed series. Thus, the parameters that better fit the model are found solving the following optimisation problem

$$\widehat{\boldsymbol{\theta}} = \arg\min_{\theta} S(\boldsymbol{\theta})\,, \tag{I.4}$$

where

$$S(\boldsymbol{\theta}) = \sum_{i=1}^{N} \varepsilon_i^2(\boldsymbol{\theta})\,. \tag{I.5}$$

The estimates of $\boldsymbol{\theta}$ satisfy that

$$\nabla_{\boldsymbol{\theta}} S(\boldsymbol{\theta} = \widehat{\boldsymbol{\theta}}) = 0\,. \tag{I.6}$$

In case $\mu(\cdot)$ is linear, as seen in Equation (3.16), the function $S(\boldsymbol{\theta})$ can be written as

$$S(\boldsymbol{\theta}) = (\boldsymbol{y} - \boldsymbol{x}\boldsymbol{\theta})^\top \boldsymbol{\Sigma}^{-1} (\boldsymbol{y} - \boldsymbol{x}\boldsymbol{\theta})\,. \tag{I.7}$$

In addition, the linear structure allows to write Equation (I.6) as

$$\nabla_{\boldsymbol{\theta}} S(\boldsymbol{\theta}) = -2\boldsymbol{x}^{\top}\boldsymbol{\Sigma}^{-1}(\boldsymbol{Y} - \boldsymbol{x}\boldsymbol{\theta}) = 0\,. \tag{I.8}$$

Hence, solving Equation (I.8) allows writing the parameter estimator in closed for as

$$\widehat{\boldsymbol{\theta}} = (\boldsymbol{x}^{\top}\boldsymbol{x})^{-1}\boldsymbol{x}^{\top}\boldsymbol{y}\,. \tag{I.9}$$

I.ii Prediction error method

Notice that, in case the proposed model structure contains a MA term, the vector $\boldsymbol{x}$ will contain values of past residuals, ε_t. In such case, Equation (I.9) can not be used to compute the estimator due to, by definition, the value of the residuals are not known prior model estimation.

The prediction error method is a generalisation of the LS estimation method were the residuals are recursively estimated one-step ahead. In practice, there are two approaches to use the prediction error method:

- *Conditioned estimation*. In this case, it is assumed that all residuals

$$\varepsilon_p = \varepsilon_{p-1} = \cdots = \varepsilon_{p+1-q} = 0\,.$$

  Then, at every time-step, ε_t can be computed.

- *Unconditioned estimation*. This estimation method defines a stationary model to predict past residuals by back-forecasting.

More details on the estimation methods can be found in Madsen [44].

I.iii Maximum likelihood estimation

The MLE method aims at maximising the joint probability of observing $\boldsymbol{y}$ given the parameters $\boldsymbol{\theta}$ and inputs $\boldsymbol{x}$. In general, the likelihood function can be written as

$$L(\boldsymbol{y}; \boldsymbol{\theta}, \sigma_{\varepsilon}^2) = \prod_{i=1}^{N} f(\mu(\boldsymbol{x}_i, \boldsymbol{\theta}), \sigma_{\varepsilon}^2)\,, \tag{I.10}$$

where $f(\cdot)$ represents the distribution that characterise the residuals.

Thus, the MLE method requires an assumption about the distribution. Typically, it is assumed that ε is normally distributed so $f(\cdot)$ can be written explicitly as

$$f(\mu(\boldsymbol{x}_i, \boldsymbol{\theta}), \sigma_{\varepsilon}^2) = \frac{1}{\sigma_{\varepsilon}\sqrt{2\pi}}\,\mathsf{exp}(-\varepsilon_i^2(\boldsymbol{\theta})/2\sigma_{\varepsilon}^2)\,. \tag{I.11}$$

Inserting Equation (I.11) in Equation (I.10) yields

$$L(\boldsymbol{y}; \boldsymbol{\theta}, \sigma_{\varepsilon}^2) = (\sigma_{\varepsilon}^2 2\pi)^{-\frac{N}{2}}\,\mathsf{exp}\left(-\frac{1}{2\sigma_{\varepsilon}^2}\sum_{i=1}^{N}\varepsilon_i^2(\boldsymbol{\theta})\right)\,, \tag{I.12}$$

and taking the logarithm yields

$$\log L(\boldsymbol{y};\boldsymbol{\theta},\sigma_\varepsilon^2) = \frac{N}{2}\log(\sigma_\varepsilon^2) - \frac{1}{2\sigma_\varepsilon^2}\sum_{i=1}^{N}\varepsilon_i^2(\boldsymbol{\theta}) + c\,, \tag{I.13}$$

where c is a constant. Then, in order to find the value of σ_ε^2 that maximises the log-likelihood, we solve which gives the

$$\frac{\partial \log L}{\partial \sigma_\varepsilon^2} = 0 \rightarrow \widehat{\sigma}_\varepsilon^2 = \frac{\sum_{i=1}^{N}\varepsilon_t^2(\boldsymbol{\theta})}{N} \tag{I.14}$$

Finally, inserting $\widehat{\sigma}_\varepsilon^2$ in Equation (I.13) it is seen that the parameters $\boldsymbol{\theta}$ that maximise the likelihood are obtained by minimising $S(\boldsymbol{\theta})$ from Equation (I.5). Thus, for linear systems with normally distributed noise the LS method is analogous to using the MLE.

II ARMAX to state space transformation

Chapter 3 proposed using state space models as a foundation to develop physics-based ARMAX model. This section introduces a basic structure to showcase how to transform an ARMAX(p,q) to state-space.

Consider the model defined as

$$Y_t + \phi_1 Y_{t-1} + \cdots + \phi_p Y_{t-p} = \beta_1 U_{1,t} + \cdots + \beta_m U_{m,t} + \varepsilon_t + \theta_1\varepsilon_{t-1} + \cdots + \theta_q\varepsilon_{t-q}\,. \tag{II.1}$$

First, let's define the state vector as

$$\boldsymbol{X}_t = \begin{pmatrix} X_{1,t} & X_{2,t} & X_{3,t} & \cdots & X_{d,t} \end{pmatrix}^\top, \tag{II.2}$$

and the vector of inputs

$$\boldsymbol{U}_t = \begin{pmatrix} U_{1,t} & U_{2,t} & \cdots & \cdots & U_{m,t} \end{pmatrix}^\top. \tag{II.3}$$

Notice that, since the inputs are considered deterministic, past measurements of external inputs can be re-arranged such that $U_{i,t-1} \rightarrow U_{j,t}$ for an arbitrary i.

Then, it is possible to define the following matrices

$$\begin{gathered} \boldsymbol{A} = \begin{pmatrix} -\phi_1 & 1 & 0 & \cdots & 0 \\ -\phi_2 & 0 & 1 & \cdots & 0 \\ \vdots & \vdots & \vdots & \ddots & \vdots \\ -\phi_{d-1} & 0 & 0 & \cdots & 1 \\ -\phi_d & 0 & 0 & \cdots & 0 \end{pmatrix}, \quad \boldsymbol{G} = \begin{pmatrix} 1 \\ \theta_1 \\ \vdots \\ \theta_{d-1} \end{pmatrix}, \\ \boldsymbol{B} = \begin{pmatrix} \beta_1 & 0 & \cdots & 0 \\ 0 & \beta_2 & \cdots & 0 \\ \vdots & \vdots & \ddots & \vdots \\ 0 & 0 & \cdots & \beta_m \end{pmatrix}, \quad \boldsymbol{C} = \begin{pmatrix} 1 & 0 & \cdots & 0 \end{pmatrix}, \end{gathered} \tag{II.4}$$

to write the following state space

$$\begin{aligned} \boldsymbol{X}_t &= \boldsymbol{A}\boldsymbol{X}_{t-1} + \boldsymbol{B}U_t + \boldsymbol{G}\varepsilon_t \\ Y_t &= \boldsymbol{C}\boldsymbol{X}_t \end{aligned} \tag{II.5}$$

where $d = \max(p, q+1)$ and additional parameters are set to zero.

For the sake of simplicity, the observation noise has been omitted. In case this assumption is not valid, there might be issues with the uniqueness of the estimated model as the observation noise and system noise might not be distinguishable.

III Time constants and eigenvalues

The time constants of a system can be computed using the eigenvalues of the design matrix describing the system in state-space form. To present this approach and to link it to the method described in Chapter 3, we use an arbitrary example. For the sake of clarity, the example is based on a simple deterministic model; however the interpretation is equally valid for the stochastic system with additive noise.

Given a linear system system defined by

$$\frac{\mathrm{d}\boldsymbol{x}}{\mathrm{d}t} = \boldsymbol{A}\boldsymbol{x} \tag{III.1}$$

with $\boldsymbol{x}$ being a state vector of dimension p, the general solution of the system in Equation (III.1) is given by

$$\boldsymbol{x}(t) = \exp(\boldsymbol{A}(t - t_0))\boldsymbol{x_0}\,, \tag{III.2}$$

where $\boldsymbol{x_0}$ represents the initial conditions of the state and t_0 the initial time; from now on, it is assumed that $t_0 = 0$. As discussed in Chapter 3, Equation (III.2) underlines that the dynamic behaviour of $\boldsymbol{x}(t)$ is defined by the design matrix $\boldsymbol{A}$.

The matrix $\boldsymbol{A}$ can be diagonalised such that

$$\boldsymbol{x}(t) = \exp(\boldsymbol{P}\boldsymbol{\Lambda}\boldsymbol{P}^{-1}t)\boldsymbol{x_0}\,, \tag{III.3}$$

where $\boldsymbol{P}$ contains the *eigenvectors* of the system as columns and $\boldsymbol{\Lambda}$ is a diagonal matrix with the *eigenvalues* in the diagonal.

Equation (III.3) can be further decomposed such that the solution of the ODE in Equation (III.1) is written as a linear combination of the eigenvectors $\boldsymbol{v}_k\ \forall k \in [1, \cdots, p]$ as

$$\boldsymbol{x}(t) = c_1 e^{\lambda_1 t}\boldsymbol{v}_1 + c_2 e^{\lambda_2 t}\boldsymbol{v}_2 + \cdots + c_p e^{\lambda_p t}\boldsymbol{v}_p\,, \tag{III.4}$$

where λ_k represent the *eigenvalues* and c_k are constants that depend on the initial conditions $\boldsymbol{x}_0$.

Finally, the time constants of the system in Equation (III.1) can be computed by

$$\tau_k = -\frac{1}{\lambda_k}\,. \tag{III.5}$$

Equation (III.4) indicates that the temporal evolution of the state can be split into different exponential processes. Then, the magnitude of each time constant quantifies the relative importance of each different process as time advances; e.g. a small time constant ,τ_k, is given by a large eigenvalue, λ_k, which suggests that the influence of the process defined by $\boldsymbol{v}_k$ diminishes fast.

Notice that the exponential terms in Equation (III.4) and the definition on Equation (III.5) echo the definition of the time constants given a transfer function in Equation (3.21).

For a detailed example of the use of eigenvalues and eigenvectors to study the evolution of indoor temperatures inside of a building, the reader may check Madsen and Holst [30].

Bibliography

[1] D Mariano-Hernández, L Hernández-Callejo, A Zorita-Lamadrid, O Duque-Pérez, and F Santos García. “A review of strategies for building energy management system: Model predictive control, demand side management, optimization, and fault detect & diagnosis”. In: *Journal of Building Engineering* 33 (2021), p. 101692.

[2] European Commission and Directorate-General for Communication. *European green deal: delivering on our targets*. Publications Office, 2021.

[3] *The European Green Deal: On Track or In Trouble?* https://www.globe-eu.org/the-european-green-deal-on-track-or-in-trouble/. Accessed: 24-02-2022.

[4] Pantelis Capros, Maria Kannavou, Stavroula Evangelopoulou, Apostolos Petropoulos, Pelopidas Siskos, Nikolaos Tasios, Georgios Zazias, and Alessia DeVita. “Outlook of the EU energy system up to 2050: The case of scenarios prepared for European Commission’s “clean energy for all Europeans” package using the PRIMES model”. In: *Energy strategy reviews* 22 (2018), pp. 255–263.

[5] Shan Zhou and Marilyn A Brown. “Smart meter deployment in Europe: A comparative case study on the impacts of national policy schemes”. In: *Journal of Cleaner Production* 144 (2017), pp. 22–32.

[6] Chao Wang, Martina Ferrando, Francesco Causone, Xing Jin, Xin Zhou, and Xing Shi. “Data acquisition for urban building energy modeling: A review”. In: *Building and Environment* (2022), p. 109056.

[7] Xing Shi, Binghui Si, Jiangshan Zhao, Zhichao Tian, Chao Wang, Xing Jin, and Xin Zhou. “Magnitude, causes, and solutions of the performance gap of buildings: A review”. In: *Sustainability* 11.3 (2019), p. 937.

[8] Han Li, Zhe Wang, Tianzhen Hong, and Mary Ann Piette. “Energy flexibility of residential buildings: A systematic review of characterization and quantification methods and applications”. In: *Advances in Applied Energy* 3 (2021), p. 100054.

[9] Chirag Deb and Arno Schlueter. “Review of data-driven energy modelling techniques for building retrofit”. In: *Renewable and Sustainable Energy Reviews* 144 (2021), p. 110990.

[10] Ying Sun, Fariborz Haghighat, and Benjamin CM Fung. “A review of the-state-of-the-art in data-driven approaches for building energy prediction”. In: *Energy and Buildings* 221 (2020), p. 110022.

[11] Pieter De Wilde. “The gap between predicted and measured energy performance of buildings: A framework for investigation”. In: *Automation in construction* 41 (2014), pp. 40–49.

[12] David Hsu. “How much information disclosure of building energy performance is necessary?” In: *Energy Policy* 64 (2014), pp. 263–272.

[13] Cheng Fan, Fu Xiao, Chengchu Yan, Chengliang Liu, Zhengdao Li, and Jiayuan Wang. “A novel methodology to explain and evaluate data-driven building energy performance models based on interpretable machine learning”. In: *Applied Energy* 235 (2019), pp. 1551–1560. ISSN: 0306-2619.

[14] Nicola Moretti, Xiang Xie, Jorge Merino, Justas Brazauskas, and Ajith Kumar Parlikad. “An openbim approach to iot integration with incomplete as-built data”. In: *Applied Sciences* 10.22 (2020), p. 8287.

[15] Mahabir Bhandari, Som Shrestha, and Joshua New. “Evaluation of weather datasets for building energy simulation”. In: *Energy and Buildings* 49 (2012), pp. 109–118.

[16] Kadir Amasyali and Nora M El-Gohary. “A review of data-driven building energy consumption prediction studies”. In: *Renewable and Sustainable Energy Reviews* 81 (2018), pp. 1192–1205.
[17] Giovanni Barone, Annamaria Buonomano, Cesare Forzano, and Adolfo Palombo. “Building energy performance analysis: an experimental validation of an in-house dynamic simulation tool through a real test room”. In: *Energies* 12.21 (2019), p. 4107.
[18] Zakia Afroz, Tania Urmee, GM Shafiullah, and Gary Higgins. “Real-time prediction model for indoor temperature in a commercial building”. In: *Applied energy* 231 (2018), pp. 29–53.
[19] Zhanhong Jiang, Jonathan Francis, Anit Kumar Sahu, Sirajum Munir, Charles Shelton, Anthony Rowe, and Mario Bergés. “Data-driven thermal model inference with armax, in smart environments, based on normalized mutual information”. In: *2018 Annual American Control Conference (ACC)*. IEEE. 2018, pp. 4634–4639.
[20] Susen Döbelt, Markus Jung, Marc Busch, and Manfred Tscheligi. “Consumers’ privacy concerns and implications for a privacy preserving Smart Grid architecture—Results of an Austrian study”. In: *Energy Research & Social Science* 9 (2015), pp. 137–145.
[21] Christoph F Reinhart and Carlos Cerezo Davila. “Urban building energy modeling–A review of a nascent field”. In: *Building and Environment* 97 (2016), pp. 196–202.
[22] TRANSSOLAR Energietechnik GmbH. *TRNSYS 16. Multizone Building modeling with Type56 and TRNBuild.* English. 2007.
[23] Jan LM Hensen and Roberto Lamberts. *Building performance simulation for design and operation*. Routledge, 2012.
[24] Simon Rouchier. “Solving inverse problems in building physics: An overview of guidelines for a careful and optimal use of data”. In: *Energy and Buildings* 166 (2018), pp. 178–195.
[25] Miguel J Jimenez and Henrik Madsen. “Models for describing the thermal characteristics of building components”. In: *Building and Environment* 43.2 (2008), pp. 152–162.
[26] Henrik Madsen, Peder Bacher, Geert Bauwens, An-Heleen Deconinck, Glenn REynders, Staf Roels, Eline Himpe, and Guillaume Lethé. *Annex 58. Reliable building energy performance characterisation based on full scale dynamic measurements. Report of Subtask 3, part 2. Thermal Performance Characterisation Using Time Series Data – Statistical Guidelines*. International energy agency, 2016.
[27] Clarence Agbi, Zhen Song, and Bruce Krogh. “Parameter identifiability for multizone building models”. In: *2012 IEEE 51st IEEE conference on decision and control (CDC)*. IEEE. 2012, pp. 6951–6956.
[28] Bernt Oksendal. *Stochastic differential equations: an introduction with applications*. Springer Science & Business Media, 2013.
[29] Yanfei Li, Zheng O’Neill, Liang Zhang, Jianli Chen, Piljae Im, and Jason DeGraw. “Grey-box modeling and application for building energy simulations-A critical review”. In: *Renewable and Sustainable Energy Reviews* 146 (2021), p. 111174.
[30] Henrik Madsen and Jan Holst. “Estimation of continuous-time models for the heat dynamics of a building”. In: *Energy and buildings* 22.1 (1995), pp. 67–79.
[31] Peder Bacher and Henrik Madsen. “Identifying suitable models for the heat dynamics of buildings”. English. In: *Energy and Buildings* 43.7 (2011), pp. 1511–1522. ISSN: 0378-7788.
[32] Glenn Reynders, Jan Diriken, and Dirk Saelens. “Quality of grey-box models and identified parameters as function of the accuracy of input and observation signals”. In: *Energy and Buildings* 82 (2014), pp. 263–274.

[33] Eline Himpe and Arnold Janssens. “Characterisation of the thermal performance of a test house based on dynamic measurements”. In: *Energy Procedia* 78 (2015), pp. 3294–3299.
[34] Simon Rouchier, Mickaël Rabouille, and Pierre Oberlé. “Calibration of simplified building energy models for parameter estimation and forecasting: Stochastic versus deterministic modelling”. In: *Building and Environment* 134 (2018), pp. 181–190.
[35] Christian Ankerstjerne Thilker, Henrik Madsen, and John Bagterp Jørgensen. “Advanced forecasting and disturbance modelling for model predictive control of smart energy systems”. In: *Applied Energy* 292 (2021), p. 116889.
[36] Julien Leprince, Henrik Madsen, Clayton Miller, Jaume Palmer Real, Kaustav Basu, Wim Zeiler, et al. “Fifty shades of grey: Automated stochastic model identification of building heat dynamics”. In: *Energy and Buildings* (2022), p. 112095.
[37] Rune Juhl, Jan Kloppenborg Møller, and Henrik Madsen. “ctsmr-Continuous time stochastic modeling in R”. In: *arXiv preprint arXiv:1606.00242* (2016).
[38] Christian Ankerstjerne Thilker, Peder Bacher, Hjörleifur G Bergsteinsson, Rune Grønborg Junker, Davide Cali, and Henrik Madsen. “Non-linear grey-box modelling for heat dynamics of buildings”. In: *Energy and Buildings* 252 (2021), p. 111457.
[39] MJ Jiménez, Henrik Madsen, JJ Bloem, and Bernd Dammann. “Estimation of non-linear continuous time models for the heat exchange dynamics of building integrated photovoltaic modules”. In: *Energy and Buildings* 40.2 (2008), pp. 157–167.
[40] Nynne Friling, María José Jiménez, Hans Bloem, and Henrik Madsen. “Modelling the heat dynamics of building integrated and ventilated photovoltaic modules”. In: *Energy and Buildings* 41.10 (2009), pp. 1051–1057.
[41] Rune Grønborg Junker, Carsten Skovmose Kallesøe, Jaume Palmer Real, Bianca Howard, Rui Amaral Lopes, and Henrik Madsen. “Stochastic nonlinear modelling and application of price-based energy flexibility”. In: *Applied Energy* 275 (2020), p. 115096.
[42] John Bagterp Jørgensen. *Constrained predictive control. A computational approach*. Springer, 2015.
[43] Mohinder Grewal and Angus Andrews. “Applications of Kalman Filtering in Aerospace 1960 to the Present.” In: *Control Systems, IEEE* 30 (July 2010), pp. 69–78.
[44] Henrik Madsen. *Time series analysis*. English. Chapman & Hall, 2007.
[45] Spyros Makridakis and Michele Hibon. “ARMA models and the Box–Jenkins methodology”. In: *Journal of forecasting* 16.3 (1997), pp. 147–163.
[46] GJ Ríos-Moreno, M Trejo-Perea, R Castañeda-Miranda, VM Hernández-Guzmán, and G Herrera-Ruiz. “Modelling temperature in intelligent buildings by means of autoregressive models”. In: *Automation in construction* 16.5 (2007), pp. 713–722.
[47] Siyu Wu and Jian-Qiao Sun. “A physics-based linear parametric model of room temperature in office buildings”. In: *Building and Environment* 50 (2012), pp. 1–9.
[48] An-Heleen Deconinck and Staf Roels. “Comparison of characterisation methods determining the thermal resistance of building components from onsite measurements”. In: *Energy and Buildings* 130 (2016), pp. 309–320.
[49] Farzin Piltan, Shahnaz TayebiHaghighi, and Nasri B Sulaiman. “Comparative study between ARX and ARMAX system identification”. In: *International Journal of Intelligent Systems and Applications (IJISA)* 9.2 (2017), pp. 25–34.
[50] Hamed Shakouri G, Aliyeh Kazemi, et al. “Selection of the best ARMAX model for forecasting energy demand: case study of the residential and commercial sectors in Iran”. In: *Energy Efficiency* 9.2 (2016), pp. 339–352.
[51] Jouko Pakanen and Sami Karjalainen. “Estimating static heat flows in buildings for energy allocation systems”. In: *Energy and Buildings* 38.9 (2006), pp. 1044–1052.

[52] Marieline Senave, Glenn Reynders, Peder Bacher, Staf Roels, Stijn Verbeke, and Dirk Saelens. “Towards the characterization of the heat loss coefficient via on-board monitoring: Physical interpretation of ARX model coefficients”. In: *Energy and Buildings* 195 (2019), pp. 180–194.
[53] Stig Hammarsten. “A critical appraisal of energy-signature models”. In: *Applied Energy* 26.2 (1987), pp. 97–110.
[54] Panagiota Gianniou, Christoph Reinhart, David Hsu, Alfred Heller, and Carsten Rode. “Estimation of temperature setpoints and heat transfer coefficients among residential buildings in Denmark based on smart meter data”. In: *Building and Environment* 139 (2018), pp. 125–133.
[55] Christoffer Rasmussen, Peder Bacher, Davide Calì, Henrik Aalborg Nielsen, and Henrik Madsen. “Method for scalable and automatised thermal building performance documentation and screening”. In: *Energies* 13.15 (2020), p. 3866.
[56] Abdo Abdullah Ahmed Gassar and Seung Hyun Cha. “Energy prediction techniques for large-scale buildings towards a sustainable built environment: A review”. In: *Energy and Buildings* 224 (2020), p. 110238.
[57] Zhou Wu, Bo Wang, and Xiaohua Xia. “Large-scale building energy efficiency retrofit: Concept, model and control”. In: *Energy* 109 (2016), pp. 456–465.
[58] Jon Fernandez, Luis del Portillo, and Iván Flores. “A novel residential heating consumption characterisation approach at city level from available public data: Description and case study”. In: *Energy and Buildings* 221 (2020), p. 110082.
[59] Poul Thyregod and Henrik Madsen. *An Introduction to Generalized Linear Models.* English. 1st ed. Informatics and Mathematical Modelling, Technical University of Denmark, DTU, 2006.
[60] Karen Byskov Lindberg, Steffen J Bakker, and Igor Sartori. “Modelling electric and heat load profiles of non-residential buildings for use in long-term aggregate load forecasts”. In: *Utilities Policy* 58 (2019), pp. 63–88.
[61] Trevor Hastie, Robert Tibshirani, and Jerome Friedman. *The Elements of Statistical Learning*. Springer Series in Statistics. New York, NY, USA: Springer New York Inc., 2001.
[62] Christoffer Rasmussen, Linde Frölke, Peder Bacher, Henrik Madsen, and Carsten Rode. “Semi-parametric modelling of sun position dependent solar gain using B-splines in grey-box models”. In: *Solar Energy* 195 (2020), pp. 249–258. ISSN: 0038-092X.
[63] X Zhang, C Rasmussen, D Saelens, and S Roels. “Time-dependent solar aperture estimation of a building: Comparing grey-box and white-box approaches”. In: *Renewable and Sustainable Energy Reviews* 161 (2022), p. 112337.
[64] Cristian Ghiaus. “Experimental estimation of building energy performance by robust regression”. In: *Energy and buildings* 38.6 (2006), pp. 582–587.
[65] Ehsan Kamel, Shaya Sheikh, and Xueqing Huang. “Data-driven predictive models for residential building energy use based on the segregation of heating and cooling days”. In: *Energy* 206 (2020), p. 118045.
[66] Jimmy Vesterberg, Staffan Andersson, and Thomas Olofsson. “A single-variate building energy signature approach for periods with substantial solar gain”. In: *Energy and Buildings* 122 (2016), pp. 185–191.
[67] Subodh Paudel, Mohamed Elmitri, Stéphane Couturier, Phuong H Nguyen, René Kamphuis, Bruno Lacarrière, and Olivier Le Corre. “A relevant data selection method for energy consumption prediction of low energy building based on support vector machine”. In: *Energy and Buildings* 138 (2017), pp. 240–256.

[68] Martin Eriksson, Jan Akander, and Bahram Moshfegh. “Development and validation of energy signature method–Case study on a multi-family building in Sweden before and after deep renovation”. In: *Energy and Buildings* 210 (2020), p. 109756.
[69] Sebastian Wolf, Jan Kloppenborg Møller, Magnus Alexander Bitsch, John Krogstie, and Henrik Madsen. “A Markov-Switching model for building occupant activity estimation”. In: *Energy and Buildings* 183 (2019), pp. 672–683.
[70] Igor Sartori, Nina Holck Sandberg, and Helge Brattebø. “Dynamic building stock modelling: General algorithm and exemplification for Norway”. In: *Energy and Buildings* 132 (2016). Towards an energy efficient European housing stock: monitoring, mapping and modelling retrofitting processes, pp. 13–25. ISSN: 0378-7788.
[71] Florent Alzetto, Guillaume Pandraud, Richard Fitton, Ingo Heusler, and Herbert Sinnesbichler. “QUB: A fast dynamic method for in-situ measurement of the whole building heat loss”. In: *Energy and Buildings* 174 (2018), pp. 124–133.

Part II

Publications

Characterisation of thermal energy dynamics of residential buildings with scarce data

Jaume Palmer Real[a,*], Christoffer Rasmussen[a], Rongling Li[b], Kenneth Leerbeck[a], Ole Michael Jensen[c], Kim B. Wittchen[c], Henrik Madsen[a]

[a] *Department of Applied Mathematics and Computer Science*
Technical University of Denmark

[b] *Department of Civil Engineering*
Technical University of Denmark

[c] *Danish Building Research Institute (SBi)*
Aalborg University

Abstract

Buildings account for a large portion of the total energy consumption and they might serve as a significant thermal storage capacity that can be advantageous for the future energy grid. To utilise this capacity, it is necessary to characterise the thermal dynamics in buildings using methods that are general enough to be applicable to a significant share of the building stock. This work proposes a data-driven method to characterise thermal dynamics of thermostatically controlled buildings with *night setback*. The method includes 1) using Hidden Markov Models to systematically select data periods when the indoor temperature decays steadily during night; 2) model reduction of a Stochastic Differential Equations model of heat transfer to a discrete linear model which is fitted by utilising the selected night-time data; and 3) computing one short time constant and one long time constant, which allows to categorise buildings according to their thermal response. This method is applied to 39 different Danish residential buildings and the results reveal that this simplified model captures the main processes governing the heat transfer: the one-step predictions for the indoor air temperature return 95% of the residuals $\in [-0.05°\text{C}, 0.05°\text{C}]$. For all buildings, the short time constants are lower than an hour, and the long time constants range from 20 hours to 100 hours. Finally, this method is used in simulated data to validate that the time constants provide insight about the energy flexibility potential of a building. The results show that dynamic thermal response of buildings can be discovered using limited data.

Keywords: Thermal building characterisation, data analysis, modelling, energy flexibility, demand response

Nomenclature

Variables

T_i	Indoor air temperature	[K]
T_m	Thermal mass temperature	[K]
T_a	Outdoor air temperature	[K]
Φ_h	Space heating	[kW]
I_g	Solar irradiation	[kW/m^2]
$v_t^{(i)}$	white noise term $\forall i, j \in [1, 2]$	-

Parameters

R_i	Thermal resistance: indoor air ↔ thermal mass	[K/kW]
R_a	Thermal resistance: indoor air ↔ outdoor air	[K/kW]
C_i	Thermal capacity of the indoor air	[kWh/K]
C_m	Thermal capacity of the thermal mass	[kWh/K]
A_w	Effective window area	[m^2]
σ_1	Incremental variance of T_i	$[K]$
σ_2	Incremental variance of T_m	$[K]$
θ_i	Auto-regressive parameter of order i $\forall i \in [1, 2]$	-
Γ_{ij}	Parameter of the discrete inputs matrix $\forall i, j \in [1, 2]$	-
ϕ_{ij}	Parameter of the discrete design matrix $\forall i, j \in [1, 2]$	-

Acronyms

SDE	Stochastic Differential Equation
DR	Demand Response
FI	Flexibility Index
FF	Flexibility Function
AR	Auto-Regressive
ARX	Auto-Regressive with eXogenous inputs
HMM	Hidden Markov Model
OLS	Ordinary Least Squares
WLS	Weighted Least Squares
TES	Thermal Energy Storage

1. Introduction

In order to successfully transition from fossil fuel to renewable energy based supply at a large scale, it is necessary to understand buildings' thermal dynamics as they will be a key asset in the future flexible energy systems [1].

*Corresponding Author
Email address: jpre@dtu.dk
Postal Address: Anker Engelunds vej 1, Building 101A, 2800 Kongens Lyngby, Denmark

A main contributor to this green transition, will be the deployment of *Demand-Response* (DR) strategies [2], i.e., altering the demand-side of the buildings energy load to match the requirements of the grid. These requirements range from, balancing frequency, maximising the renewable energy share, or reducing energy peaks [3].

Space heating takes a major part of the energy load in buildings, specially in colder regions. Then, in order to use DR strategies, buildings need to be prepared to store and release heat when needed, without affecting severely the comfort of their users. Residential buildings in particular, can be used as *thermal storage units* (TES), and heavy buildings are specially suited for that task without risking indoor comfort [4]. In addition, the DR potential of residential buildings can be increased through adequate retrofitting [5]. Thus, there is a need for tools that can assess how buildings are able to store and release heat. Moreover, these tools need to be general, considering the existing variety of residential buildings in place [6].

1.1. Literature review

There are several approaches for estimating the main indicators of the building energy performance: the *heat loss coefficient* (or its inverse, the thermal *resistance*) and the thermal capacity [7]. The approach will depend on the chosen model for the energy flow in the building. In their review, Foucquier et al., separated the main modelling methods for buildings in three categories: physics-based methods (*white box*), purely statistical methods (*black-box*) and hybrid methods (*grey-box*) [8].

In the first category, it is possible to find numerical tools, such as the finite volume methods (FVM)[9]. This approach is computationally expensive, and relies either on simulated data or complex experimental assemble. Often, these methods require going into detail to component level to gain insight about the building's thermal characteristics, such as the outer wall structure and its composition [10, 11]. A different approach, was presented as the *co-heating* method [12]. This method is based on simplified heating dynamic equations describing the heat transfer inside a building. The co-heating method showed accurate results assessing the energy performance of buildings; however, it needs a meticulous experimental set up to control and measure the temperature, and the experiment can take multiple days. In addition, the measurements are bound to the external conditions during the experimental period. Finally, due to the necessary infrastructure for the assessment, it can only be performed in empty houses. Alternatively, Alzetto et al. introduced a new method that could evaluate the building thermal response in a two days experiment [13]. This represents an improvement from the traditional co-heating method. Nevertheless, it still requires an extensive experimental set up. In addition, there often exists a performance gap between the model prediction using thermal parameters estimated with the above methods and the real operational energy performance of the building [14, 15].

Black-box methods have been commonly applied for predicting energy consumption of buildings. For example, D'Amico et al. used *Multi Criteria Decision-Making* to compare three different methods when forecasting energy demand [16], and Finck et al. trained *Artificial Neural Networks* models in their simulation and demonstration work [17, 18]. Nevertheless, these methods are not used for characterisation purposes, as their outputs are difficult to interpret physically. Thus, they have been omitted from this review.

For existing buildings, the grey-box model approach is often used, as it takes into account building physics in data-driven modelling. Bacher and Madsen studied multiple variations of the lumped resistance-capacity (RC) model are presented [19]. In their work, it is shown that such models make it possible to estimate the heat resistance and capacity for different components of the house. This method allows the use of in-situ measures of operative houses. However, this approach still needs a considerable amount of data to decouple the different processes that are part of the energy flow. Also, the complexity of these models can easily grow, burdening the computation. For this reason, and specially when working with large data sets, it is important to use strategies to reduce the order of the models, as Goyal and Barooah suggested [20]. Even with high quality data, it could be difficult to gain insights into the building dynamics. For instance, during the periods where the building is thermostatically controlled, the impact of external variables over the indoor air temperature might be masked by the effects of the controller, which makes it impossible to estimate the thermal capacities.

The thermal characteristics of buildings, can also be computed statically, by using daily averages of the consumption and outdoor temperature. Nielsen et al. and Rasmussen et al. studied the impact of weather conditions in a set of danish residential buildings [21, 22]. These approach relies on having consumption data. In addition, by using daily values, they omit the dynamic nature of using buildings thermal mass as TES.

1.2. Work description

In this study, we suggest a simple and efficient method to scan residential buildings and retrieve their thermal characteristics using only indoor and outdoor temperature measurements. Specifically, we compute the *time constants* of the two main dynamic processes that govern the heat loss in buildings.

Most of the characterisation work presented in the literature review rely on complex model configurations that try to fit in many building components taking part in the heat transfer of buildings. Such studies are based on data sets with a large number of variables, e.g. temperatures of all components, which are not commonly measured in existing buildings. In this work, in an effort to pursue generality, we take the opposite direction to build simple models that can capture energy dynamics of buildings using scarce data that is easy to measure. Moreover, this method does not require a particular experimental set-up as it is developed based on the data that is available in many existing dwellings in Denmark.

We focus the study to data periods that are following a *night setback* schedule; i.e., periods with no heat input, where the indoor temperature decays steadily. This schedule is a commonly used strategy to decrease the energy consumption dur-

ing night with a lower temperature setpoint than during daytime. During night, it can be assumed that there is no significant influence on the indoor temperature from the users as they most likely are asleep. There is also no solar irradiation affecting the indoor temperature. Thus, the pattern of decreasing temperature can be understood as a fingerprint that explains the energy storage performance of the building.

There are multiple methods to identify decaying behaviours. One example is the use of statistical change point detection of the signal of interest [23]. In the present work, a Hidden Markov Model (HMM) of the indoor temperatures to identify the decaying periods. The same method was used by Wolf et al. to detect various human activities using CO_2 concentration data [24]. The relevant data is selected and it is used to fit an auto-regressive model. This model is derived from a Stochastic Differential Equation system describing the thermal dynamics in buildings.

Our method is general and can be applied to a significant portion of the current building stocks. Moreover, the method presented in this work is easily scalable and can be used to identify groups of buildings with similar energy response. Grouping buildings into clusters where the energy response is known, can be specially relevant since it could reduce the uncertainty of DR policies [25].

This study is divided into three sections, followed by a conclusion. In Section 2, the mathematical background of the applied method is explained; the model structure and its physical interpretation are discussed, and the method for data selection and the concepts used in the flexibility analysis are described. Section 3 describes the data used in the study. Section 4 shows the modelling results, an interpretation of the system dynamics and the estimated values of time constant for a number of buildings. In Section 5, a simulation framework is used to show how the building intrinsic parameters affect the time constants, and how the time constants provide information about the flexibility potential of the building.

2. Method

In this section, it is shown how an auto-regressive model is derived from a stochastic RC model. The purpose of this approach is to offer a physical interpretation of the parameters. Then, it is explained how the time constants are computed using the *transfer function* form of the auto-regressive model.

Our proposed method only works for specific periods of time; here, the method to select the relevant data periods is presented.

Finally, the concepts of *flexibility index* (FI) and *flexibility function* (FF) that we use in section 5 are presented.

2.1. Building as a second order dynamical system

Equation (1) describes a general continuous time model for heat dynamics inside of a building. It tracks the temporal evolution of two main variables inside the building: the indoor air temperature, T_i, and the thermal mass temperature, T_m. The model is represented as a second order linear stochastic differential equation (*SDE*) system. This system has three main external inputs: the outdoor temperature, T_a, the global solar irradiation, I_g, and the space heating input, Φ_h. This model has five parameters $\{R_i, R_a, C_i, C_m, A_w\}$ that are described in the nomenclature section. The uncertainty in the system is captured by the stochastic term, $d\omega_i \ \forall i \in [1, 2]$. This term represents a Wiener process with incremental variances $\sigma_i^2 \ \forall i \in [1, 2]$.

The external inputs affect only the indoor air temperature; in turn, there is a heat transfer between the indoor air and the thermal mass. Madsen described this model in detail [26].

$$\begin{cases} dT_i = \dfrac{1}{C_i}\left(\dfrac{1}{R_i}(T_i - T_m) - \dfrac{1}{R_a}(T_i - T_a) + \Phi_h + I_g A_w\right)dt + \sigma_1 d\omega_1 \\ dT_m = \dfrac{1}{R_i C_m}(T_m - T_i)\,dt + \sigma_2 d\omega_2 \end{cases} \tag{1}$$

Since the system in Equation (1) is linear, it can be re-written using the following matrix form,

$$\begin{pmatrix} \frac{dT_i}{dt} \\ \frac{dT_m}{dt} \end{pmatrix} = \begin{pmatrix} \frac{1}{R_i C_i} & -\left(\frac{1}{R_a C_i} + \frac{1}{R_i C_i}\right) \\ \frac{-1}{R_i C_m} & \frac{1}{R_i C_m} \end{pmatrix} \begin{pmatrix} T_i \\ T_m \end{pmatrix} + \begin{pmatrix} \frac{1}{R_a C_i} & \frac{1}{C_i} & \frac{A_w}{C_m} \\ 0 & 0 & 0 \end{pmatrix} \begin{pmatrix} T_a \\ \Phi_h \\ I_g \end{pmatrix} + \begin{pmatrix} \sigma_1 & 0 \\ 0 & \sigma_2 \end{pmatrix} \begin{pmatrix} \frac{d\omega_1}{dt} \\ \frac{d\omega_2}{dt} \end{pmatrix}. \tag{2}$$

Now, the model variable is a vector: $\boldsymbol{T}(t) = (T_i(t),\ T_m(t))^\top$, and $\boldsymbol{U}(t) = (T_a(t),\ \Phi_h(t),\ I_g(t))^\top$ is the vector of external inputs. We can write Equation (2) in a compact form as

$$\frac{d}{dt}\boldsymbol{T}(t) = \boldsymbol{A}\boldsymbol{T}(t) + \boldsymbol{B}\boldsymbol{U}(t) + \boldsymbol{\Sigma}\frac{d}{dt}\boldsymbol{\omega}(t)\,, \tag{3}$$

where $\boldsymbol{A}$ is the design matrix describing the dynamic characteristics of the building, and $\boldsymbol{B}$ describes how the input variables enter the system. Finally, $\boldsymbol{\omega}(t) = (\omega_1(t),\ \omega_2(t))^\top$ is the stochastic term, and $\boldsymbol{\Sigma}$ is the matrix of incremental variances.

In this work, only the indoor air temperature, T_i is observed. It is important to notice that the system described in Equation (1) has no measurement equation. Thus, we assume that the error measurements for T_i are small enough to be disregarded.

2.2. From SDEs to auto-regressive

The system in Equation (3) can be discretized by integrating over a sample interval, $[t, t + s)$, where s is the *sampling time* of the system. Then, assuming that the input $(U(t))$ is constant in the sampling interval, the system can be re-written as

$$\boldsymbol{T}(t + s) = \boldsymbol{\Phi}(s)\boldsymbol{T}(t) + \boldsymbol{\Gamma}(s)\boldsymbol{U}(t) + \boldsymbol{\nu}(t, s)\,. \tag{4}$$

If the sampling time is small enough, the discrete time model structure will capture the relevant dynamics described in the continuous case. We can fix the sampling time to an arbitrary time unit, $s = 1$, and find he explicit expression for the elements describing Equation (4):

$$\boldsymbol{\Phi}(s=1) = \exp(\boldsymbol{A}\cdot 1) = \begin{pmatrix} \phi_{11} & \phi_{12} \\ \phi_{21} & \phi_{22} \end{pmatrix} \tag{5}$$

$$\boldsymbol{\Gamma}(s=1) = \int_0^{s=1} \exp(\boldsymbol{A}\cdot r)\boldsymbol{B}dr = \begin{pmatrix} \Gamma_{11} & \Gamma_{12} & \Gamma_{13} \\ \Gamma_{21} & \Gamma_{22} & \Gamma_{23} \end{pmatrix} \tag{6}$$

$$\boldsymbol{\nu}(t, s=1) = \begin{pmatrix} \nu_t^{(1)} \\ \nu_t^{(2)} \end{pmatrix} \text{ with } \nu_t^{(i)} = \mathcal{N}(0,\, \varsigma_i^2)\ \ \forall i \in [1,2]\,. \tag{7}$$

In this case, $\boldsymbol{\Phi}$ describes the discrete dynamics of the system and $\boldsymbol{\Gamma}$ the effect from the external inputs. The vector $\boldsymbol{\nu}$ is normally distributed white noise with zero mean and variance $\varsigma_i^2\ \forall i \in [1,2]$, and it accounts for the stochastic part of the system.

This study is focused on the dynamics of buildings with a night heating setback. Thus, if there is no solar irradiation and the space heating is turned off, the input term can be simplified to $\boldsymbol{U} = (T_a, 0, 0)^\top$. It is then possible to write discrete explicit expressions for the indoor air temperature and the thermal mass:

$$\begin{cases} T_{t+1}^i &= \phi_{11}T_t^i + \phi_{12}T_t^m + \Gamma_{11}T_t^a + \nu_t^{(1)} \\ T_{t+1}^m &= \phi_{21}T_t^i + \phi_{22}T_t^m + \Gamma_{21}T_t^a + \nu_t^{(2)}\,, \end{cases} \tag{8}$$

where the notation has been changed to highlight the discrete nature of the expression. Notice that the terms from the matrices described in equations (5)-(7), appear now in the transformed difference equation system (8).

Now, we want to remove the thermal mass variable from the model, since we do not have access to its associated temperature measurements. In order to do this, the equations from Equation (8) have been merged, adjusting the index t,

$$T_{t+1}^i = \phi_{11}T_t^i + \phi_{12}\overbrace{(\phi_{21}T_{t-1}^i + \phi_{22}T_{t-1}^m + \Gamma_{21}T_{t-1}^a + \nu_{t-1}^{(2)})}^{T_t^m} + \Gamma_{11}T_t^a + \nu_t^{(1)}\,. \tag{9}$$

For houses with regular heating schedules that have not been ventilated recently, the temperature of the thermal mass should be very similar to the temperature of the indoor air [27]. Assuming that $T_{t-1}^i \approx T_{t-1}^m$, it is possible to reduce the expression to Equation (10), where all variables are observed.

$$\begin{aligned} T_{t+1}^i = \phi_{11}T_t^i + (\phi_{12}\phi_{21} + \phi_{12}\phi_{22})T_{t-1}^i + \\ \Gamma_{11}T_t^a + \phi_{12}\Gamma_{21}T_{t-1}^a + \nu_t^{(1)} + \phi_{12}\nu_{t-1}^{(2)}\,. \end{aligned} \tag{10}$$

In Denmark, the cold weather conditions of winter, present slow outdoor temperature variations during night, as shown in Figure 1. For a small enough time step, there is little change from one measurement to the next one, i.e. $T_t^a \approx T_{t-1}^a\ \forall t$. This simplification allows us to reduce the system complexity:

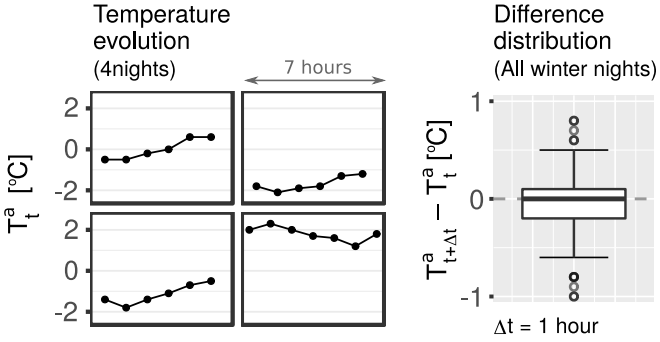

Figure 1: The lattice on the left shows the temporal evolution of the outdoor temperature for 4 randomly selected nights. On the right, the temperature hourly differences for all winter nights is shown.

$$T_{t+1}^i = \overbrace{\phi_{11}}^{\theta_1}T_t^i + \overbrace{(\phi_{12}\phi_{21} + \phi_{12}\phi_{22})}^{\theta_2}T_{t-1}^i + \overbrace{(\Gamma_{11} + \phi_{12}\Gamma_{21})}^{\omega}T_t^a + \nu_t^{(1)} + \phi_{12}\nu_{t-1}^{(2)}\,, \tag{11}$$

where the final model parameters, $\{\theta_1, \theta_2, \omega\}$, have been introduced.

Finally, a new stochastic variable is defined, $\nu_t = \nu_{t-1}^{(1)} + \phi_{12}\nu_{t-2}^{(2)}$. Since $\nu_t^{(1)}$ and $\nu_t^{(2)}$ are independent and normally distributed with zero mean $\forall t$; the new variable, ν_t, is also normally distributed with zero mean. Thus, it is possible to write the final model as the following *auto-regressive* model,

$$T_t^i = \theta_1 T_{t-1}^i + \theta_2 T_{t-2}^i + \omega T_t^a + \nu_t\,, \tag{12}$$

where the time index, t, has been adjusted for clarity. Figure 2 summarizes the process leading from equation (1) to equation (12), highlighting the necessary assumptions.

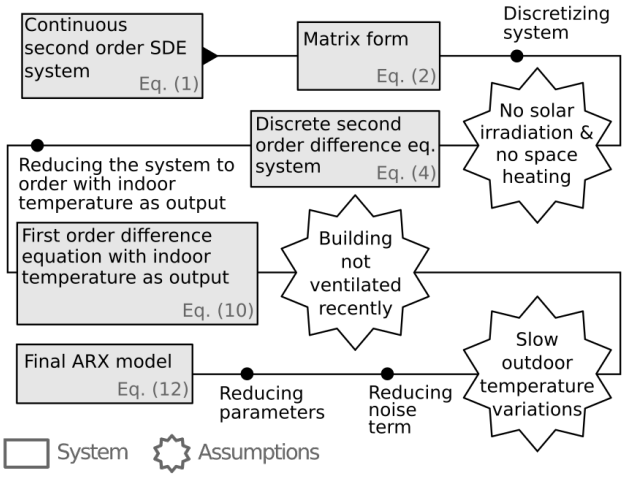

Figure 2: Flowchart describing the method to transform the initial SDE system into a reduced discrete linear model.

2.3. A system with two time constants

In order to study the heat loss between the indoor air and the outdoor air, we focus on the interaction between T_t^i and T_t^a from model (12) using the *transfer function* as shown in Equation (13),

$$T_t^i = \underbrace{\frac{\omega}{1-\theta_1 B-\theta_2 B^2}}_{H(B)} T_t^a\,, \tag{13}$$

where B is the *backshift operator* defined as $B^j X_t = X_{t-j}$ for an arbitrary dynamic random variable $\{X_t\}$, and $H(B)$ is the transfer function of the system (12). As described in [28], in order to compute the time constant of the system (12) it is necessary to find the roots of the denominator of $H(B)$, i.e., the *poles* of the system. In this case, there are two poles, q_1 and q_2, as the polynomial in the denominator is order two. Finally, each pole has an associated time constant which can be computed as:

$$\tau_j = \frac{s}{\ln|q_j|} \quad \forall\, j \in [1,2]\,. \tag{14}$$

Hence, in this case there are two different time constants that characterize the heat flow between indoor air and outdoor air. Each of these time constants has time units and they reveal information about the two processes described by the initial system (2) as illustrated in Figure 3. In general, when the heating is shut down, there is a quick heat transfer between the indoor air and the thermal mass due to the low thermal capacity of the air. The initial heat transfer is captured by the parameter τ_1. The heat transfer between indoor air and outdoor air is the second process, which is characterized by τ_2, is slower and will dominate the dynamics as indoor temperature keeps decreasing [26].

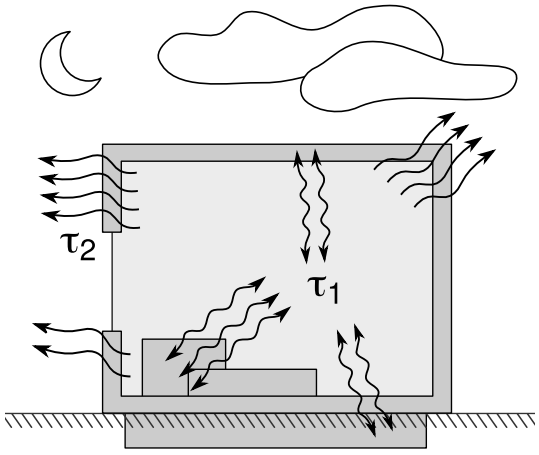

Figure 3: This figure shows a schematic of the two main processes governing the heat flow between indoor air and outdoor air. First, the heat transfers from the indoor air to the thermal mass, characterized by τ_1. Meanwhile, τ_2 characterises the heat transferred from the indoor air to the outdoor air.

2.4. Identification of night setback temperature curves

Hidden Markov Models consist of two components: an observed sequence of states and a corresponding hidden state sequence. The current state only depends on the state of the previous observation. The states change according to a fitted transition matrix, which is a matrix providing the probability of a state change. For each state, the observations are Gaussian, and the mean and variance depends on the state.

All studied houses showed a temperature decay of the indoor air during night hours. The goal, was to identify the state where the temperature is decaying constantly. In order to identify it, a new variable was created to be used as an input for the model:

$$d_t = T_t^i - T_{t-1}^i\,. \tag{15}$$

When temperature is continuously dropping, the data points of d_t are distributed differently from the rest, as can be seen in Figure 4. The Viterbi algorithm [29] was used to find the most likely sequence of states given a sequence of observed d_t.

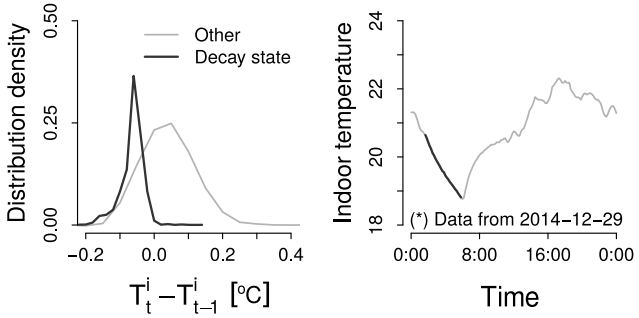

Figure 4: An example of the distribution of decay points for one arbitrary building with night setback. The figure on the left shows that the decay states distribute different from other states. The figure on the right shows the indoor temperature of a day with the thicker curve indicating the decay period identified using the HMM method.

For some houses, the selected periods are not only the long night decaying periods, but also shorter decays during the day time due to the dead-band of the controller. The long night decays are selected with a threshold. This threshold was computed by clustering all d_t data points into two based on the length of the period. In general, it is concluded that this process is sufficient to reveal the natural split between short daytime decays (unwanted) and long night decays, although the time spans vary from house to house because of their different time constants.

2.5. Flexibility index (FI) and Flexiblity Function (FF)

In order to gain insights into the relationship between the time constant and the flexibility of a building, the concepts of the Flexibility Index (FI) [30] and the Flexibility Function (FF) [31] are used. The FI quantifies the savings caused by allocating energy consumption in a flexible way. This is done by comparing the cost of the consumption adapted to a flexible control signal (*flexible cost*) and the cost of the consumption if the system was unaware of the price signal (*ignorant cost*). The idea behind the FI can be seen in equation (16). FI = 1 characterizes a building with an extreme flexibility potential, and FI = 0 the opposite.

$$\mathrm{FI} = 1 - \frac{\text{Flexible cost}}{\text{Ignorant cost}} \tag{16}$$

The *flexibility function* (FF) describes the energy that is available at a particular moment, or *state of charge*; and the resources it can allocate and how it can allocate them before reaching the system limits. This function provides information about how an energy system would adapt to changes in the control signal or changes in its state of charge. Moreover, an energy system has limited resources that can be turned on/off in case of need, and the rate at which it is able to move those resources depends on the dynamic characteristics of each system. The FI and FF used in this work are based on the work introduced by Junker et al. [30, 31].

When calculating the FI and FF in this work, the energy systems are buildings that have their indoor air temperature controlled with an MPC controller. Then, the state of charge translates into the room temperature: the building is completely charged when the indoor temperature reached its daily maximum inside the comfort boundaries and vice-versa. The heating input is controlled by a price signal which is built using the wind speed data. This price signal can also be based on other data and be used for other purposes such as peak shaving, or lowering CO_2 emissions.

3. Data description

This study is based on measurements from a set of 39 Danish single family houses in the Middelfart region in Denmark. None of the studied buildings was built after 1980s, and their construction years vary as described in figure 5. They also vary in size and plant blueprint: the built area ranges from 80 to 226 m^2. Most of the houses are detached family houses, although there are also, semi-detached houses, town-houses and a few farms. In this work, these details have been omitted as the focus is set on characterising the buildings solely based on how they lose heat.

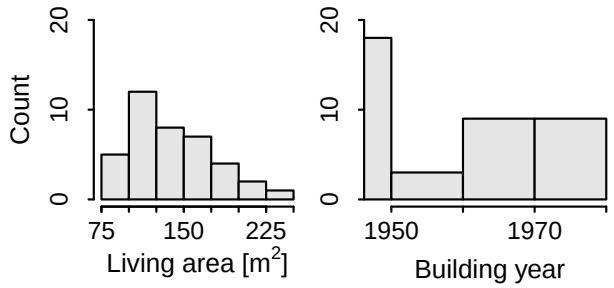

Figure 5: Summary description of the studied set of 39 buildings. Almost half of the buildings were built before 1950.

There are two data sets. The first data set contains the indoor temperature measurements from December 2014 to December 2015. We used only the winter data between December 2014 and March 2015 and with a 10 min resolution. The second data set consists of hourly outdoor temperature values. This data set has been selected to match the dates of the indoor temperature

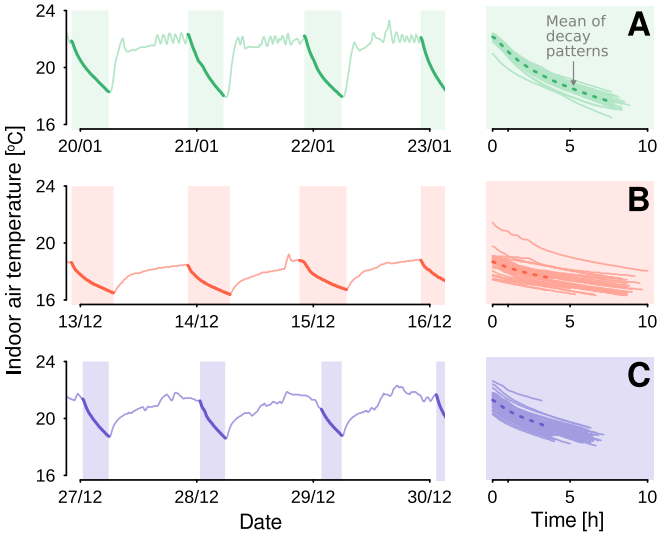

Figure 6: On the left, 4 day period for the three example households (A, B, C). On the right, the lines corresponding to all decay periods present in the data are shown. Each building has its clear decay pattern.

data. In order to compensate the lower resolution, the hourly values are interpolated using linear interpolation. This interpolation are carried under the assumption that, during winter nights the fluctuations in outdoor temperature are slow.

For better presentation and visualisation of the work, the rest of this work focuses on three buildings with characteristic decay patterns, as shown in Figure 6. The three buildings have been chosen due to they present qualitative differences in their continuous heat loss pattern. It can be noticed that building B shows a sharp decay at the beginning and then a slower decaying trend; building A has a fast temperature drop; and building C has a shorter decay curve, but still steeper than the curve in B. For all the three example buildings, the decaying patterns are consistent during different nights. For instance, it can be noticed that in building C, the decaying trend is similar in every case even though the initial indoor temperature varies.

4. Results and discussions

This section presents the results from the modelling process. These results are also discussed to understand how the thermal dynamics are captured. Afterwards, this section offers a classification of the buildings based on their time constants.

4.1. Model validation

The parameters from the model in Equation (12) were estimated using *Ordinary Least Squares* (OLS) method in the first place, since the model is linear and the noise is supposed to be normally distributed. This revealed that the term related to the outdoor temperature, ω, was not significant in most of the tested buildings. However, as presented in Section 2, the outdoor air temperature affects the heat loss dynamics. This impact is more noticeable at the end of the decaying curve, when the heat exchange with the outdoor air is more significant than

the heat exchange with the thermal mass. In addition, at the beginning of the decay trend, the assumption that $T_t^i \approx T_t^m$ is less accurate, since in reality both temperatures converge over time. Lastly, at the beginning of the decaying curve there is a higher chance than the users might be awake. All these reasons suggest that the noise over time, $\{v_t\}$, might not be independent. In fact, the system noise is expected to be at its maximum at the beginning of the decay and then continuously decrease over time. In order to cope with this, the *weighted least squares* (WLS) method was used, where the models is fitted giving a specific weight to each observation. These weights are proportional to the time since the temperature decay started, given that the observations become more reliable as time moves forward. The following equation was used for the weighting process,

$$w(k) = 1 - \frac{1}{\alpha + (1-\alpha)k} \quad \text{with } 0 \leq \alpha \leq 1\,, \tag{17}$$

where k is an integer counting the number of measurements since the beginning of the decay period and α is a tuning parameter. Notice that $w \in [0, 1]$, it is minimum right at the beginning of the decay period, $w(1) = 0$, and then grows monotonically. The parameter α defines how fast is this growth; i.e. how the weights are distributed along the decay period. Notice that this parameter depends on the time constants of the building and it could be fine-tuned in a recursive method in order to fit a particular building. Thus, it is important to remark that this weighting function is not unique and it could be adapted to each case.

Table 1 compares the results after fitting the model with OLS and WLS. Notice how, after using WLS, the p-values of the parameter estimates are below 0.1, confirming that the parameters are highly significant. It can also be noticed that the estimate of the contribution of the outdoor temperature, $\hat{\omega}$, increased significantly using the WLS, especially for houses A and C, which confirms the influence of the external conditions.

		Estimate		**Std. error**		**p-value**	
		OLS	WLS	OLS	WLS	OLS	WLS
A	$\hat{\theta}_1$	1.768	1.779	0.016	0.017	<1E-16	<1E-16
	$\hat{\theta}_2$	-0.769	-0.781	0.016	0.017	<1E-16	<1E-16
	$\hat{\omega}$	4.3E-4	3.3E-4	2.5E-4	2.9E-4	0.09	0.26
B	$\hat{\theta}_1$	1.111	1.273	0.024	0.023	<1E-16	<1E-16
	$\hat{\theta}_2$	-0.113	-0.275	0.024	0.023	<1E-16	<1E-16
	$\hat{\omega}$	1.8E-3	1.5E-3	2.4E-4	2.6E-4	<1E-16	<1E-16
C	$\hat{\theta}_1$	1.624	1.707	0.015	0.015	<1E-16	<1E-16
	$\hat{\theta}_2$	-0.625	-0.708	0.015	0.015	<1E-16	<1E-16
	$\hat{\omega}$	2.8E-4	1.3E-4	1.4E-4	1.7E-4	0.05	0.45

Table 1: Table comparing the parameter estimates for each example building. The table compares the results using WLS (weighted with the function in (17)) and using OLS.

Figure 7 reveals that the ordinary residuals, after using the WLS, behave like white noise regardless of the outdoor conditions. It also can be seen that most of the residuals are in the $[-0.1, 0.1]$ range, which show the accuracy of the one-step prediction. The values that fall outside of this range are from the beginning of the decaying periods when it is expected to be noisy, as explained previously. The distribution of residuals can be seen in Figure 8, which shows that the errors are small and centered around zero.

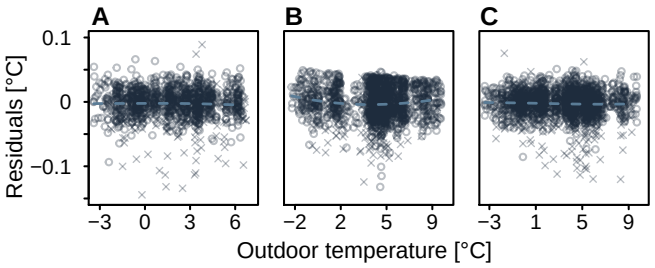

Figure 7: The figure compares the outdoor temperature and the residuals using the WLS model. The residuals from the first hour of each decay are marked with an x. The trend of all residuals is plotted as a dashed line. All residuals are centered around 0 and evenly spread across all temperature range.

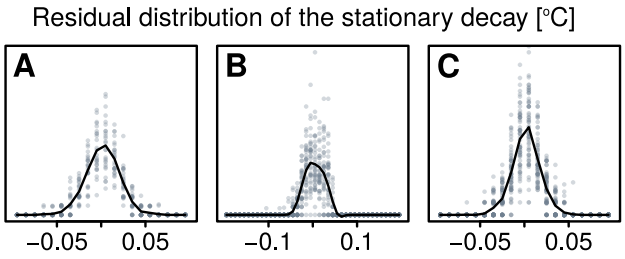

Figure 8: Distribution of residuals after using the WLS model. The figures include all the decays in the time span of interest ignoring the first hour of each decay. For each building a smooth curve was plotted for better visibility.

In Figures 7 and 8 it is not possible to see if the residuals are biased on a daily basis. For this reason, the evolution of residuals are plotted for 3 arbitrary days picked at random for each example building in Figure 9. It can be seen from this figure that in all cases the prediction follows the same pattern. At the beginning of the decay period, the model is over-predicting so the residuals are negative and larger. This bias comes from the simplification $T_t^i \approx T_t^m$, since it forces the stochastic part to account for the changes in T_t^m. However, shortly after the start the residuals converge to white noise, since $T_t^i \to T_t^m$ quickly [26]. These transient periods are the cause of the larger residuals seen in Figure 7.

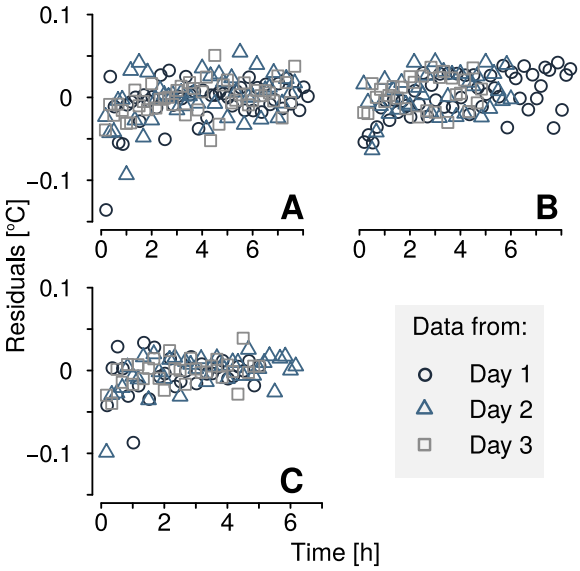

Figure 9: Temporal evolution of the residuals during each decay period. Only 3 decays are plotted for better visibility. It can be seen that the ordinary residuals are larger at the beginning of the decay period, but shortly after there is no observable trend.

4.2. *Time constant of 39 houses*

The time constants of the three example buildings are shown in Table 2; it is important to notice that τ_1 is expressed in minutes, whereas τ_2 is expressed in hours. These results can be compared with the qualitative behaviour observed in Figure 6. In comparison with the other two, building B shows a flatter decay trend at the end of each night. This translates into having $\tau_2^{(B)} > \tau_2^{(C)} > \tau_2^{(A)}$. In addition, the numerical results in Table 2 reveal that building B loses energy swiftly at the beginning of the decay, which is different from house A where the heat transfer between the indoor air and thermal mass also has a significant contribution to the decay period.

	A	**B**	**C**
τ_1 [min]	38.8	4.6	21.5
τ_2 [hour]	36.7	65.6	49.7

Table 2: Results for the example houses.

Moreover, the results of house A were compared with the results computed using a different method presented in [32], where a more complex auto-regressive model (including heating data) was fitted using a time span of 11 days. The difference between results were smaller than an 8%. In addition, it is important to remark that it is possible to further reduce the difference between the results by fine-tuning the weighting function (17), specifically for house A.

The simplicity and generality of this method has allowed us to use it in the total pool of 39 buildings and to categorize their parameters τ_1 and τ_2. Figure 10 shows the distribution of the time constants for all 39 buildings. It can be observed that: i) the long time constant, τ_2, has the same order of magnitude as

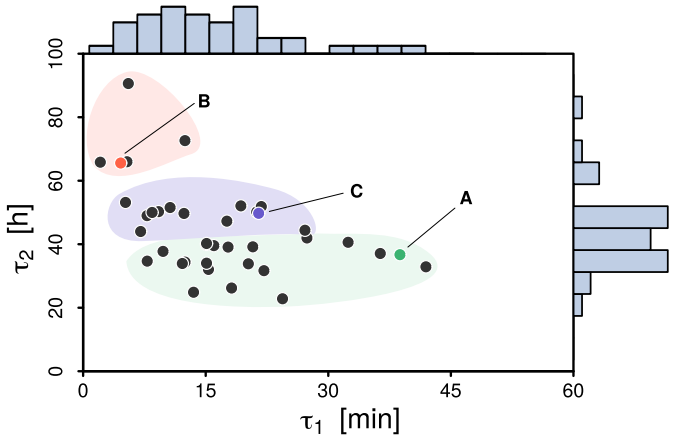

Figure 10: Scatter plot of the two time constants for 39 buildings. As the result of a K-means clustering, three regions are marked in the figure. In each cluster, the example house is highlighted.

the time constant one would expect from Danish family houses [33, 34]; ii) for the short time constant, τ_1, all values are shorter than one hour, which highlights the importance of a small time step to capture this part of the dynamics. From Figure 10 it can be seen that the 39 buildings are clustered in groups. K-means clustering method [35] was used and as the result three clusters are marked in the figure. Note that each of the three selected buildings falls in different categories, confirming the qualitative differences in their heat loss dynamics spotted at the beginning of this work.

In Figure 10, one can get a clear picture at the available classes of buildings in the studied set. On the short time constant axis, τ_1, the time values are mostly scattered, contrarily to the τ_2 where most of the values lie around the bottom half of the plot. Furthermore, it can be seen how the main driver for clustering comes from the long time constant τ_2, i.e., the three main regions reveal three different steps along the y-axis. The difference among three clusters could be due to the difference in insulation level, house size, the amount of thermal mass, etc. However, to investigate this level of detail would require more information about these houses which we do not have, thus it was left out of the current study.

5. Flexibility assessment

This section shows the application of using the computed time constants of the house to reveal its energy flexibility potential based on simulations.

The simulations are based on the model described in (2) and carried out using different parameter values to gain an overview of their impact. Specifically, the parameters of the indoor air heat resistance, R_i, and the capacity of the indoor air, C_i, were fixed; while the heat resistance between the indoor and outdoor air, R_a, and the capacity of the thermal mass, C_m, were changed in each simulation. The first two parameters depend on intrinsic magnitudes of the air; meanwhile, the last two parameters are easier to interpret and they characterize magnitudes from a building that are easier to correct through

renovation. Finally, the only external output of the model, the outdoor temperature, follows an arbitrary pattern that matches the order of magnitude of danish winter time.

For each combination of parameters, a time series of four days was simulated with a night-setback schedule. Using those values, the time constants were computed, and the results can be seen in Figure 11. It can be seen that both parameters are directly proportional to the value of the time constants, as expected. Three cases have been highlighted (H1, H2 and H3) to represent three buildings with a different parameter combination. These have been chosen to further assess the effects of the parameters on the building thermal performance.

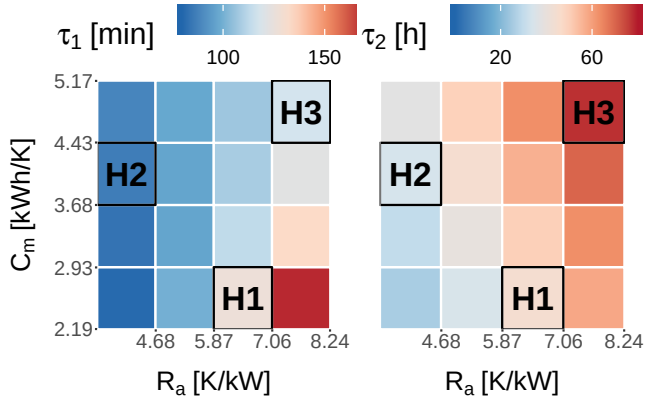

Figure 11: Resulting time constant values for different values of C_m and R_a. The increase of R_a yields higher values of both time constants. The increase of C_m benefits only τ_2. H1, H2 and H3 represent three different houses with different characteristics.

For each combination of parameters shown in Figure 11, we simulated four days using two different control strategies: one ignores the price signal and only tries to keep the indoor temperature inside a defined comfort region. In the other simulation, the heating system is controlled using *Model Predictive Control* (MPC), where the control signal is the price of energy. The MPC controller tries to minimize the operation cost using the aforementioned price signal, while also keeping the indoor temperature within the comfort region. These two strategies represent the *Ignorant Cost* and *Flexible Cost* as described in Section 2.

For the simulations, we created a price signal that depends on the wind speed during an arbitrary period of time, to simulate a system powered by wind energy. The energy price decreases as the wind speed increases, assuming that energy supply is always sufficient.

The results of the controlled simulation for the three highlighted cases (H1, H2, H3) are presented in Figure 12. It can be seen that when the price is low, the heating is switched on and when the price increases the heating is turned off until the temperature approaches the lower boundary. It can be noticed that the heating in H3 could be turned off for a longer time due to the building's higher time constants. The indoor air temperature in building H2 never reached the upper boundary of the comfort region due to higher heat losses.

It can be seen in Figure 13 that the resistance R_a is the key

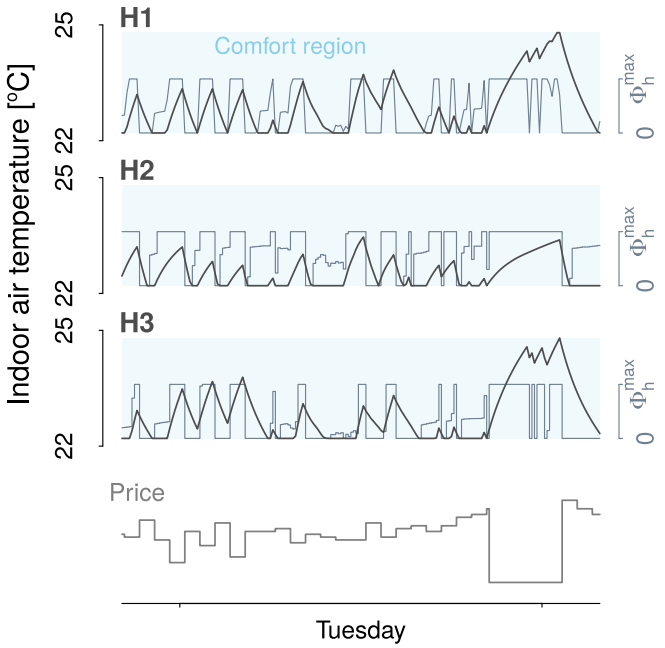

Figure 12: Simulation of the flexible control scenario for the representative houses. The indoor temperature follows the the heat supply, which is controlled by the price signal. It can be seen that H3, is able to keep indoor temperature within the comfort region with the heating system running for a shorter time comparing to H1 and H2.

parameter to increase savings using the flexibility of the building.

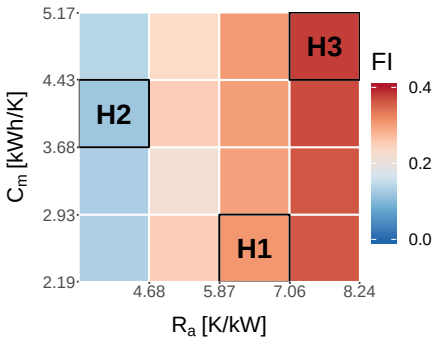

Figure 13: Resulting Flexibility Index value for different values of C_m and R_a. It can be noticed that the main driver for the FI is the thermal resistance. H1, H2 and H3 represent three different houses with different characteristics.

Lastly, the results of the flexibility function of the three houses can be seen in Figure 14. This figure summarizes how the three different houses react to a change in the two main drivers of the energy consumption: the room temperature and the energy price. This reaction is presented as the deviation from the ignorant consumption; i.e. the consumption of the system ignoring the flexible price signal. The three houses display a similar response to the state of charge: a flat section, where the system ignores the variations of the indoor temperature, and two steep curves at the ends of the temperature range. When the room temperature reached the low boundary, the system was forced to increase consumption to maintain comfort; similarly, the system decreases consumption when the room temperature reached the high boundary. It can be noted that H3 is able to stay on the flat region for a wider temperature range

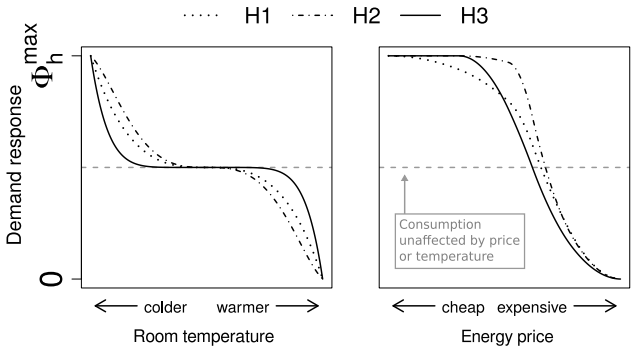

Figure 14: The figure shows that the energy demand is affected by changes on the state of the system (room temperature) and the variations in the control signal (energy price). The curve above the dashed line means that the consumption is increased, and vice-versa. It can be seen that H3 is more resilient to changes in the room temperature, and it is able to consume less during the most expensive hours.

than the other two. This suggests that H3 is more resilient to changes in the room temperature than the H1 and H2.

The response to energy price follows a decreasing curve for the three houses. For lower prices, the power demand of H1 is below H2 and H3. As the price increases, H3 consumption gets below H1 and H2. This result is in line with the results in Figure 13, and confirms that the high value of the FI of H3 is the result of avoiding expensive prices. The savings of H1 compared to H2 come mainly from decreasing consumption during cheaper hours.

6. Conclusions

This study shows how one can obtain insights from the thermal characteristics of a building with limited data. First of all, Hidden Markov Models were used to select the relevant periods to extract measurements from the periods with a night-setback. By focusing on these long decaying periods, it has been possible to transform a complete physical system to a simple auto-regressive structure. This model structure only uses the indoor air temperature and the outdoor air temperature, which are normally easy to measure.

It is important to use a high resolution sampling to capture the fast dynamics inside the building. In this study, 10-minute time interval data was used. This small time step made it possible to reduce the model structure by taking advantage of the slow changes and small variations of the outdoor temperature. Additionally, the resulting time constants highlighted the importance of choosing a small time step. The only external input of our model, the outdoor temperature, was measured hourly and was transformed to 10-minute data using linear-interpolation taking advantage of its slow dynamics. The linear interpolation is expected to represent accurately the real outdoor temperature, without affecting the posterior analysis.

It is critical to understand the physical meaning of the model. In order to fit the model, it was necessary to take into account the decreasing trend of the system noise during the night by using the WLS method. Only by doing this, all parameters in the model became significant. This is important because the temperature decay inside of a building could potentially be caused by other factors: such as the air mixing in the same room, or a heat transfer to a much colder contiguous room. The significance of the parameter corresponding to the outdoor air confirms that the indoor air decreases due to a heat loss to the outdoor air, which validates our model assumptions.

This method offers a general and computationally light model that can be scaled to a large portion of the existing building stocks. By visualising the two time constants for all 39 buildings as shown in Figure 10, three clusters of buildings with similar characteristics could be easily found. In this study, we used a simple clustering method to identify those building clusters.

The usability of each time constant depends on the specific problem. The long time constant is the one that gives a clearer picture of buildings' characteristics for thermal storage and it is also closely related to the classical time constant used in building physics. However, the short time constant could be relevant for studying short term flexibility and indoor comfort.

Finally, it is confirmed that there is a clear connection between the time constants and the flexibility potential of buildings. It is shown that the long time constant dominates the potential usage of a house as an energy storage unit in a flexible energy grid. Moreover, using the FF, it is possible to assess qualitatively the flexible response of the simulated houses. In conclusion, the results show that a house with higher values of τ_1 and τ_2 can implement more flexible strategies.

Acknowledgements

This work is part of the CITIES project (nr. DSF1305-00027B) as well as the *Smart Energi i Hjemmet* project. I would like to thank my colleague Rune G. Junker for many valuable discussions and for sharing his work and vision on the future of flexible energy systems.

References

[1] K. Foteinaki, R. Li, A. Heller, and C. Rode. Heating system energy flexibility of low-energy residential buildings. *Energy and Buildings*, 180:95–108, 2018.

[2] S. Ø. Jensen, H. Madsen, R. A. Lopes, R. G. Junker, D. Aelenei, R. Li, S. Metzger, K. B. Lindberg, A. J. Marszal, M. Kummert, B. Bayles, E. Mlecnik, R. Lollini, and W. Pasut. *Annex 67: Energy Flexible Buildings - Energy Flexibility as a key asset in a smart building future*. 2017. Contribution of Annex 67 to the European Smart Building Initiatives.

[3] A. J. Marszal-Pomianowska, H. Johra, A. Knotzer, J. Salom, T. Péan, S. Ø. Jensen, E. Mlecnik, H. Kazmi, R. Pernetti, K. Klein, L. Frison, P. Engelmann, J. Parker, L. Aelenei, R. A. Lopes, D. Aelenei, R. G. Junker, H. Madsen, A. Q.Santos, B. N. Jørgensen, and Z. Ma. *Principles of Energy Flexible Buildings: Energy in Buildings and Communities Programme Annex 67 Energy Flexible Buildings*. International Energy Agency, 2020.

[4] Johan Kensby, Anders Trüschel, and Jan-Olof Dalenbäck. Potential of residential buildings as thermal energy storage in district heating systems – results from a pilot test. *Applied Energy*, 137:773 – 781, 2015.

[5] T. H. Pedersen, R. E. Hedegaard, and S. Petersen. Space heating demand response potential of retrofitted residential apartment blocks. *Energy and Buildings*, 141:158 – 166, 2017.

[6] G. Reynders, J. Diriken, and D. Saelens. Generic characterization method for energy flexibility: Applied to structural thermal storage in residential buildings. *Applied Energy*, 198:192 – 202, 2017.
[7] V. Dimitriou, S. K.Firth, T. M.Hassan, T. Kane, and M. Coleman. Data-driven simple thermal models: The importance of the parameter estimates. *Energy procedia*, 78:2614–2619, 2015.
[8] A. Foucquier, S. Robert, F. Suard, L. Stéphan, and A. Jay. State of the art in building modelling and energy performances prediction: A review. *Renewable and Sustainable Energy Reviews*, 23:272 – 288, 2013.
[9] C. Luo, B. Moghtaderi, H. Sugo, and A. Page. A new stable finite volume method for predicting thermalperformance of a whole building. *Building and Environment*, 43:37–43, 2008.
[10] L. Wang, P. Ma, E. Hu, D. Giza-Sisson, G. Mueller, and N. Guo. A study of building envelope and thermal mass requirements for achieving thermal autonomy in an office building. *Energy and Buildings*, 78:79 – 88, 2014.
[11] L. Evangelisti, C. Guattari, F. Asdrubali, and R. de Lieto Vollaro. In situ thermal characterization of existing buildings aiming at nzeb standard: A methodological approach. *Developments in the Built Environment*, 2:100008, 2020.
[12] G. Bauwens and S. Roels. Co-heating test: A state-of-the-art. *Energy and Buildings*, 82:163–172, 2014.
[13] F. Alzetto, G. Pandraud, R. Fitton, I. Heusler, and H. Sinnesbichler. Qub: A fast dynamic method for in-situ measurement of the whole building heat loss. *Energy and Buildings*, 225:175–182, 2018.
[14] S. Roels, P. Bacher, G. Bauwens, S. Castano, M. J. Jiménez, and H. Madsen. On site characterisation of the overall heat loss coefficient: Comparison of different assessment methods by a blind validation exercise on a round robin text box. *Energy and buildings*, 153:179–189, 2017.
[15] D. Cali, T. Osterhage, R. Streblow, and D. Müller. Energy performance gap in refurbished german dwellings: Lesson learned from a field test. *Energy and buildings*, 127:1146–1158, 2016.
[16] A. D'Amico, G. Ciulla, L. Tupenaite, and A. Kaklauskas. Multiple criteria assessment of methods for forecasting building thermal energy demand. *Energy and Buildings*, 224:110220, 2020.
[17] C. Finck, R. Li, and W. Zeiler. Optimal control of demand flexibility under real-time pricing for heating systems in buildings: A real-life demonstration. *Applied Energy*, 263:114671, 2020.
[18] C. Finck, R. Li, R. Kramer, and W. Zeiler. Quantifying demand flexibility of power-to-heat and thermal energy storage in the control of building heating systems. *Applied Energy*, 209:409 – 425, 2018.
[19] P. Bacher and H. Madsen. Identifying suitable models for the heat dynamics of buildings. *Energy and Buildings*, 43:1511–1522, 2011.
[20] S. Goyal and P. Barooah. A method for model-reduction of non-linear thermal dynamics of multi-zone buildings. *Energy and Buildings*, 47:332–340, 2012.
[21] H. Nielsen, S. Mortensen, P. Bacher, and H. Madsen. *Analysis of energy consumption in single family houses*. 01 2010.
[22] C. Rasmussen, P. Bacher, D. Calì, H. A. Nielsen, and H. Madsen. Method for scalable and automatised thermal building performance documentation and screening. *Energies*, 13(15):3866, 2020.
[23] C. Rasmussen, R. Relan, and H. Madsen. Identification of occupancy status by statistical change point detection of CO_2 concentration. In *2018 IEEE Conference on Control Technology and Applications (CCTA)*, pages 1761–1766. IEEE, 2018.
[24] S. Wolf, J. Kloppenborg Møller, M. A. Bitsch, J. Krogstie, and H. Madsen. A markov-switching model for building occupant activity estimation. *Energy and Buildings*, 183:672–681, 2019.
[25] A. Wang, R. Li, and S. You. Development of a data driven approach to explore the energy flexibility potential of building clusters. *Applied Energy*, 232:89 – 100, 2018.
[26] H. Madsen and J. Holst. Estimation of continuous-time models for the heat dynamics of a building. *Energy and buildings*, 22:67–79, 1995.
[27] K. Foteinaki, R. Li, A. Heller, M. H. Christensen, and C. Rode. Dynamic thermal response of low-energy residential buildings based on in-wall measurements. *E3S Web of Conferences*, 111, 2019.
[28] H. Madsen. *Time series analysis*. Chapman Hall, 2008.
[29] C. Bishop. Pattern recognition and machine learning. chapter 13, page 629. Springer, 2006.
[30] R. G. Junker, A. Gashem Azar, R. Amaral Lopes, K. Byskov Lindberg, G. Reynders, R. Relan, and H. Madsen. Characterizing the energy flexibility of buildings and districts. *Applied energy*, 225:175–182, 2018.
[31] R. G. Junker, C. S. Kallesøe, J. Palmer, B. Howard, R. A. Lopes, and H. Madsen. Stochastic nonlinear modelling and application of price-based energy flexibility. *Applied Energy*, 275, 2020.
[32] S. Nordli. Statistical methods for optimizing renovation projects. Master's thesis, DTU Compute, 2018.
[33] P. Bacher, H. Madsen, H. A. Nielsen, and B. Perers. Short-term heat load forecasting for single family houses. *Energy and Buildings*, 65:101–112, 2013.
[34] J. Le Dréau and P. Heiselberg. Energy flexibility of residential buildings using short term heat storage in the thermal mass. *Energy*, 111:991–1002, 2016.
[35] T. Hastie, R. Tibshirani, and J. Friedman. The elements of statistical learning. chapter 13, page 460. Springer, 2009.

Simulating heat load profiles in buildings using mixed effects models

J Palmer Real[1], J Kloppenborg Møller[1], C Rasmussen[1], K B Lindberg[2], I Sartori[2] and H Madsen[1]

[1] DTU Compute, Asmussens Allé, Building 303B, Lyngby, Denmark
[2] SINTEF Building and Infrastructure, Oslo, Norway

E-mail: jpre@dtu.dk

Abstract. The landscape of buildings is a diverse one and long-term energy system planning requires simulation tools that can capture such diversity. This work proposes a model for simulating the space-heating consumption of buildings using a linear mixed-effects model . This modelling framework captures the noise caused by the differences that are not being measured between individual buildings; e.g. the preferences of their occupants. The proposed model uses outdoor temperature and space-heating consumption measured at hourly resolution; thus, the model is able to predict the intra-day variations as well as longer effects. Given the stochastic nature of the simulation, the prediction interval of the simulation can be estimated, which defines a region where the consumption of any unobserved building will fall in. A whole year has been simulated and compared to out-of-sample measurements from the same period. The results show that the out-of-sample data is virtually always inside the estimated 90% prediction interval. This work uses data from Norwegian schools, although the model is general and can be built for other building categories. This amount of detail allows energy planners to draw a varied and realistic map of the future energy needs for a given location.

1. Introduction

In order to plan and develop strategies for the future power market, it is necessary to create tools that reliably represent it. Such tools need to be able to predict the energy consumption of the different systems that form the energy landscape. The current tools dedicated to this task are often based on trends based on historical data [1; 2; 3]. As the power sector shifts towards a more flexible framework with high integration of renewable energy sources, it is necessary to re-visit these methods used for long-term forecasting [4].

Buildings take a significant portion of the total energy use [5]; thus, modelling their consumption is a key task in order to develop suitable forecasting tools. From the total energy consumed in buildings, in Europe, the major part is dedicated to space heating [6], and there exist an extensive literature focused on modelling it [7]. A well-known example is the energy signature method (ES); a data driven approach that quantifies a building thermal performance based, mainly, on the outdoor temperature [8]. In general, the ES is a static method, even though their parameters might change over the course of the year [9].

The proposed model in this work aims to capture the dynamic nature of heat consumption; given that, when predicting the energy use of a building, capturing the peaks that take place

during the day is of particular interest. Similarly, it is crucial to see how this pattern changes as buildings become more efficient.

There are factors that impact the heat consumption of a building that can be specially difficult to measure. A clear example is the behaviour of the occupants; predicting it is far from being trivial due to their noisy nature and intrusive measurement set ups [10]. A long-term forecasting tool needs to account for such phenomena to be general enough to represent the existing variety of the building stock. This means capturing the inherent differences from building to building, caused by random unobserved events. In this work, this is done by using a mixed effects model. We depart from the work done in [11], where a linear fixed model was fit to generate an hourly profile of the energy consumption in buildings. Then, a random term is added to the fixed model structure, to account for the individual differences between buildings. This addition reduces model complexity, quantifies the differences between observed buildings and facilitates predicting the consumption from unobserved ones.

The outline of this work is as follows: first, in section 2, the mixed effects model structure is introduced and explained in the context of modelling building energy load; section 3 presents the data used to fit the model; section 4 displays the results using mixed effects; finally, section 5 discusses the main results and presents the following steps.

2. Method

Mixed effects models allow to quantify the noise introduced by random qualities that are inherent to the modelled system. This section introduces the main concepts, and later focuses on using mixed effects for modelling the heat load of buildings.

2.1. Mixed models

Linear mixed effects models, or linear mixed models, are a generalization of the classical linear model which follows the structure

$$\boldsymbol{Y} = \boldsymbol{X}\boldsymbol{\beta} + \boldsymbol{Z}\boldsymbol{U} + \boldsymbol{\epsilon}\,; \tag{1}$$

where $\boldsymbol{Y}$, $\boldsymbol{X}$ and $\boldsymbol{Z}$ are known matrices, $\boldsymbol{\epsilon} \sim N(\mathbf{0}, \boldsymbol{\Sigma})$ and $\boldsymbol{U} \sim N(\mathbf{0}, \boldsymbol{\Psi})$. In Equation (1), $\boldsymbol{\beta}$ represents the *fixed effects*, while $\boldsymbol{U}$ are the *random effects*. Therefore, these models follow a hierarchical structure since there is an underlying model structure, defined by $\boldsymbol{X}$ and $\boldsymbol{Z}$, which is affected by a higher-level random variable, $\boldsymbol{U}$. Then, an arbitrary observation of $\boldsymbol{Y}$, Y_{ij}, has two sources of noise: the random effects $U_i \subset \boldsymbol{U}$, and the noise of the model, ϵ_{ij}. Hence, given the linear structure of Equation (1), Y_{ij} can be written as

$$Y_{ij} = \sum_{l=1}^{L} X_{jl}\beta_l + Z_i U_i + \epsilon_{ij}\,. \tag{2}$$

Notice that the sub-index i denotes a category of observations, which introduces the noise U_i; whereas j marks the number of available observations. In addition, the term $l \in \{1, \ldots, L\}$ represents the number of fixed effects.

When the measurements of the random variable, Y_{ij}, are taken at regular time intervals, the model in Equation (2) can be interpreted as a time-series. In this case, the sub-index j is substituted by t, to denote the time dependency. This formulation, has been extensively used in pharmaco-kinetics, when testing a medicine in a subset of a population [12]. The metabolism of each tested individual might affect the response to the medicine; however, there are latent effects that are common to all subjects. In this simplified example, the latent effects are captured by $\boldsymbol{\beta}$, whereas $\boldsymbol{U}$ characterizes the variability of the results introduced solely by the individuals that are part of the experiment. For more details and examples on mixed models, see [13].

2.2. Mixed models for buildings

There are factors that affect the energy consumption of buildings that are difficult to identify and measure; such as the preferences of the building users. Such factors cause random differences between the energy behaviour of individual buildings. The cause of those differences can be understood as a random effect. Then, using a mixed model, it is possible to identify the distribution that characterizes the differences between individual buildings. As summarized in Figure 1, estimating the distribution has two different outcomes:

- *Profiling.* Using the observations to estimate the random effects of each particular building from the measured ensemble of buildings, i.e. estimating $\hat{U}_i \ \forall i \in \{1, \dots, k\}$.
- *Sampling.* Simulating a representative realization of a building that has not been observed, using random effects sampled from the estimated distribution $\hat{\boldsymbol{U}}$.

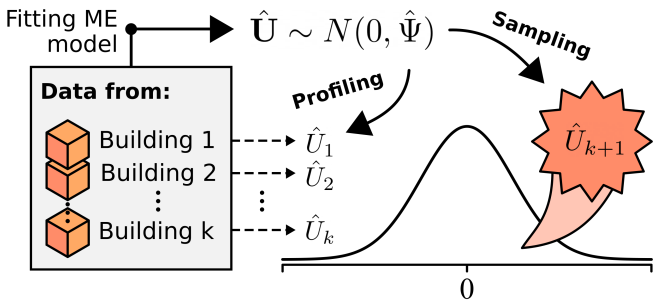

Figure 1: Schematic representation of the outcomes of fitting a mixed effects model

2.2.1. A mixed energy signature. The energy signature (ES) is a method to evaluate the energy performance of buildings. The ES model is a linear model that, using coarse data aggregation, returns the heat loss coefficient (HLC) and the base temperature (T_b). The former coefficient quantifies the energy efficiency of a building, and the latter is the outdoor temperature at which that building is in thermal balance. Thus, both parameters characterize the energy efficiency of a single building. In its simplest form, the ES has the following structure

$$\Phi = \begin{cases} \alpha_0 + \beta_0 T_{\text{out}} + \epsilon & \text{if heating period} \\ \Phi_0 + \epsilon & \text{otherwise} \end{cases}, \tag{3}$$

where Φ is the heat load, T_{out} is the outdoor temperature. The independent term, α_0, represents unmodelled heat losses; β_0 is the HLC, and $T_b = \alpha_0/\beta_0$; lastly, Φ_0 represents the residual heat load during periods where there is no weather dependence, i.e. $T_{\text{out}} > T_b$. Working with multiple buildings, it is fair to assume that there will be differences in their parameters, $\{\alpha_0, \beta_0, \Phi_0\}$, due to un-measured differences across the building population. Then, the model in Equation (3) can be extended to a mixed effect formulation to capture those differences as random effects. Hence, the heating regime of Equation (3) becomes

$$\Phi_i = \underbrace{\alpha + \beta T_{\text{out}}}_{\text{Fixed effects}} + \underbrace{U_{i,0} + U_{i,1} T_{\text{out}}}_{\text{Random effects}} + \epsilon\,, \tag{4}$$

where $U_{i,0} \sim N(0, \sigma_0)$ and $U_{i,1} \sim N(0, \sigma_1)$. Re-writing Equation (4) into

$$\Phi_i = \alpha + U_{i,0} + (\beta + U_{i,1}) T_{\text{out}} + \epsilon\,, \tag{5}$$

it can be notice that, the unmodelled heat losses now contain the random effects $U_{i,0}$; similarly, the heat loss coefficient, depends on $U_{i,1}$. Then, using the model described in Equation (5), it is possible to retrieve the heating performance parameters from each of the buildings of the population. In other words, for each building, it is possible to obtain its heat loss coefficient, $\beta_i = \beta + U_{i,1}$, and its base temperature, $T_{b,i} = (\alpha + U_{i,0})/\beta_i$.

2.2.2. The simulation model. The objective of this work is creating a stochastic simulation tool, that predicts the hourly consumption of buildings given the weather conditions. The model needs to be dynamic and be able to predict consumption for the whole year. The proposed model for simulating the heat load is

$$\begin{aligned} \Phi_{i,t} = & \\ \text{Fixed hour effects} \rightarrow \quad & \left[\sum_{j=1}^{24} \varrho_j I_{\{t\in j\}} + W_t \sum_{j=1}^{24} \rho_j I_{\{t\in j\}}\right] I_{\{t\in\Omega_{\text{WD}}\}} + \\ \text{Fixed seasonal intercepts} \rightarrow \quad & \theta_1 + \theta_2 W_t + \\ \text{Fixed weather effects} \rightarrow \quad & \theta_3 \Delta T_{i,t} + \\ \text{Random effects} \rightarrow \quad & U_{i,2} + U_{i,3} W_t + U_{i,4} \Delta T_{i,t} + \\ \text{Residuals} \rightarrow \quad & \epsilon_{i,t} = \varphi_1 \epsilon_{i,t-1} + \xi_{i,t}\,, \end{aligned} \tag{6}$$

where, $I_{\{\cdot\}}$ is the indicator function, which equals to 1 when the condition in $\{\cdot\}$ is fulfilled and equals 0 otherwise. $S_t = I_{\{T_{b,i}<T_{\text{out},t}\}}$, $W_t = I_{\{T_{b,i}>T_{\text{out},t}\}}$ and $\Delta T_{i,t} = (T_{b,i} - T_{\text{out},t}) I_{\{T_{b,i}>T_{\text{out},t}\}}$; lastly, Ω_{WD} is the subset of work days. Hence, the model in Equation (6) uses the previously introduced $T_{b,i}$, to discern between heating and non-heating season. The model accounts for a fixed hourly schedule, which depends on the season. Additionally, each season has a fixed heating baseline. Then, the weather effects are introduced through the variable $\Delta T_{i,t}$, that is positive during heating season, and zero otherwise. Furthermore, the variables $\{S_t, W_t, \Delta T_{i,t}\}$ have a random effect over the heat load; i.e. the seasonal heating intercept and the effects of the weather might vary from building to building. Finally, given the hourly sampling, an auto-correlation term has been added in the residuals. Thus, in the model described in Equation (6), the estimated fixed parameters are $\boldsymbol{\beta} = \{\rho_1, \ldots, \rho_{24}, \varrho_1, \ldots, \varrho_{24}, \theta_1, \theta_2, \theta_3, \varphi_1\}$.

3. Description of the data set

The data set used in this work contains hourly measurements of the heat load of 33 different Norwegian schools. The heating has been split into electric heating and space heating. In this work, only the space heating is used. In addition, the outdoor temperature for the different schools is available. For each building, the measurements span from 1 to 3 years with no gaps in the data. Other general information about all buildings is known, this information contains details like location, efficiency label and built area. In the following results, all schools have the *Regular* efficiency label, which means that they do not comply with the TEK10 efficiency standards and above. Lastly, to normalize the data, the heat load of the schools has been divided by the area of each building, i.e. $[\Phi_{i,t}] = kWh/m^2$.

In order to validate the results of the stochastic simulation, the data has been split into two sets: one for training and one for testing. The training set contains data from 25 buildings. In order to have a balanced data set for training, one year has been chosen arbitrarily for each of the 25 buildings. The final training set contains data from 2009, 2010, 2011, 2012 and 2017. On the other hand, the test set contains data from 8 different buildings. The data from the test set is all from 2010, to ensure consistency with the time stamps and weather data.

4. Results

As explained in the method section, mixed effects models can be used to study the differences between the measured buildings (profiling), or to simulate the behaviour of a new unobserved building (sampling). In this section, both outcomes are presented: first, the results of fitting model in Equation (5) are shown, which allows computing the variable $T_{b,i}$ $\forall i \in \{1, \ldots, 33\}$. Then, the model in Equation (6) has been fit using the training set and the simulated consumption has been compared to the test data.

4.1. Profiling energy performance

All buildings in this work have the same energy efficiency label, implying that their response to weather conditions should be similar. Using the model in Equation (5) it has been possible to retrieve energy performance parameters, $\{\beta_i, T_{b,i}\}$, from all individual buildings and compare the population of available buildings. The results can be seen in Figure 2, where it can be noticed that, the base temperature, as well as the HLC, vary significantly from building to building. For reference, a global T_b has been computed fitting the classical fixed effects ES, using data from all schools simultaneously. Notice that, even though numerous buildings signature lie close to the global one, the differences between individual buildings vary significantly, with the HLC of some of the worst performers doubling the HLC of the best ones.

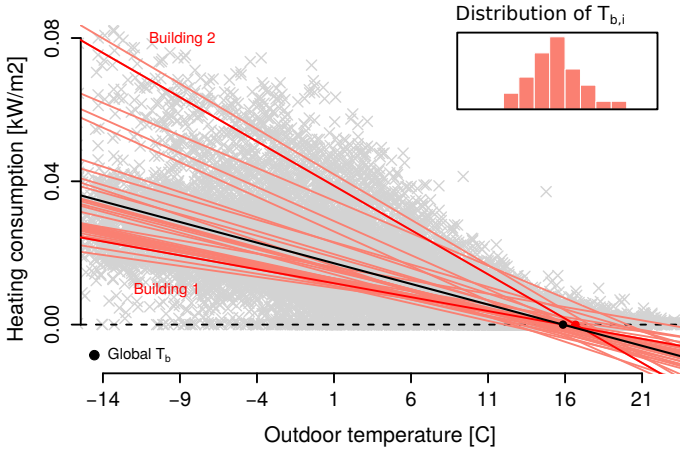

Figure 2: Energy signature for the total building population of regular schools. Two arbitrary buildings have been highlighted in red. It can be seen that the performance parameters change significantly from building to building.

4.2. Sampling energy profiles

The previous section showed that mixed models allow us to assess the differences across individual buildings that are present in the building population. This section, shows the results simulating the consumption of an unobserved school. This simulation is based on the model in Equation (6), that has been fit using data from 25 schools.

Figure 3 shows the model prediction given the temperatures of the month of February 2010; where, it can be noticed that the model simulation follows closely the trend of the test data. As expected, this trend shows clear peaks during the work days and a flatter trend during the weekends. The simulation under-predicts the highest peaks taking place in the morning of work days. When the morning peaks are captured, the valleys at night are over-predicted, which highlights the difficulty of capturing sudden changes in heat consumption.

Since the simulation is stochastic, the prediction interval (PI) of the simulation has been computed. As expected, this prediction interval shows a constant width during the whole time-series due to the assumption of normally distributed noise. It is easy to see that, in this February example, the prediction interval includes practically all test data points.

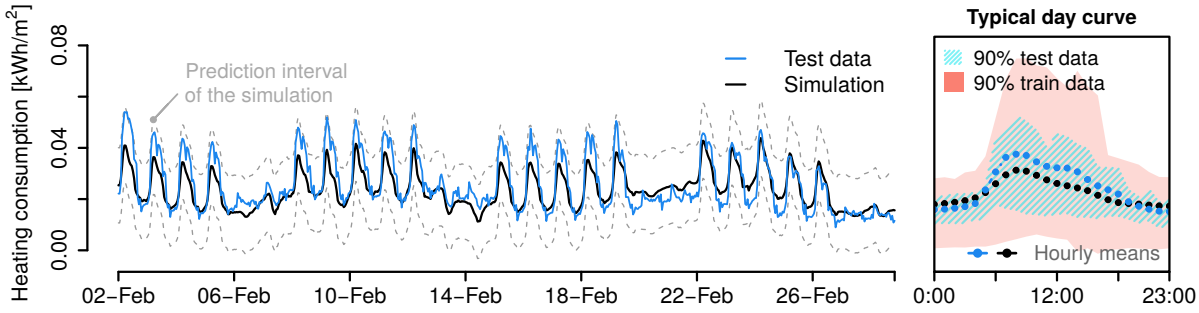

Figure 3: Comparison of the simulated data and a test set for the month of February 2010.

In addition, Figure 3 includes the daily profile of the prediction and the test data. It can be observed that the typical day curve of the simulation is lower than the testing data during the working hours. This damped trend in the simulation might be due to the range difference between the training and testing set. As it can be seen that the hourly range of data points of the training set is significantly wider than test set.

This model is fitted with data from all year round, so it has been possible to simulate heat consumption for every month. Figure 4 shows the typical daily consumption for every month of 2010. The simulated curve and the test curve follow a similar pattern during the colder months. Notice that the daily baseline consumption decreases during the summer, where only the hour effects are present. During June, July and August the test consumption is virtually zero, and the simulation still shows a low periodic hourly pattern. Nevertheless, Figure 4 also includes the percentage of test data points that fall inside the 90% prediction interval of the simulation. It can be seen that, for the whole year, practically all test data falls inside the expected region.

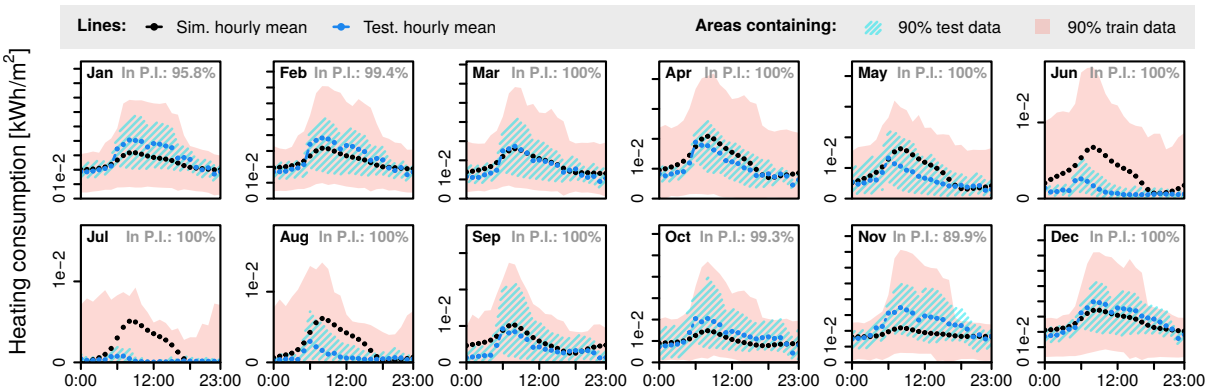

Figure 4: Typical days for every month of the year 2010. Every month includes the % of test data that falls inside the 90% prediction interval, denoted by "In P.I.".

5. Discussion

The results in this work show the potential of mixed effects models to be used to forecast long-term energy consumption of buildings. These models are a natural extension of fixed effects models, that have been proven successful in past work. Mixed effects are able, not only to generate a representative prediction of the heat consumption in buildings, but also they estimate the inherent uncertainty of the simulation due to non-measured events.

Fitting a mixed effects version of the energy signature, has showed that the range of energy performance varies significantly, even though all schools have the same efficiency label. This result highlights the importance of working with stochastic simulations, given the wide variety of energy performance in the building stock.

There is still room for improvement in the current version of the model. Although all test values fall inside the prediction interval, the simulation mean shows damped peaks, when compared to the test data. In addition, practically 100% of test data falls inside the 90% prediction interval; which hints that such interval should be narrower. Similarly, it can be seen that the interval is symmetric and constant. However, a more realistic model would have a prediction interval that: i) is asymmetric since consumption can only take positive values; and ii) is wider when consumption is expected to be higher. These limitations come from the assumption that the modelled data follows a gaussian distribution. In the future, different distribution families will be used, to take into account such issues. In addition, the dependence of the weather can be improved, to make the base temperature variable over the year, and then skip the need for fitting first the mixed effects energy signature. Despite the aforementioned issues, the results are promising enough and the next steps well defined to pursue further this methodology with a more complete model. Ultimately, given the generality of modelling with mixed effects, the work presented here can be extended to other building categories to simulate a broader energy landscape.

Acknowledgments

The authors would like to thank the Flexbuild project for providing the motivation, data and foundation to build this work on. In addition, funding from the Centre for IT-Intelligent Energy Systems in Cities (CITIES) and Flexible Energy Denmark (FED) have made possible this research.

References

[1] Carvallo J P, Larsen P H, Sanstad A H and Goldman C A 2018 *Energy Policy* **119** 410–422 URL `https://ideas.repec.org/a/eee/enepol/v119y2018icp410-422.html`

[2] Chen T and Wang Y C 2012 *International Journal of Electrical Power Energy Systems* **43** 454–464 ISSN 0142-0615 URL `https://www.sciencedirect.com/science/article/pii/S0142061512002645`

[3] Boßmann T, Elsland R, Lickert F and Wietschel M 2013 The german load curve in 2050: Structural changes through energy efficiency measures and their impacts on the electricity supply side

[4] Lindberg K, Seljom P, Madsen H, Fischer D and Korpås M 2019 *Utilities Policy* **58** 102–119 ISSN 0957-1787 URL `https://www.sciencedirect.com/science/article/pii/S0957178719300116`

[5] Pérez-Lombard L, Ortiz J and Pout C 2008 *Energy and Buildings* **40** 394–398 ISSN 0378-7788 URL `https://www.sciencedirect.com/science/article/pii/S0378778807001016`

[6] Taylor P G, d'Ortigue O L, Francoeur M and Trudeau N 2010 *Energy Policy* **38** 6463–6474 ISSN 0301-4215 energy Efficiency Policies and Strategies with regular papers. URL https://www.sciencedirect.com/science/article/pii/S0301421509003280

[7] Foucquier A, Robert S, Suard F, Stéphan L and Jay A 2013 *Renewable and Sustainable Energy Reviews* **23** 272–288 ISSN 1364-0321 URL https://www.sciencedirect.com/science/article/pii/S1364032113001536

[8] Hammarsten S 1987 *Applied Energy* **26** 97–110 ISSN 0306-2619 URL https://www.sciencedirect.com/science/article/pii/0306261987900122

[9] Rasmussen C, Bacher P, Calì D, Nielsen H and Madsen H 2020 *Energies* **13** ISSN 1996-1073

[10] Wolf S, Møller J K, Bitsch M A, Krogstie J and Madsen H 2019 *Energy and Buildings* **183** 672–683 ISSN 0378-7788 URL https://www.sciencedirect.com/science/article/pii/S0378778818320887

[11] Lindberg K, Bakker S and Sartori I 2019 *Utilities Policy* **58** 63–88 ISSN 0957-1787 URL https://www.sciencedirect.com/science/article/pii/S0957178719300128

[12] T K, C S, MG S and M E 2012 *Clinical Pharmacokinetics* **51** 512–515

[13] Madsen H and Thyregod P 2011 *Introduction to general and generalized linear models* Texts in statistical science (CRC Press) ISBN 9781420091557

Revealing the hidden dynamics of the energy signature model

Jaume Palmer Real[1], Christoffer Rasmussen[1], Davide Calì[1], Henrik Madsen[1]
[1]Department of Applied Mathematics and Computer Science
(Technical University of Denmark), Lyngby, Denmark

Abstract

The energy signature (ES) model is a well-known method to measure the energy performance of a building. This method uses coarse data aggregation that omits valuable information about the dynamics of the thermal elements of a building. This work presents a method to reconstruct these hidden dynamics without increasing the measuring complexity. The proposed method uses a state space formulation of the ES, that is filtered using hourly measurements of outdoor temperature and heat consumption. It is shown that the reconstructed state variable works as a proxy of the indoor temperature, and reacts to the weather conditions. These results highlight the potential of this method for real-time heating performance evaluation, as well as anomaly detection.

Key innovations

- Implementing a dynamical version of the energy signature method using high frequency measurements.
- Reconstructing a dynamic variable that is a proxy of the indoor temperature, i.e., measurements of the indoor air temperature are not needed.

Practical implications

High frequency data such as hourly resolution is required for the proposed method. Special attention should be put on the reliability of the estimated hidden proxy of the indoor temperature state for new case studies.

Introduction

The energy signature (ES) is a popular method used to characterize the heat loss of a building. As explained by Hammarsten (1987), the method uses linear regression to estimate a set of parameters that describe the energy performance of a building. In its simplest form, the ES has the following structure

$$\Phi = \begin{cases} \alpha_0 + \beta_0 T_{\text{out}} + \epsilon & \text{if heating period} \\ \Phi_0 + \epsilon & \text{otherwise} \end{cases}, \quad (1)$$

where Φ and T_{out} are the average heating power and outdoor temperature, respectively, during a period of time—typically 24 hours. Notice that the model presents two different regimes. The first regime corresponds to periods with heat demand, where the model is characterized by two parameters: α_0, which represents fixed passive heat losses; and the *heat loss coefficient*, β_0, that quantifies the heat losses to the outdoor air. The second regime corresponds to periods without heating demand. For buildings without a cooling system, such as the one used in this work, the heat load during this regime is characterized by a constant, Φ_0. Both regimes have the error term, $\epsilon \sim \mathcal{N}(0, \sigma_0)$; where σ_0 is an arbitrary standard deviation. The model in Equation (1) assumes that there is a constant outdoor temperature at which the building is in thermal balance; that is the *base temperature*, T_b. Then, the base temperature works as a boundary between both regimes: if $T_{out} < T_b$, there is heating demand, therefore the first regime is used; otherwise, the second regime is used. The model in Equation (1) is static and it is based on the assumption that, using coarse data aggregation, the contribution of dynamic elements of the building get smoothed out. Hence, fitting the model in Equation (1) reveals two key values: the previously introduced heat loss coefficient, and the base temperature. This static approach already provides valuable insight about the energy performance compared to other classic metrics like the A-temp (Rohdin et al. (2018)).

As data collection in buildings has become easier, more refined versions of the ES method have sprouted. For instance, Ghiaus (2006) compute the energy performance parameters using quantile regression, in order to ensure robustness of the estimates. Eriksson et al. (2020) proposed a method to fit the energy signature selecting night data from heating periods, which improved the parameter estimation. Rasmussen et al. (2020) used a smoothing function to create a smooth transition between the two regimes in Equation (1); this yielded a continuous model that can be fit using data from all year round. In addition, they suggested that the estimated base temperature is not constant, as they observe daily variations of

this parameter throughout the year.

Nevertheless, the heat load of buildings is affected by dynamic phenomena due to the inertia provided by the thermal mass of the building. Revealing the impact of such effects could help monitoring building energy performance, detect anomalies in real time or assess the potential of a building to be used as a short term thermal storage unit. Therefore, it is of interest to study the energy signature with higher time resolution. As already discussed by Hammarsten (1987), if faster dynamic effects are to be taken into account, the basic ES structure would be

$$\Phi_t = \Phi_{x,t} + \beta_0(T_{i,t} - T_{\text{out},t}) + C\frac{dT_i}{dt} + \epsilon_t\,, \qquad (2)$$

where the sub-index t has been added to highlight the dynamic nature of the expression. Compared to the static case, the most noticeable addition in Equation (2) is the indoor temperature, $T_{i,t}$, and its time derivative. In addition, the independent term α_0 has been substituted by $\Phi_{x,t}$, which represents passive heat losses in the building, which now change over time. This term represents a combination of all heat gains and losses that are not being modelled; examples of these could be infiltration, ventilation losses, solar gains or occupancy effects. These variables are often difficult to measure and identify, which is one of the main reasons that literature focuses on the static case.

This work aims to capture the information that is lost due to the static assumption. This is done by reconstructing a proxy variable that is representative of the indoor thermal conditions. In order to do so, the high resolution ES in Equation (2) is transformed into an auto-regressive model with exogenous inputs (ARX). This time-series approach has been widely used for characterizing the energy performance in buildings (Senave et al. (2019), Palmer et al. (2021)), and forecasting of energy load (Rasmussen et al. (2016)). Then, the ARX model is written in state space form, which allows to reconstruct non-observed variables using only measurements of heat consumption and outdoor temperature; i.e., without increasing the number of measured variables. These two variables can be collected non-intrusively, which would facilitate large scale applications of the method.

Method

In order to reconstruct the unobserved variables from Equation (2), it is necessary to transform the system to state space form. Then, a Kalman filter is used to estimate the unobserved state variables using the measurements of the observed variables. In addition, the parameters of the model need to be estimated, so the filtering process is wrapped around an optimization algorithm that estimates the model parameters by maximizing their likelihood. The outline of the method presented in this article can be seen in Figure 1. In this section, the transformation to state space and the subsequent optimization are presented. Lastly, the data used during the filtering process is described.

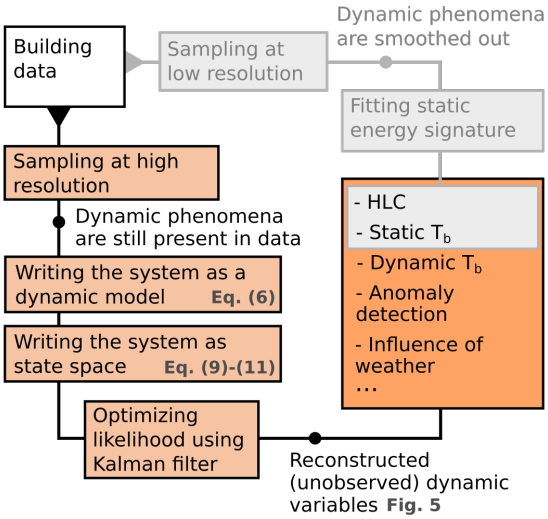

Figure 1: Flow chart of the suggested method. In grey, the classic approach. In color, the proposed alternative, that contains and expand the outcome of using the static Energy Signature

Dynamic model

Before writing the state space formulation of the high resolution ES, it is necessary to expand the current model to account for short term dynamics. First, a new variable is introduced, α_t, defined as

$$\alpha_t = \Phi_{x,t} + \beta_0 T_{i,t}\,. \qquad (3)$$

This variable quantifies the heat gains and losses inside the building, due to unmodelled effects. It also takes into account the influence that the current indoor temperature has on the heat load. Hence, α_t combines the variables that are often difficult to measure. This re-parametrization allows writing Equation (2) as

$$\Phi_t = \alpha_t - \beta_0 T_{\text{out},t} + C\frac{dT_i}{dt} + \epsilon_t\,. \qquad (4)$$

When the resolution is high enough, it is fair to assume that, the heating input is highly dependent of the heating input during previous time steps. Thus, a second order auto-regressive term has been added for the main variable. Then, the ES model becomes

$$\Phi_t = \alpha_t + \beta_1 T_{\text{out},t} + \varphi_1\Phi_{t-1} + \varphi_2\Phi_{t-2} + \epsilon_t\,. \qquad (5)$$

Where the coefficient that multiplies $T_{\text{out},t}$ has been changed from β_0 to β_1 since the parameter value will

change when changing the model structure. Additionally, the term $C\frac{dT_i}{dt}$ has been removed when transforming Equation (4) to Equation (5); given that, in a thermostatically-controlled building, such as the one used in this work, the changes of indoor temperature will be captured by Φ_t, Φ_{t-1} and Φ_{t-2}. Equation (5) represents an ARX model with the outdoor temperature as an input. In order to compare this model to the initial model in Equation (1), Equation (5) has been transformed to steady state. This is done by: i) introducing the backshift operator B (defined as $BX_t = X_{t-1}$, for an arbitrary random variable X_t), which yields

$$(1 - \varphi_1 B - \varphi_2 B^2)\Phi_t = \alpha_t + \beta_1 T_{\text{out},t} + \epsilon_t \,; \qquad (6)$$

and ii) writing the transfer function form and setting $B = 1$. This transformation of Equation (5) results in

$$\Phi_t = \tfrac{1}{1-\varphi_1-\varphi_2}\alpha_t + \tfrac{\beta_1}{1-\varphi_1-\varphi_2}T_{\text{out},t} + \tfrac{1}{1-\varphi_1-\varphi_2}\epsilon_t \,, \quad (7)$$

which can be re-parametrized to

$$\Phi_t = \bar{\alpha}_t + \bar{\beta} T_{\text{out},t} + \bar{\epsilon}_t \,. \qquad (8)$$

For more details on the steady state transformation, see Madsen (2007).

Notice that the structure in Equation (8) echoes the structure seen in the static ES in Equation (1). As shown in Figure 1, using the dynamic ES, it is still possible to retrieve the heat loss coefficient and the base temperature. However, in Equation (8), $\bar{\alpha}_t$ is a dynamic variable, instead of a constant intercept. Having access to this variable allows to study the dynamic variations of the heat consumption.

Kalman filter

Equation (5) already represents a high-resolution version of the energy signature, however α_t is not being observed. In order to reconstruct α_t, it is necessary to transform the system into state space form and use the Kalman filter. First, the state vector is defined as

$$\boldsymbol{X}_t = \begin{pmatrix} \Phi_t \\ \Phi_{t-1} \\ \alpha_t \end{pmatrix} \,; \qquad (9)$$

which contains all the information of the system at a given time. Then, it is possible to write Equation (5) as the following state space model:

$$\boldsymbol{X}_t = \boldsymbol{A}\boldsymbol{X}_{t-1} + \boldsymbol{B}\boldsymbol{U}_t + \boldsymbol{G}\boldsymbol{\varepsilon}_t \qquad (10)$$
$$\boldsymbol{Y}_t = \boldsymbol{C}\boldsymbol{Y}_{t-1} + e_t \,, \qquad (11)$$

where Equation (10) is the *system equation* and Equation (11) is the *observation equation*. Using this formulation, the elements of the system are

$$\boldsymbol{A} = \begin{pmatrix} \varphi_1 & \varphi_2 & 1 \\ 1 & 0 & 0 \\ 0 & 0 & 1 \end{pmatrix}, \boldsymbol{B} = \begin{pmatrix} \beta_1 \\ 0 \\ 0 \end{pmatrix},$$
$$\boldsymbol{G} = \begin{pmatrix} 1 & 0 \\ 0 & 0 \\ 0 & 1 \end{pmatrix}, \boldsymbol{U} = \begin{pmatrix} T_{\text{out},t} \end{pmatrix}$$
$$\text{and } \boldsymbol{C} = \begin{pmatrix} 1 & 0 & 0 \end{pmatrix}.$$

Lastly, $e_t \sim \mathcal{N}(0, \sigma_e)$ and $\boldsymbol{\varepsilon_t} = (\epsilon_t \ \omega_t)^\top$, which is a two-dimensional normally distributed variable with variance-covariance matrix,

$$\boldsymbol{\Sigma}_1 = \begin{pmatrix} \sigma_\epsilon^2 & 0 \\ 0 & \sigma_\omega^2 \end{pmatrix}.$$

Notice that α_t is a random walk,

$$\alpha_t = \alpha_{t-1} + \omega_t \,, \qquad (12)$$

with $\omega_t \sim \mathcal{N}(0, \sigma_\omega)$. This formulation allows α_t to adapt to the measured observations of $T_{\text{out},t}$ and Φ_t, within the bounds dictated by the model structure of Equations (10) and (11).

Optimization

The main model described in Equation (5) is characterized by the set of parameters $\boldsymbol{\theta} = \{\varphi_1, \varphi_2, \beta_1, \sigma_\epsilon, \sigma_\omega, \sigma_e\}$. These parameters can be estimated by maximizing the log-likelihood of $\boldsymbol{\theta}$ ($\log L(\boldsymbol{\theta})$), as explained in detail by Rouchier (2018). Using this approach, the parameter estimator is defined as

$$\hat{\boldsymbol{\theta}} = \left\{ \max_{\boldsymbol{\theta}} \log L(\boldsymbol{\theta}; \mathcal{Y}_{N^*}) \right\}, \qquad (13)$$

where $L(\boldsymbol{\theta}; \mathcal{Y}_{N^*})$ is the conditional likelihood given the observations of the states. In practical terms, this means that the filtering process is wrapped in an unconstrained optimization routine that has $L(\boldsymbol{\theta}; \mathcal{Y}_{N^*})$ as cost function. When using the Kalman filter, this cost function is computed using the one-step prediction errors as described by Madsen (2007). Finally, the process is filtered using $\hat{\boldsymbol{\theta}}$ to reconstruct the state variables.

Data description

The data used in this work comes from an experiment realized in a test building at the Fraunhofer-Institut in Holzkirchen, Germany, part of International Energy Agency's Energy in Buildings and Communities Programme (IEA EBC), Annex 71 (Kersken and

Strachan (2019); Roels (2020)). A two-storey single family house was monitored during the experiment that lasted one month, starting December 2018. The house was unoccupied and equipped with multiple sensors and equipment to monitor and mimic real-living condition. The measured variables included: heat load from electric heaters, weather variables, indoor air from different rooms, ventilation flow rates and humidity. The heat load is divided in two categories: heating dedicated to space heating and heating to simulate the heat generated by occupants. All measures were taken every 10 minutes, and they have been aggregated to hourly values. In this work, the variables used are the electric heating input from different heaters $[kW]$ and outdoor temperature $[C]$. Afterwards, indoor temperature measurements are used for validating the results from α_t. Figure 2 shows a 5 days period of the data used. It can be seen that there are two clear heating patterns: the building is regularly heated during the day, and the heat is turned off during the night.

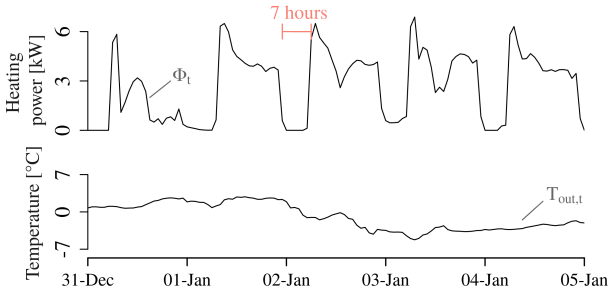

Figure 2: Subset of the data used in this work. A clear night-setback pattern can be observed in the heat consumption.

Pursuing generality, the entire test building has been treated as a single unit. Hence, the heat load from different electric heaters have been aggregated to constitute the main dependent variable, Φ_t. Those heaters are electric, they are located in the different rooms of the house, and they are the main source of space heating. Other sources of heat, such as artificial occupants and solar gains, have been disregarded and are not part of Φ_t. Similarly, this work focuses on the analysis of one single output variable, which is the re-constructed α_t. Hence, this work characterizes the whole test building by its hourly heat consumption, and the output α_t. Figure 3 shows a schematic representation of the approach followed in this work, using an arbitrary floor-plan.

Results

In order to validate the results, first the residuals of the model in Equation (10) and (11) are presented. Afterwards, the re-constructed state variable α_t, from the state vector in Expression (9), is analyzed.

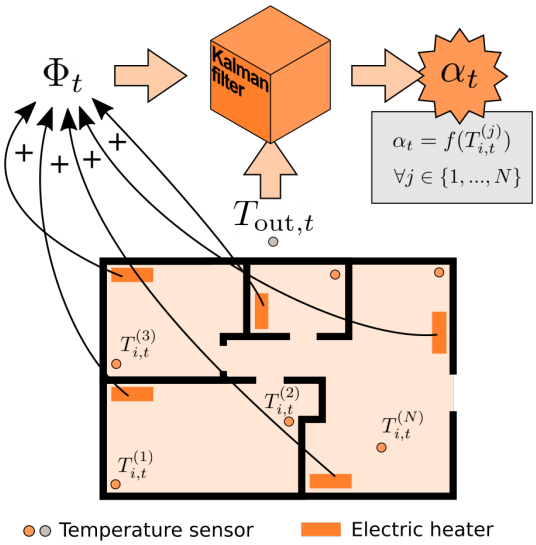

Figure 3: Sketch of the procedure. The studied house is treated as a single unit, with the aggregated consumption from all heaters as dependent variable.

Analysis of residuals

After applying the Kalman filter to the model in Equations (10) and (11), the resulting one-step prediction errors are depicted in Figure 4. It can be observed that the residuals are clearly non-gaussian, due to the regular spike pattern they present. When checking the auto-correlation function (ACF) and partial auto-correlation function (PACF), it can be seen that the value at lags 7, 17 and 24 are high, whereas the rest fall very close to the 95% confidence interval. The peaks are caused by the scheduled heating of the building, which is turned off at night during a 7-hour period, as shown in Figure 2. These daily variations have not been introduced in the modelling process, therefore it is not surprising to see this pattern in the residuals. Nevertheless, the rest of the lag values in the ACF and PACF fall very close of the confidence interval. Thus, the cause of the non-gaussian effects in the residuals has been identified. Therefore, as a preliminary result, we claim that the rest of the relevant dynamics have been captured.

Figure 5 shows the hourly distribution of the residuals. Notice that during night hours, when the heating system is turned off, the model tends to over-predict the heat load. This phenomenon causes a distinct pattern in the residuals, where the hourly residuals are significantly less spread than during the rest of the day. During night hours the heat is turned off; then, recalling Equation (5), the contribution of the auto-regressive terms is not present. Additionally, the outdoor temperature contribution is fairly constant due to its slow dynamics. These combined suggests that, the decaying pattern in the night residuals is caused mainly by α_t.

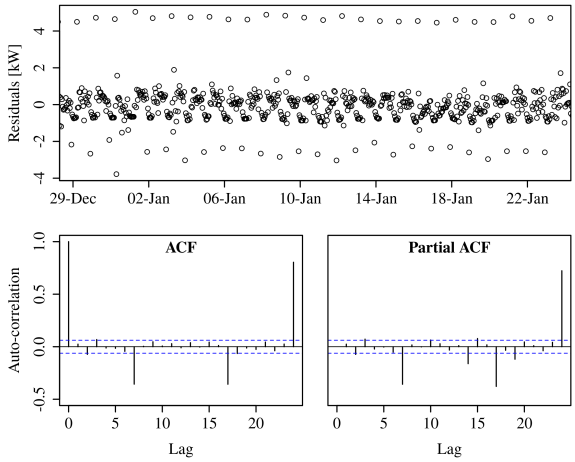

Figure 4: Residual analysis after using the Kalman filter. The residuals are centered around 0 with constant variance, except for a periodic pattern caused by the setback schedule. This can be observed in the ACF and PACF which have only three important peaks at lag 7,17 and 24.

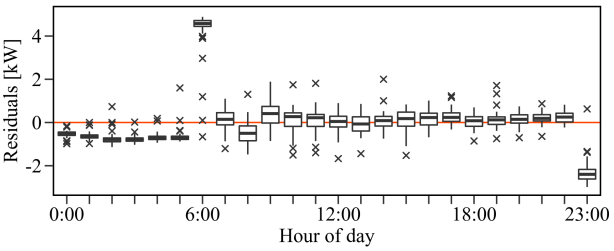

Figure 5: Hourly distribution of the residuals after using the Kalman filter. The residuals are centered around 0 during the day, but they show a decaying pattern during night.

Analysis of α_t

Figure 6 shows the reconstructed variable $\bar{\alpha}_t$ for a period over 3 weeks. It can be seen that the variations of $\bar{\alpha}_t$ are centered around the static parameter α_0. When $\bar{\alpha}_t$ is aggregated to coarser resolution, it converges to the static α_0. The reconstructed variable shows a periodic pattern, that falls during night hours and is maintained fairly constant during the day, following the heating pattern observed in Figure 2.

Additionally, it has been possible to compare the value of the model parameters for the static and dynamic cases, which can be seen in Table 1. Notice that the static parameter, α_0, is compared to the mean of $\bar{\alpha}_t$ over the filtering interval, $\bar{\bar{\alpha}} = \frac{\sum_{t=1}^{T} \bar{\alpha}_t}{T}$, where T is the number of data points. As hinted by Figure 6, α_0 is approximately the mean of $\bar{\alpha}_t$. On the other hand, the value of heat loss coefficient in the dynamic and static case are practically the same, i.e. $\beta_0 \approx \bar{\beta}$. In addition, table 1 shows that the uncertainty of the dynamic model estimators are always larger than the static case. This increase is a consequence of the larger number of parameters to

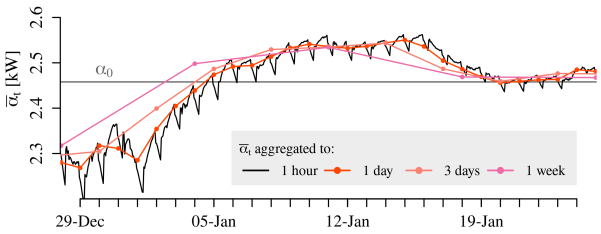

Figure 6: Evolution of the variable $\bar{\alpha}_t$ compared to the static parameter α_0. In color, different aggregation levels of $\bar{\alpha}_t$.

estimate through the filtering process: $\bar{\bar{\alpha}}$ and $\bar{\beta}$ are function of the estimated parameters $\{\beta, \varphi_1, \varphi_2\}$, and the random walk, α_t.

Table 1: Parameter estimates comparison between dynamic and static models. In parentheses, the standard deviation of the parameter estimators.

	Static ES	**Dynamic ES**
α [kW]	α_0	$\bar{\bar{\alpha}}$
	2.46 (0.07)	2.48 (0.16)
β [kW/K]	β_0	$\bar{\beta}$
	0.064 (0.019)	0.065 (0.026)

Now, departing from Equation (8), and recalling the definition of α_t in Equation (3), it is possible to define the indoor temperature as a function of α_t and the other internal heat gains and losses,

$$\hat{T}_{i,t} = \frac{\alpha_t - \Phi_{x,t}}{\beta_1} \,. \tag{14}$$

For now, the contribution of $\Phi_{x,t}$ to Equation (14) is difficult to assess, and that is out of the scope of this work. Then, in order to compare $\hat{T}_{i,t}$ to real measurements of the indoor temperature, it has been assumed that the $\Phi_{x,t}$ is a constant value $K \approx 0.35$ kW. The value of K has been chosen arbitrarily to make $\hat{T}_{i,t} \approx 21$ °C and facilitate visualization; nevertheless, the order of magnitude of K matches the expected losses in a system such as the one studied in this work. Figure 7 compares $\hat{T}_{i,t}(\alpha_t, K)$ to measurements from sensors located at 40 different positions in the house. It can be seen that the reconstructed variable follows the same pattern as the indoor temperature: showing flat periods during the daylight hours, and a decay pattern during the night, when the heating system is turned off. Notice that, comparing to $\hat{T}_{i,t}$, the measured indoor temperature has larger decays at night. This difference is caused by the assumption that α_t is a normally-distributed random walk, while the heating data is clearly non-gaussian. This damped decay in α_t was already hinted in Figure 5, where it can be noticed the residuals are systematically negative at night, highlighting that during those hours, the model tend to over-predict.

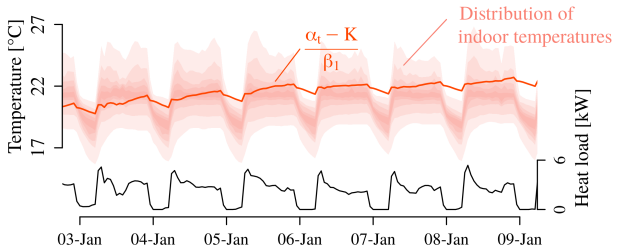

Figure 7: Comparison of the indoor temperature, and the re-constructed α_t, with $K = 0.35$ kW. Indoor temperature is measured in $N = 40$ different locations and, for every hour, the quantile distribution is shown.

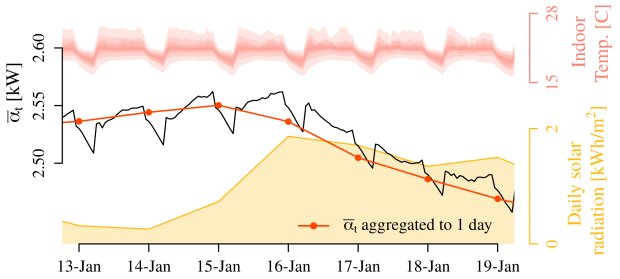

Figure 8: Comparison of the reconstructed $\bar{\alpha}_t$ and the daily solar radiation. The distribution of indoor temperatures is shown at the top of the figure.

As said earlier, $\Phi_{x,t}$ represents the heat gains in the building that are not part of the model. Even though its exact structure is not known, we know that a big contributor to the heat gains of a building comes from the solar radiation. Comparing the solar radiation and the evolution of α_t confirms this hypothesis, as there is a clear correlation between both variables. This can be seen in Figure 8, where $\bar{\alpha}_t$ decreases when the solar radiation increases. Additionally, notice that the indoor temperature is kept constant during the same interval. This echoes the relationship between the $\bar{\alpha}_t$ and the base temperature $T_{b,t}$: when the solar gains are high, the outdoor temperature at which the building is in thermal balance, will decrease.

Conclusion

Based on solely hourly heat consumption and outdoor temperature time series measurements, this work has proposed a method to reconstruct the hidden dynamics—i.e. the indoor temperature and the remaining unknown net heat gain consisting of solar gain, ventilation loss, etc.—that impact on the heating load of a building.

Departing from the classical energy signature method, a state space model was fitted to reveal the effects that were not accounted for explicitly in the model. This approach represent a non-intrusive way of monitoring the energy performance of a building, where the variations of the indoor temperature, unknown heat losses and gains, are captured in the proxy variable α_t. The estimated variable α_t reveals that assuming a constant base temperature can be an over-simplification; given that, α_t presents significant hourly and daily variations. This variable, that was reconstructed using only weather and heating consumption data, has been shown to replicate the fluctuating indoor temperature to a high extent, given an average unobserved net heat gain of 350 watts. The dynamic behaviour of this reconstructed variable, α_t, displays a plateau during the daylight hours, followed by a decay during the night, echoing the night setback of the indoor temperature.

The lack of indoor information is a common issue when monitoring the energy usage of a building. This opacity complicates assessing the portion of the heat load that is due to poor energy performance or simply caused by occupants' preferences. The method presented in this work allows computing the thermal building performance parameters, as well as a reconstructed variable that provides insight of the thermal state inside the building, without increasing the data requirements. Moreover, since the energy signature is translated into a dynamic model, the time resolution can be increased and the measuring period shorted. The aforementioned reasons, and the reduced number of variables involved, make the method easier to apply at large scale, compared to other alternatives for evaluating energy performance. This is specially relevant, considering that the presented method avoids using the indoor temperature, which often represents a variable difficult to capture reliably.

The proposed model still has room for improvement. The analysis of residuals showed that the model fails to reconstruct the dynamics of the system at night; which is due to the non-gaussian structure of the heat consumption.The choice of α_t as a random walk is not well suited for the abrupt changes that take place around 23:00 and 06:00 every day. Moreover, the performance parameters shown a larger uncertainty than in the static case. Nevertheless, the authors believe that the uncertainty is mainly caused by the quality of the data used, and the parameters are still representative of the building heating performance. The next steps to take in this direction, will be to improve the model so it can incorporate the setback schedule that was present in the data. Furthermore, the model will need to be tested in different data sets, to validate its generality. Finally, more weather variables will be incorporated into the state space model as done by Rasmussen et al. (2020), to evaluate their influence over the α_t variable. Understanding the effects of other external variables over α_t, will allow to get better insight of the indoor temperature and overall heating performance, using only the minimum measurements.

Acknowledgment

The authors would like to thank four different projects that have made this research possible: Centre for IT-Intelligent Energy Systems in Cities (CITIES), Flexible Energy Denmark (FED), Flexbuild, and the IEA EBC Annex 71 for providing the data.

References

Eriksson, M., J. Akander, and B. Moshfegh (2020). Development and validation of energy signature method – case study on a multi-family building in sweden before and after deep renovation. *Energy and Buildings 210*, 109756.

Ghiaus, C. (2006). Experimental estimation of building energy performance by robust regression. *Energy and Buildings 38*(6), 582 – 587.

Hammarsten, S. (1987). A critical appraisal of energy-signature models. *Applied Energy 26*(2), 97 – 110.

Annex 71 (2019). *Empirical Whole Model Validation – Modelling Specification –Twin House Experiment*.

Madsen, H. (2007). *Time Series Analysis*. Chapman Hall.

Palmer, J., C. Rasmussen, R. Li, K. Leerbeck, O. Jensen, K. Wittchen, and H. Madsen (2021). Characterisation of thermal energy dynamics of residential buildings with scarce data. *Energy and Buildings 230*.

Rasmussen, C., P. Bacher, D. Calì, H. Nielsen, and H. Madsen (2020). Method for scalable and automatised thermal building performance documentation and screening. *Energies 13*(15).

Rasmussen, L. B., P. Bacher, H. Madsen, H. A. Nielsen, C. Heerup, and T. Green (2016). Load forecasting of supermarket refrigeration. *Applied Energy 163*, 32 – 40.

Roels, S. (2020). Ebc annex 71.

Rohdin, P., V. Milic, M. Wahlqvist, and B. Moshfegh (2018, 09). On the use of change-point models to describe the energy performance of historic buildings.

Rouchier, S. (2018). Solving inverse problems in building physics: An overview of guidelines for a careful and optimal use of data. *Energy and Buildings 166*, 178 – 195.

Senave, M., G. Reynders, P. Bacher, S. Roels, S. Verbeke, and D. Saelens (2019). Towards the characterization of the heat loss coefficient via on-board monitoring: Physical interpretation of ARX model coefficients. *Energy and Buildings 195*, 180 – 194.

A data-driven framework for characterising building archetypes: a mixed effects modelling approach

Jaume Palmer Real[a,*], Jan Kloppenborg Møller[a], Rongling Li[b], Henrik Madsen[a,c]

[a] *Department of Applied Mathematics and Computer Science*
Technical University of Denmark

[b] *Department of Civil Engineering*
Technical University of Denmark

[c] *FME-ZEN, Norwegian University of Science and Technology*

Abstract

Building archetypes are a common solution to study the energy demand of cities and districts. These are generally based on building information such as construction year and function. However, there can be large differences in the energy demand of buildings of the same archetype due to factors such as the preferences of occupants, quality of the building construction, and unrecorded renovations. This work uses a non-linear mixed effects model to capture these random differences. The model uses weather measurements to generate the daily heating load of buildings for the whole year. The model is generated and tested using data from 56 Norwegian apartments. Results show that 91% of measurements from an out-of-sample test set fall inside the 95% prediction interval. Additionally, the model allows us to compute a proxy of the heat loss coefficient, which characterises the heating performance of the population of apartments. Finally, two sub-categories of apartments are identified by clustering the model estimates for the studied population. The model is general, computationally light and uses existing data that are commonly collected in many buildings. The suggested method offers a more robust and reliable method to segment building archetypes using only weather data and energy demand.

Keywords: Building archetype, thermal characterisation, mixed-effects modelling, data-driven modelling

Nomenclature

Acronyms

ES	Energy signature
EUI	Energy use index, kWh/m^2
GMM	Gaussian mixture model
HLC	Heat loss coefficient, kW/^{o}C
ME	Mixed effects
UBEM	Urban building energy model

Indices

i	Observation/measure
k	Individual building

Variables

Φ	Heat load, kW/m^2
Φ^{sol}	Solar irradiation, W/m^2
T^{out}	Outdoor temperature, ^{o}C
W^{s}	Wind speed, m/s

1. Introduction

Around 55% of the world's population live in cities, and this number is expected to increase to 70% by 2050 [1]. This implies higher energy demand in concentrated areas, thus meticulous planning is necessary to guarantee sustainable growth. Moreover, a city is a complex system, and to increase its sustainability, it is necessary to understand its components and how they interact. Buildings are a key factor to manage when planning the energy use in cities; they represent 40% of the total energy demand in urban areas. Therefore, increasing buildings' efficiency will reduce total energy use considerably. In addition, buildings can be used to balance the energy supply grid by using strategies such as demand response facilitated by smart infrastructures [2]. When modelling districts and cities, the inclusion of individual buildings is challenging, as this increases the complexity of the model. A potential solution to this is using urban building energy models (UBEM), which aim to divide the building stock into categories (*segmentation*) and capture their attributes to simulate a typical consumption of each category of building (*characterisation*) [3].

In general, the categorisation is based on qualitative attributes of the buildings, such as the year of construction, location and the functionality. In each category, a building model is calibrated to simulate the energy consumption of the specific category [4]. Often, the building models used are based on

*Corresponding Author
Email address: jpre@dtu.dk
Postal Address: Anker Engelunds vej 1, Building 101A, 2800 Kongens Lyngby, Denmark

previously identified archetypes, which are deterministic models that disregard the variability of the heat consumption inside each category. However, buildings that are grouped based on qualitative or quantitative characteristics, such as their usage or year of construction, present significantly different heat responses [5, 6]. The causes behind these differences in energy use inside a building can be difficult to identify. They may include occupant behaviour, different geometry, or renovations that have not been declared [7, 8]. The effects of occupants have been evaluated through measurements of CO2 concentration [9], tracking appliance usage [10] or survey activity diaries [11]. Assessing the effects of geometry and renovation requires data about the building construction that may not be up to date or even accessible. Thus, monitoring the possible sources of uncertainty is not always an option.

This study proposes using random effects to model the energy consumption of a population of similar buildings. The focus is set to characterise the heating load and generate stochastic simulations; thus, we pursue a reduced-order model that can be easily interpreted. Instead of seeking a model structure that relies on extensive measured variables to incorporate the causes behind differences in building consumption, this study accepts those differences and aims to quantify their impact using limited data that is easy to access.

1.1. Review of hierarchical methods in building modelling

Random effects are used to model and quantify random differences between individuals in a population. Often, they are used to model the inner sample variations in clinical studies [12]. In buildings science, a similar example is found in the work by Rupp et al. [13], where they used random effects to model impact of the occupants on the heating of an office in a sub-tropical city in Brazil. In their work, they identified parameters that determine the level of comfort of the office workers, such as the habit of drinking hot beverages or wearing warm clothing. Since these attributes depend on individual preferences, random effects were added to the model to account for them.

Random effects were also explored by Capozzoli et al. [14] when they used a linear mixed effects model (LMEM) to simulate the annual energy consumption of healthcare buildings in northern Italy. The mixed effects structure allowed them to characterise a big ensemble of buildings with a single model and capture their common attributes, despite the buildings presenting qualitative differences. However, their model is only able to simulate annual values, and it is designed for coarse energy benchmarking. The model proposed in the present work uses daily values and takes into account the weather's influence, thereby offering a richer simulation of the heating demands of building categories.

Palmer et al. [15] presented a linear model that used random effects to simulate stochastic hourly profiles of building categories. The model was an extension of the work done by Lindberg, Bakker, and Sartori [16] that developed a linear fixed effect model to simulate the above-mentioned energy profiles. The model by Palmer et al. [15] was linear and the uncertainty was purely Gaussian, which limited the overall performance of the simulation tool.

Mixed effects models are often formulated as hierarchical models, where a random variable that describes a subset of a population is nested inside a broader and more general model. Cerezo et al. [17] compared methods to characterise building archetypes to simulate yearly consumption. Starting with a physics-based archetype model, they assigned a probability distribution to its most uncertain parameters; later, they calibrated these parameters using a Bayesian approach. Their work showed that a model based on this stochastic calibration provided more reliable simulation results than a purely deterministic method. The work by Cerezo et al. [17] was continued by Sokol, Davila, and Reinhart [18], using a similar approach to a different group of buildings in a different climate. In this way, they validated the concept of using a hierarchical structure to define building archetypes. Additionally, they repeated the experiment using yearly and monthly values of energy consumption and found that simulating monthly values and later aggregating provides more accurate estimation of the distribution of heating loads.

Kristensen, Hedegaard, and Petersen [19] suggested a hierarchical approach to model a population of Danish houses. In their work, they used a complex building model that returns the hourly energy use. Given the model complexity, it was only feasible to calibrate a subgroup of the model parameters for a segmented building population. De Jaeger, Lago, and Saelens [20] proposed a stochastic characterisation of the thermal performance of buildings by estimating the probability distribution of the U-values for different Flemish building categories. To perform such a study, they needed to have access to a region-wide energy certificate database.

Gholami et al. [21] used a Bayesian calibration method to tune 11 different building archetypes from a neighbourhood in the Italian city of Bologna. Their results showed robust long-term prediction with an improvement in the computational requirements. Still, their study focused on the annual energy use index (EUI) and relied on a model structure provided by the building modelling software Energy+.

A trend can be observed in the previous studies reviewed here: they focus on assigning a density distribution to a subset of parameters using established archetype building models, and these distributions are then calibrated, so the building models account for random differences within building categories. In the present study, the differences between buildings are captured by the random effects, as part of a reduced-order model. The model is based on a non-linear sigmoid-based energy signature that, as stated by Nageler et al. [22], gives reliable simulation results when heating measurements are available. The model uses daily energy consumption and weather data as input and can simulate the daily heating load continuously for the whole year. Since the uncertainty caused by buildings' differences is captured, it is separated from other sources of noise, which renders the model fit more reliable.

The proposed model highlights the potential of mixed effects (ME) models to study building populations. Instead of limiting the use of hierarchical models for calibration of known

building models, ME models can be developed in more general model structures to satisfy specific goals; in this case, the simulation of daily heating load and the characterisation of the weather response of a category of buildings. The flexibility of this framework is a valuable asset to develop reliable and representative models for large districts and cities.

1.2. Paper outline

This paper is organised as follows. Section 2 introduces the modelling method where, first, the non-linear model is presented for one single building; then, the model is extended with the addition of random effects to model a building population. To introduce the reader to the concept of random effects, Section 2.2.1 presents an example studying the annual energy demand of a population of schools. Section 3 presents the main findings of this work and is divided in two sub-sections: first, a fixed effects (FE) non-linear model is presented to study the heating load pattern of an individual building and a detailed description of the model is given to assess the quality of the fit. The FE model is extended with the addition of random effects, which converts it into a mixed effects (ME) model. Figure 1 schematically presents the workflow of this section, where one can see that the outcome of the ME model is two-fold. On the one hand, the ME model allows a richer study of the known set of buildings used to train the model (*profiling*); on the other hand, the ME model is used to generate new observations of buildings (*sampling*), i.e., simulating unknown buildings. Section 4 uses the outcome of the profiling to refine the segmentation of the initial population of buildings. Finally, Section 5 discusses the major outcomes of this work.

2. Methods

This section introduces the model structure to model one single building. Later, the model is extended to account for the whole category.

2.1. One building: a continuous energy signature

The heating needs of buildings change throughout the year as they are affected by weather conditions, which as a first approximation can be represented by the outdoor temperature; thus, the outdoor temperature is considered the main driver of the heating demand. In absence of cooling, the heating load of a building presents the following trend: when the outdoor temperature is high enough and there are no other heating requirements, the heating load of a building is zero; as temperature decreases, the load starts to increase; eventually, in the coldest period of the year, the heating load curve will flatten out because the heating system reaches its capacity. Qualitatively, this heating behaviour matches a monotonic increase between two plateaus: one at zero heating demand and one at the maximum heating capacity. This S-shape behaviour can be modelled by a sigmoid curve, a model found in numerous and diverse systems. Such curves are continuous functions that are characterized using a small number of parameters.

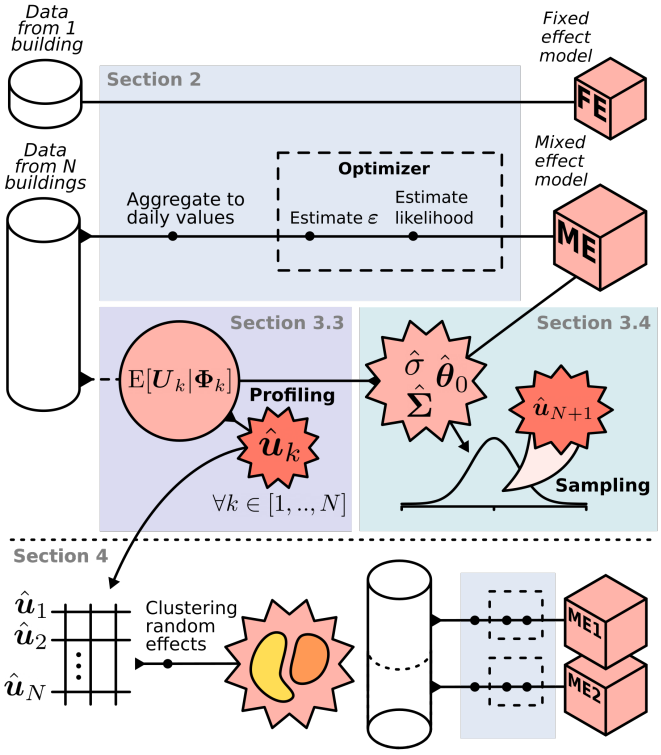

Figure 1: Flowchart showing the main blocks of this work.

A specific type of sigmoid is the Gompertz curve. This model has typically been used to model population growth in biological systems [23], although it has also been used to model wind power curves [24]. This model has the following structure

$$y = Ae^{-e^{-C(x-Q)}}, \tag{1}$$

which describes a continuous curve that starts at $y = 0$ (at $x = \infty$) and eventually reaches a horizontal asymptote. This curve is characterised by three parameters: $A > 0$ represents the upper asymptote (at $x = -\infty$), C gives the growth rate from 0 to A, lastly, Q acts as a horizontal offset of the curve. The function from Equation (1) can be seen in Figure 2, where different combinations of its parameters have been plotted to visualise their effects on the shape of the curve.

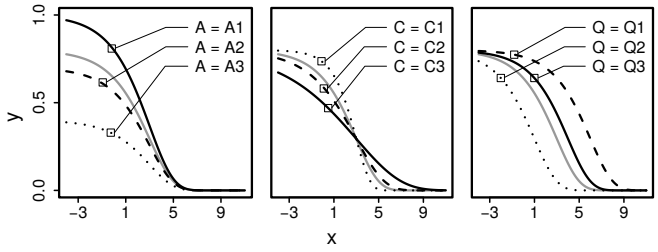

Figure 2: Comparison of different Gompertz curves for arbitrary values of its defining parameters.

In this study, Equation (1) is used to model the heating load curve of a building, where y represents the heating load of a

building, Φ, and x is the outdoor temperature, T^{out}. Then, Equation (1) becomes

$$\Phi_i = A \exp[-\exp(-C(T_i^{\text{out}} - Q))] + \varepsilon_i \,, \tag{2}$$

where the notation is changed to improve the readability. In Equation (2), the sub-index i represents the ith observation of the heating load and the outdoor temperature; in addition, a noise term is added, which is represented by the random variable $\varepsilon_i \sim N(0, \sigma^2)$.

The parameters $\{A, C, Q\}$ describe how the daily heating demand changes with the outdoor air temperature; still, this temperature is coupled with other climatic variables that affect the heating load of a building. In this work, we modelled these effects by defining $\{A, C, Q\}$ as a function of the weather conditions. As introduced in Figure 2, each of these three parameters defines a distinct attribute of the heating load curve, so each parameter has been handled separately as follows:

- The parameter A represents the heating capacity, thus it is defined as constant regardless of the weather conditions.
- The parameter C characterises the slope of the heating load curve. This dependence echoes the heat loss coefficient, which is often influenced by the wind conditions [25]. For this reason, the parameter C is modelled as a linear function of the wind speed, W^{s}, such that

$$C \rightarrow C(W^{\text{s}}) = \alpha + \beta W^{\text{s}} \,. \tag{3}$$

- The parameter Q horizontally shifts the heating load curve, which represents the passive heat gains and losses in the building. In particular, the effects of solar irradiation are a major contributor of the heat gains in highly insulated buildings [26]. For this reason, the parameter Q is defined as a function of the solar irradiation, $Q(\Phi^{\text{sol}})$. This relationship might not have an explicit expression, since the effects of the solar irradiation depend on variables such as the incidence angle or the shading of nearby objects. Here, we use B-spline curves to capture the non-linear effects of the solar irradiation on the heating of a building. Thus, the parameter $Q(\Phi^{\text{sol}})$ is defined as

$$Q \rightarrow Q(\Phi^{\text{sol}}) = \sum_i^n b_i B(\Phi^{\text{sol}}) \,, \tag{4}$$

  where n is the chosen number of spline curves, $B(\cdot)$ the basis spline function and $b_i \; \forall i \in [1, .., n]$ are scalar parameters representing the weight of each spline curve. The use of spline curves offers flexibility to model complex relationships between variables; more information on their application is found in the work of Rasmussen et al. [27].

The newly defined $\{A, C(W^{\text{s}}), Q(\Phi^{\text{sol}})\}$ introduced a lower level of parameters, namely $\boldsymbol{\theta} = \{A, \alpha, \beta, b_1, ..., b_n\}$ which represents the fixed effects parameter vector of the proposed model:

$$\Phi_i = A \exp\left[-\exp\left[\left(\alpha + \beta W_i^{\text{s}}\right)\left(T_i^{\text{out}} - \sum_i^n b_i B(\Phi_i^{\text{sol}})\right)\right]\right] + \varepsilon_i \,. \tag{5}$$

Notice that Equation (5) has the same non-linear structure as Equation (1). Thus, for the sake of clarity, the final model can be re-written as

$$\Phi_i = A \exp\left[-\exp\left(-C(W_i^{\text{s}})\left(T_i^{\text{out}} - Q(\Phi_i^{\text{sol}})\right)\right)\right] + \varepsilon_i \,, \tag{6}$$

where the parameters $\{C(W^{\text{s}}), Q(\Phi^{\text{sol}})\}$ are given by Equations (3)-(4).

2.1.1. Interpretability

The model introduced in Equation (6) captures the dependence of the heating load on the outdoor temperature, wind speed and solar irradiation. Often, the dependence between the heating load of a building and the weather conditions is modelled using a piece-wise differentiable model known as the *energy signature* (ES), which is a well known method to assess the thermal performance of buildings [28]. For buildings without cooling, such as the ones studied in this work, this model has the following expression

$$\Phi_i = \begin{cases} HLC \cdot (T_b - T_i^{\text{out}}) + \epsilon_i & \text{if heating period} \\ 0 & \text{otherwise} \end{cases} \,, \tag{7}$$

where $\{T_b, HLC\}$ are model parameters and ϵ_i represents independent and identically normally distributed residuals. In Equation (7), the parameter HLC stands for the *heat loss coefficient*, a performance indicator to evaluate the thermal insulation of the envelope of the building. Thus, the energy signature assumes a linear relationship between the heating load and the outdoor temperature in the heating regime. The change of regime in Equation (7) depends on the relationship between the outdoor air temperature and the parameter T_b: if $T^{\text{out}} < T_b$ the building requires heat to maintain comfortable indoor conditions; typically in Norwegian buildings $T_b \approx 17^{\text{o}}C$ [29]. Hence, the classic ES requires prior knowledge from the modeller to be able to separate the different heating regimes and adjust the fitting of the curve [30].

The model introduced in this work is continuous and presents a smooth transition between heating regimes. As shown in Equation (6), the model has the following structure

$$\Phi_i = f(T_i^{\text{out}}, \Phi_i^{\text{sol}}, W_i^{\text{s}}) + \varepsilon_i \,, \tag{8}$$

where $f(\cdot)$ captures the weather dependence of the heating load. This makes it possible to define

$$g(T_i^{\text{out}}, \Phi_i^{\text{sol}}, W_i^{\text{s}}) = \frac{\partial f}{\partial T^{\text{out}}} \,, \tag{9}$$

a closed form continuous function that is completely described by the parameter $\{A, C(W^{\text{s}}), Q(\Phi^{\text{sol}})\}$.

The function in Equation (9) describes the change rate between the heating load and the outdoor temperature, and it can be used to compute a proxy of the classic HLC. Yet, HLC is a constant parameter, whereas $g(\cdot)$ is a continuous function that is defined for the whole range of weather variables. As seen in Figure 2, the Gompertz curve presents three different regions: two plateaus at the ends, and a slope in the middle. Near the inflection point, the middle region of the Gompertz function is well approximated by a linear model. Then, we define $HLC^* = g(T^{\text{out}*})$, where $T^{\text{out}*}$ is the outdoor temperature at the inflection point of $f(\cdot)$. Hence, physical information about the performance of the envelope of the building can be computed directly from Equation (6).

2.2. *One category: randomness at the building level*

This section introduces random effects to the model of Equation (6). To illustrate this concept, Section 2.2.1 presents an example where random effects are used to evaluate the differences in annual consumption of a population of schools. In the example, a simple model is developed to introduce the ME framework. The choice of schools is arbitrary, thus, this model could be applied to other building categories. If the reader is familiar with this type of modelling, they can skip this section and jump to Section 2.2.2, where the model from Equation (6) is extended using random effects.

2.2.1. *A mixed-effects example*

The energy usage index (EUI) is a metric that summarises the annual energy consumption of a building per unit area. Buildings that have similar characteristics will have a similar EUI. If we are interested in estimating the mean value EUI of a population of similar schools, a model (M0) would be

$$EUI_i = \mu + \upsilon_i\,, \tag{10}$$

where i denotes the ith observation of EUI and $\upsilon_i \sim N(0, \sigma_0^2)$ represents residual noise. Equation (10) contains only one fixed parameter, μ, also known as a *fixed effect*. Notice that, since the model structure is chosen for its simplicity, it is assumed that the EUI does not depend on any other variable and it is distributed around the mean value, μ.

However, in reality, the yearly heating consumption of different schools is different from the mean value. Then, for individual buildings, an alternative model (M1) would be

$$EUI_{i,k} = \mu + U_k + \epsilon_{i,k}\,, \tag{11}$$

where, $\epsilon_{i,k} \sim N(0, \sigma_1^2)$ and μ still represents the mean value EUI for the given population. The added term, U_k, captures the deviations of the individual kth building around the mean value. Notice that, since U_k is added to Equation (11), the residual term $\epsilon_{i,k}$ accounts only for the deviations of measurements of $EUI_{i,k}$ coming from the same individual kth building.

In order to characterise a population of buildings, we study how U_k varies, rather than its individual values. Thus, it is modelled as a random variable $U_k \sim N(0, \sigma_u^2)$, and it is called the *random effect* of Equation (11). Notice that now, M1 is described by three parameters $\{\mu, \sigma_1^2, \sigma_u^2\}$. Since M1 contains both fixed and random effects, it is called a *mixed effects* model; for more details about this family of models please refer to Madsen and Thyregod [31].

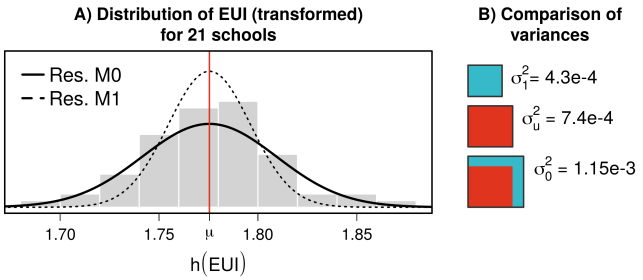

Figure 3: Comparison of uncertainty for models M0 and M1. Figure A) shows the distribution of the residuals. Figure B) compares the different estimated variances, where the size of the rectangles is proportional to the variance.

Figure 3 shows the results after fitting M0 and M1 using data from different Norwegian schools ($N = 21$). Sub-figure A) compares the estimated models over the distribution of the used data; sub-figure B) offers a visual comparison of the variances of the three random variables υ_i, $\epsilon_{i,k}$ and U_k. In order to ensure the data were normally distributed, the data were transformed using the Box-Cox transformation [32]

$$h(y_i) = \frac{y_i^{-0.5} - 1}{-0.5}\,. \tag{12}$$

Notice that the mean value of both M0 and M1 are the same, and the main difference is found in the variances σ_0^2 and σ_1^2. Since M1 includes the random effects, U_k, to account for the differences in individual $EUI_{i,k}$ the residuals $\epsilon_{i,k}$ are smaller. This can be clearly observed in sub-figure B) where it is shown that in model M1, most of the noise is caused by U_k.

Fitting model M1 with data from 21 schools allows us to use Equation (11) to estimate the value of the individual values of u_k $\forall k \in [1, ..., 21]$. As explained in Chapter 5 of Madsen and Thyregod [31], the random effects are estimated by

$$\hat{u}_k = E[U_k | EUI_i = \boldsymbol{y}_k] = \omega\hat{\mu} + (1 - \omega)\bar{y}_k \tag{13}$$

where $\omega = 1/(1 + n\gamma)$, with n being the number of observations of the kth building, and $\gamma = \sigma_u^2/\sigma_1^2$. It is important to highlight that $\hat{u}_k$ is an estimated value, whereas U_k is a random variable. In addition, as introduced in Figure 1, given the estimated parameters, it is possible to sample values from $N(0, \hat{\sigma}_u^2)$. Introducing these sampled values to Equation (11) makes it possible to simulate the energy usage index for similar schools that have no available energy data.

2.2.2. *Including the inner-category randomness in the heating load curve*

The heating load curve of a single building can be modelled with Equation (6). This model is extended to represent an entire category of buildings by including random effects, defined in this work by the random variable $\boldsymbol{U} \sim N(\boldsymbol{0}, \boldsymbol{\Sigma})$. This constitutes a non-linear mixed effects model where on

the one hand, the mean heating load curve of a category of buildings is characterised by $\boldsymbol{\theta}$ and on the other hand, the deviations from the mean curve of the kth building are described by $\boldsymbol{u}_k = \{u_{A,k}, u_{\alpha,k}, u_{\beta,k}, u_{Q,k}\}$, which is a sample from $\boldsymbol{U}$.

The final mixed effects model is

$$\Phi_{i,k} = (A_0 + u_{A,k}) \exp\Bigg[- \exp\Big[\Big(\alpha + u_{\alpha,k} + (\beta + u_{\beta,k}) W_i^{\mathrm{s}}\Big) \times (T_{i,k}^{\mathrm{out}} - (1 - u_{Q,k}) \sum_i^n b_i B(\Phi_{i,k}^{\mathrm{sol}}))\Big]\Bigg] + \varepsilon_{i,k}\,, \tag{14}$$

where, $\boldsymbol{u}_k$ is included in Equation (6) under the following assumptions:

- The variable $u_{A,k}$ accounts for the differences in the upper limit of the heating load between individual buildings.
- The variables $u_{\alpha,k}$ and $u_{\beta,k}$ capture the small differences in the effects of the wind on a individual building.
- The influence of the solar irradiation is modelled as a sum of B-spline curves to adapt to possible non-linear effects. The small differences around the mean value of $Q(\Phi^{\mathrm{sol}})$ are captured by adding $u_{Q,k}$.

Recalling the non-linear structure of the Gompertz curve, Equation (14) can be re-parameterised, defining the three high-level parameters as:

$$\begin{cases} A \to A_k = A_0 + u_{A,k} \\ C \to C_{i,k} = \alpha_0 + u_{\alpha,k} + (\beta_0 + u_{\beta,k}) W_i^{\mathrm{s}} \\ Q \to Q_{i,k} = (1 - u_{Q,k}) \cdot \sum_j^n b_j B(\Phi_i^{\mathrm{sol}}) \end{cases} \tag{15}$$

Notice that, for the sake of clarity, a sub-index is added to the fixed effects so that $\boldsymbol{\theta} \to \boldsymbol{\theta}_0$. Adding the newly defined parameters in Equation (14) yields the final model,

$$\Phi_{i,k} = \underbrace{A_k \exp\left[- \exp[C_{i,k}(T_i^{\mathrm{out}} - Q_{i,k})]\right]}_{f_{\mathrm{ME}}(T_{i,k}^{\mathrm{out}}, \Phi_i^{\mathrm{sol}}, W_i^{\mathrm{s}})} + \varepsilon_{i,k}\,, \tag{16}$$

which characterises the daily heating load of a building category using only the continuous function $f_{\mathrm{ME}}(\cdot)$.

2.3. Data description

All data used in this work comes from the TREASURE database supplied by SINTEF in the framework of the Flexbuild project. This database contains hourly measures of the heating load, outdoor temperature, wind speed and solar irradiation for nearly 300 Norwegian buildings. The consumption data was collected by a company that provides energy management services (EMS), and the measurements range from 2009 to 2018; the meteorological data was extracted from the Norwegian Meteorological Institute (MET). The data was cleaned so each measured building has continuous measurements that span from 1 year up to 3 years. The data quality is good, only the wind speed and solar irradiation presented minor gaps in their measurements; the missing measurements were addressed using linear interpolation. Since this work only focuses on static characteristics, the data has been aggregated to daily values.

The data set also includes building information, for example, the geographic regions, building floor area, and functions. Additionally, the buildings are labelled according to their energy efficiency in one of the categories: E, T, R. Category E refers to buildings with efficiency near the *Passivhaus* standards; category T refers to buildings that have been recently renovated and are compliant with the Norwegian standards TEK10 [33]; finally, the buildings labelled R do not comply with any of the above two standards. Some of the buildings use district heating and others use electric heaters. Regardless of the heating sources, this study focus on the space heating load normalised using the area of each building with the unit of kW/m^2.

The proposed model is developed using a subset of the main database containing measurements from 56 apartment buildings. In order to validate the results, the data were split randomly into a training set, containing 41 buildings, and a testing set containing the remaining 15 buildings. The training set data are from 2013, 2017 or 2018, depending on the availability of the data for individual buildings; to ensure that the training set is balanced, only one year of data is chosen for each building. All measurements from the testing set are from 2017.

2.4. Parameter estimation

The parameters of the model in Equation (16) are estimated by maximizing the likelihood function,

$$L(\boldsymbol{y}; \boldsymbol{\Theta}) = f_Y(y_1, y_2, ..., y_n; \boldsymbol{\Theta})\,, \tag{17}$$

where n is the number of observations and $f_Y(\cdot)$ is the density function of the model. Thus, the likelihood function quantifies the probability of observing $\boldsymbol{y} = [y_1, y_2, ..., y_n]$ given the parameters $\boldsymbol{\Theta}$.

In this work, $\boldsymbol{y}$ contains observations of the daily averaged heating load for 41 different buildings, so Equation (17) becomes

$$L(\boldsymbol{y}; \boldsymbol{\Theta}) = \prod_{i=1}^{41} \cdot f_Y(\boldsymbol{y}_i; \boldsymbol{\Theta})\,, \tag{18}$$

where $\boldsymbol{y}_i$ contains the observations of the ith building. For models that contain only fixed effects, $\boldsymbol{\Theta}$ includes the fixed effects and the parameters that characterise the chosen model distribution; typically, when the model is assumed to be Gaussian, such distribution is completely characterised by the variance of the residuals. The inclusion of random effects adds a new level of uncertainty which requires re-writing the density function such that

$$f_Y(\boldsymbol{y}_i, \boldsymbol{u}_k; \boldsymbol{\Theta}) = f_{Y|\boldsymbol{u}_k}(\boldsymbol{y}_i|\boldsymbol{u}_k; \boldsymbol{\Theta}_1) f_U(\boldsymbol{u}_k; \boldsymbol{\Theta}_2)\,, \tag{19}$$

where $\boldsymbol{\Theta} \equiv \boldsymbol{\Theta}_1 \cup \boldsymbol{\Theta}_2$ and $\boldsymbol{u}_k$ is a vector of length q containing the random effects of the kth building.

The formulation presented in Equation (19) is called *hierarchical likelihood*, which splits the likelihood function in two

terms, $f_U(\cdot)$ and $f_{Y|\boldsymbol{u}_k}(\cdot)$, highlighting the hierarchical structure of a mixed effects model. As depicted in Figure 4, there is an underlying random variable, $\boldsymbol{U}$, that follows the distribution $f_U(\cdot)$; an observation of such random variable, $\boldsymbol{u}_k$, conditions the upper layer of the model that follows the distribution $f_{Y|\boldsymbol{u}_k}(\cdot)$. More details about the hierarchical function can be found in Chapter 5 of Madsen and Thyregod [31].

As presented in Section 2.2.2, in this work both the individual noise and the population noise are normally distributed, with

$$f_{Y|\boldsymbol{u}_k}(\boldsymbol{y}_k; \boldsymbol{u}_k, \boldsymbol{\theta}_0, \sigma_1) = \frac{1}{\sqrt{2\pi\sigma_1^2}^n} \exp\left[-\frac{1}{2}\frac{\sum_{i=1}^{n}\left(y_{i,k} - f_{\mathrm{ME}}(\boldsymbol{u}_k, T^{\mathrm{out}}_{i,k}, \Phi^{\mathrm{sol}}_{i,k}, W^{\mathrm{s}}_{i,k})\right)^2}{\sigma_1^2}\right] \tag{20}$$

and

$$f_U(\boldsymbol{u}_k; \boldsymbol{\Sigma}) = \frac{1}{\sqrt{2\pi}^q \det \boldsymbol{\Sigma}} \exp\left[-\frac{1}{2}\boldsymbol{u}_k^\top \boldsymbol{\Sigma}^{-1} \boldsymbol{u}_k\right]. \tag{21}$$

where $\boldsymbol{\Theta_1} \equiv \{\boldsymbol{\theta}_0, \sigma_1, \boldsymbol{u}_k\}$ since Equation (20) contains the function $f_{\mathrm{ME}}(\cdot)$, and $\boldsymbol{\Theta_2} \equiv \{\boldsymbol{\Sigma}\}$.

The final expression of the likelihood function is obtained by combining Equations (18) and (20)-(21), which leaves a complicated non-linear product. To reduce the computational requirements, the negative logarithm of the likelihood function is computed, so the product from Equation (18) becomes a summation, and the maximisation becomes a minimisation. The final objective function is

$$l(\boldsymbol{y}, \boldsymbol{u}_k; \boldsymbol{\theta}_0, \sigma_1, \boldsymbol{\Sigma}) = -\log\left[\prod_{i=1}^{41} f_{Y|\boldsymbol{u}_k}(\boldsymbol{y}; \boldsymbol{\theta}_0, \sigma_1) f_U(\boldsymbol{u}_k; \boldsymbol{\Sigma})\right], \tag{22}$$

which is still a complex non-linear function to minimise. To ease this optimisation, in this work the TMB package is used [34]. This package runs in R and uses the Laplace approximation to calculate the function $l(\cdot)$ and estimates its parameters.

2.5. Simulation and validation framework

The model proposed in this work is intended for simulation purposes. Recalling Figure 1, the simulation is done by sampling realisations from the random effects distribution. Then, using outdoor air temperature, wind speed and solar irradiation measurements for a given period, it is possible to simulate the daily heating load of a building.

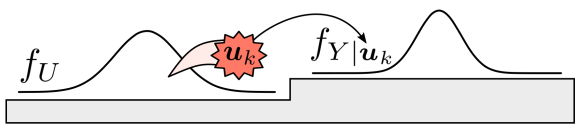

Figure 4: Schematic representation of the hierarchical likelihood structure from Equation (19).

To study the uncertainty introduced by the differences among individual buildings, the region that includes the 95% of sampled buildings is computed. This uncertainty region is computed using a Monte Carlo approach, where we simulate numerous realisations and select the region containing 95% of the sampled space. The performance of the proposed model is evaluated using the *reliability* metric, which is computed by measuring the % of test measurements that fall inside the 95% uncertainty region.

3. Results

This section introduces the results of fitting the model in Equation (6) using data from one single building. Then, the results of modelling a whole category of buildings with Equation (16) are presented. The results at category level are divided into two sub-sections: first, the model fit is analysed studying the model results compared to the training set; later the model is validated comparing the results with a set of measurements from out-of-sample buildings. Finally, the proposed model is used to study the thermal performance of a category of buildings.

3.1. One apartment

Figure 5 shows the fit of the training set for one apartment building. It can be seen that the model accurately captures the fluctuations of the daily heating load and presents a small residual noise.

Evaluating the residuals of such a model confirms the quality of the fit. Figure 6 shows the residuals are centred around zero and present no significant trends when compared with the three weather variables. However, it is noticeable that the variance decreases slightly for the outdoor temperature at the warmer side of the plot. This shrinking of the variance is caused by the change of heating behaviour during summer days: when the outdoor temperature is very high the heating load is very close to zero. The residuals term from Equation (6) has a constant variance that is unable to adapt to such behavioural changes. Moreover, it can be noticed that the residuals are slightly narrower for high values of the solar irradiation; this is caused by the coupling between bright days and high outdoor air temperature. In addition, given that the data comes from Norway, it is seen that most of the daily data points concentrate in the lower end of the solar irradiation, so it is more likely to find larger residuals in that region. Similarly, focusing on the wind speed, extreme values present small residuals, but, given the low number of observations in this range, this is not considered as a potential bias; as seen in Figure 7, changes in the wind speed will have a limited impact over the heating load.

Additionally, Figure 6 shows an exponential decay of the auto-correlation function (ACF) and a significant partial auto-correlation (PACF) in lag one. This indicates that the model omits some structure (presumably an AR(1)); yet, given the lag-one auto-correlation is only around 0.5, this is ignored. It is important to recall that the proposed model is static and does

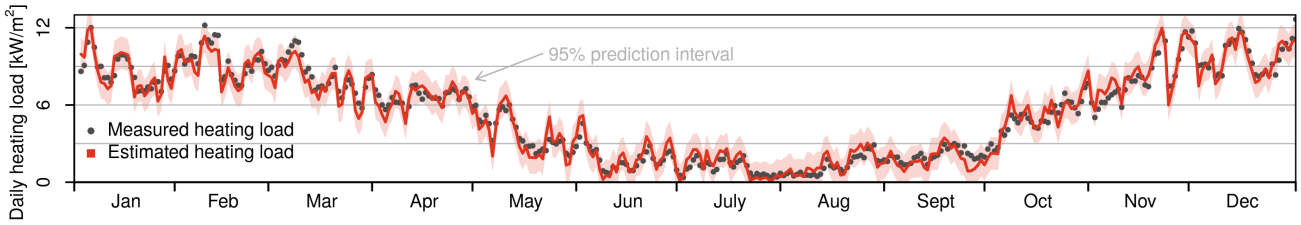

Figure 5: Yearly evolution of the simulated heating load for one building compared to measurements of the heating load during that period.

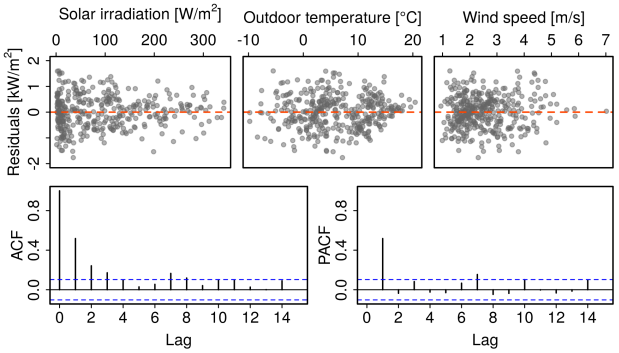

Figure 6: Residuals analysis of an arbitrary apartment building. The top row of plots show the dependence of the residuals with two main inputs. The bottom row shows the ACF and PACF.

not take into account the effects of heating inertia, which might be what causes this lag-one auto-correlation. Still, the results of the model are satisfactory for the purpose of this study.

The relation between the estimated heating load and the outdoor temperature is shown in Figure 7. There, three different curves are plotted for different weather conditions to evaluate how the model adapts to changes in the weather variables. The figure includes two sub-plots that show the dependence of parameters $\{C(W^s, Q(\Phi^{sol}))\}$ on the weather variables.

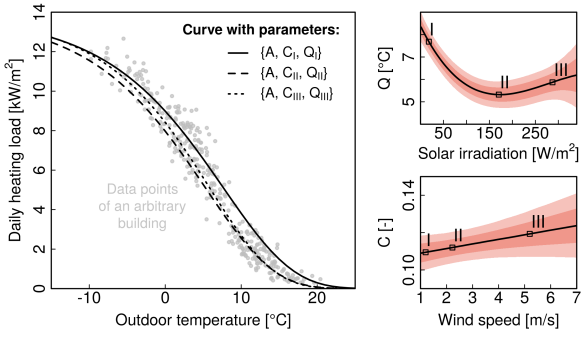

Figure 7: Main figure shows the dependence of $f_{ME}(\cdot)$ on the three weather variables. Two sub-figures show the dependence of parameters C and Q on wind speed and solar irradiation, respectively.

The C parameter grows slightly with the wind speed, confirming that the heat loss increases as wind speed increases; however, the small slope suggests that changes in the wind speed will not cause significant changes in the heating load. The parameter Q follows a sharply decreasing trend that flattens, then slightly increases during days with high solar irradiation. The initial decrease suggests that, as the solar irradiation increases (see trend from point I to point II), the heating load curve is shifted to the left (see solid and dashed curve in Figure 7 left), since the building demands less heating due to the solar gain. The increase of Q (see trend from point II to point III), suggests that, for very bright days, the internal gains decrease slightly. This is however a small and possibly not significant effect. This could be caused by some behavioural changes of the occupants during very bright days, such as an increase in the heat loss caused by window opening.

3.2. Modelling results of all apartments

To model the apartment category, random effects are introduced as described by Equation (16). After computing the Akaike information criterion (AIC) for models with different numbers of splines, the final choice was to use four spline curves. Using four spline curves yields the final model with seven fixed effects, $\hat{\boldsymbol{\theta}}_0$, which can be seen in Table 1. The p-values confirm that all parameters are significant, proving the dependence of the model on the three weather variables. Yet, β_0 presents a small value with the largest uncertainty, suggesting the effects of the wind speed are weak.

Fixed effects				**Random effects**	
	Mean	Std. dev.	p-value		Std. dev.
$\hat{A}_0$	23.60	1.08	<1e-16	$\hat{u}_A$	1.64
$\hat{\alpha}_0$	8.44e-2	2.8e-3	<1e-16	$\hat{u}_\alpha$	1.59e-2
$\hat{\beta}_0$	8.82e-4	5.2e-4	8.75e-2	$\hat{u}_\beta$	2.10e-3
-	-	-	-	$\hat{u}_Q$	2.89e-1
$\hat{b}_1$	5.91	0.30	<1e-16	-	-
$\hat{b}_2$	0.29	0.16	7.0e-2	-	-
$\hat{b}_3$	1.52	0.23	8.53e-11	-	-
$\hat{b}_4$	3.10	0.27	<1e-16	-	-

Table 1: Fixed effects estimates (left). Diagonal of the covariance matrix of random effects, $\boldsymbol{\Sigma}$ (right).

The random effects of the model are contained in a four-dimensional random vector, $\boldsymbol{u}_k$, that is distributed following a multivariate normal $N(\mathbf{0}, \boldsymbol{\Sigma})$. The right side of Table 1 includes the standard deviation of each component of $\boldsymbol{u}_k$. It can

be observed that $\hat{u}_\alpha$ $\hat{u}_\beta$ present a large standard deviation, highlighting that the wind dependence varies significantly among the training buildings.

As explained in Section 2.2.1, using the measurements in the training set, it is possible to estimate the individual values of $\boldsymbol{u}_k$ for all the observed buildings. Studying the quantiles of $\boldsymbol{u}_k$ $\forall k \in [1, ..., 41]$ confirms the estimated random effects follow a Gaussian distribution, as can be seen in Figure 8.

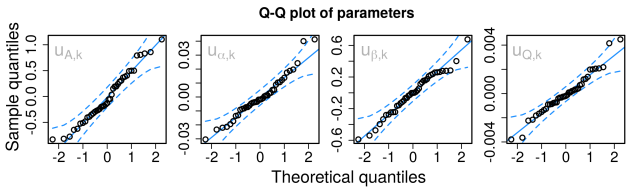

Figure 8: Quantile plots of the estimated random effects. All of the quantile points fall inside the 95% prediction interval confirming that the random effects follow a normal distribution.

The fixed effects shown in Table 1 give the mean value of the heating load curve which can be seen in Figure 9. As the parameters describing the curve depend on the solar irradiation and wind speed, to improve visualisation, three snapshots are plotted. Each sub-plot contains the observations for a range of solar irradiation, and the mean curve uses the median solar irradiation and the median wind speed of that range. There is still a large uncertainty around the mean, which is caused by the differences among the buildings. This is confirmed in Figure 9 by including the individual building curves from the buildings in the training set.

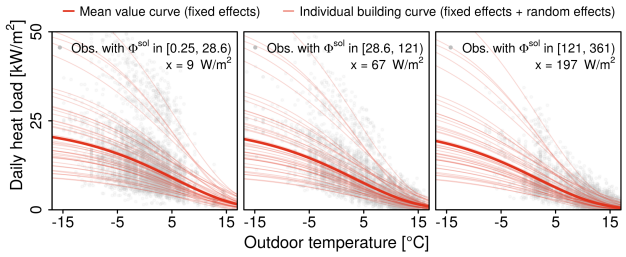

Figure 9: Three snapshots comparing the mean curve and the individual building curves for different values of the solar irradiation.

Thus, the random differences from building to building add a new layer of uncertainty that is captured by the random effects, hence, it is separated from residual noise. To visualise this result, two models were compared: the proposed model with fixed effects and random effects, denoted by $f_{\text{ME}}(\cdot)$; and another model with only fixed effects, that is, setting $\boldsymbol{U} = \boldsymbol{0}$, denoted by $f_0(\cdot)$. The comparison of $f_{\text{ME}}(\cdot)$ and $f_0(\cdot)$ can be seen in Figure 10, where the regions defined by the 95% prediction interval are highlighted for both models.

In the model without random effects, the uncertainty is constant around the mean, since the only source of uncertainty comes from the normally distributed residuals. When using the random effects, the uncertainty changes with the outdoor temperature due to the non-linear structure of the model. In the

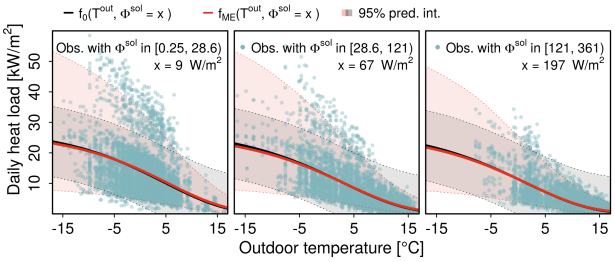

Figure 10: Comparison of the uncertainty region of the ME model and a model without random effects.

cold end of the temperature spectrum, the uncertainty is significantly wider when compared to the model without random effects, that is, during days with low outdoor temperatures the heating load differs more from one building to the other. When the outdoor temperature is high, the uncertainty is lower since all buildings have lower heating loads. The uncertainty region of f_{ME} includes more data points, which renders that model as a better representative of the studied population.

3.3. *Predicting observed buildings*

The estimated fixed effects, $\hat{\boldsymbol{\theta}}_0$, and random effects, $\hat{\boldsymbol{u}}_k$, completely characterise the buildings in the training set. Then, their only source of uncertainty is the residual noise, $\varepsilon_{i,k}$. Figure 11 shows the estimated individual curves of 6 buildings; to improve readability, these curves are computed with a fixed solar irradiation. Notice that the 95% prediction interval is much narrower, when compared to Figure 10, due to the absence of the building uncertainty. Still, most of the measured data points are included in the uncertainty region, highlighting the good fit of the model at the building level.

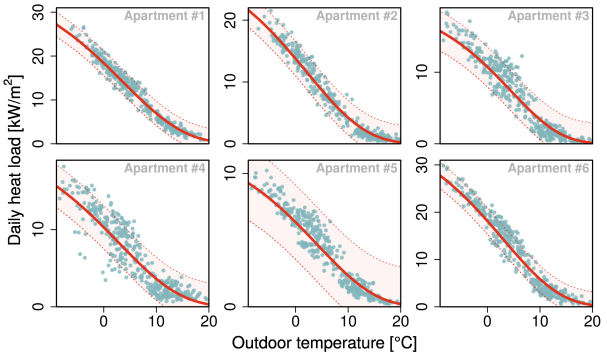

Figure 11: Heating load curves of six different buildings. The solar irradiation and the wind speed are set as constants to ease readability.

3.4. *Simulating unobserved buildings*

If the 41 buildings of the training set are a representative sample of the apartment population in Norway, then the uncertainty region from Figure 10 marks the region where 95% of observations from any unobserved Norwegian apartment buildings will fall. Although it is not possible for the authors to

examine the representativeness of these buildings, we can compare the uncertainty region to measurements from 15 apartment buildings that were not part of the training set. The daily heating load measurements of those test buildings compared to the uncertainty area of f_{ME} depicted in Figure 10. Given this region, it is possible to compute the *reliability* measure, defined as the percentage of data points that fall inside the 95% prediction interval. Figure 12 shows the distribution of the individual scores, where one will note that most of the test buildings show a reliability over 90%.

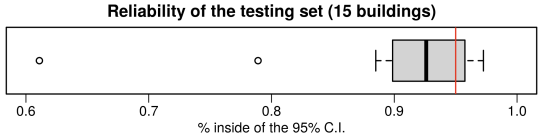

Figure 12: Boxplot that shows the distribution of reliability measure for the 15 buildings in the testing set.

3.5. *Assessing the thermal performance of the studied category*

The estimated parameters of Equation (16) were used to compute the proxy heat loss coefficient, HLC^* described in Section 2.1.1. Given the presence of random effects, HLC^* is not described by a single parameter but a distribution that characterises the studied category of buildings. The density distribution of HLC^* was estimated using a Monte Carlo approach and is shown in Figure 13. It presents a wide bell curve with a long tail in the higher side of the HLC range.

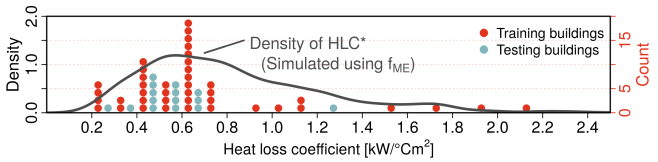

Figure 13: Distribution of the HLC^* computed using model f_{ME}. The distribution is compared to a dot plot of the classic HLC computed for the buildings in testing and training sets.

For each building, in both the training and testing set, the classic heat loss coefficient are computed following Equation (7). The distribution of these individual values is included in Figure 13 as a dot plot. Despite the low number of points, the computed values resemble the distribution, indicating that HLC^* is a valid alternative for simulating the thermal performance of the envelope of an unobserved apartment building.

4. Model application: Refining segmentation

As described in Section 3, with the proposed model it is possible to estimate the random effects, $\hat{\boldsymbol{u}}_k$, for each building in the training set. This vector, along with $\boldsymbol{\theta}_0$, completely characterises a building's response to the weather conditions, providing a deeper understanding of the set of buildings used to train the model. In this work, we propose using $\hat{\boldsymbol{u}}_k$ to group buildings based on the likeness of their heating curve. This approach offers a data-driven alternative to the conventional segmentation procedure that groups buildings using qualitative data that might be outdated or missing.

The buildings are grouped using a fuzzy analysis clustering (FANNY method) [35] and two sub-categories of buildings are found, named C1 and C2. Table 2 presents the available details of the buildings contained in each cluster. Notice that, using only qualitative details, no clear line can be drawn to separate C1 and C2, since both include buildings with similar attributes. Additionally, both clusters have buildings with missing details.

	C1 (24 buildings)	C2 (17 buildings)
Function	Apartment block	
Construction years	2010, 2012-2016	Unknown, 1998, 2005-2006, 2011, 2013, 2015-2016
# of units	4-154	9-62
Location	Unknown, Harstad, Jakobsli, Ranheim, Trondheim	Harstad, Heimdal, Moss, Ranheim, Trondheim
Area [m^2]	352-17457	640-5775
Eff. label	R, T, E	R

Table 2: Summary of characteristics found in the different buildings contained in C1 and C2.

As outlined in Figure 1, these two clusters are studied separately by splitting the original training data set and repeating the fitting process described in Section 3. This results in having two different models: ME1 and ME2. Both models follow the structure presented in Equation 16 and are governed by f_{ME1} and f_{ME2} respectively. Hence, ME1 and ME2 are described by a different set of parameters $\boldsymbol{\theta}_0^{(l)}$, $\Sigma^{(l)}$ and $\sigma^{(l)}$ for $l \in [1, 2]$. Table 3 compares the fixed effects after fitting both models. It is seen that ME2 presents a higher heating capacity and higher wind dependence than ME1, suggesting that C1 contains buildings that are better insulated. This was already hinted at in Table 2, where we noted that C1 contained buildings compliant with high efficiency standards. Furthermore, notice that the solar gains, reflected by the sum of splines, are higher for buildings in C1, which indicates again that the impact of solar irradiation is more significant in low-energy buildings.

	Train.	$A^{(l)}$	$\alpha^{(l)}$	$\beta^{(l)}$	$\sum_i^{n=4} b_i^{(l)} B(x)$
ME1	C1	2.80	9e-2	1.2e-4	4.03
ME2	C2	3.66	7.72e-2	2.02e-3	3.72

Table 3: Fixed effects for the two clusters. Notice that the term $\sum_i^{n=4} b_i B(\Phi^{\text{sol}})$ is defined for a range of solar irradiation; to improve interpretability, only the values for $x = 50\text{W/m}^2$ are given.

To assess how this finer segmentation represents the population of apartments, the models ME1 and ME2 are compared to the test set presented in Section 3.4. Since it is unknown

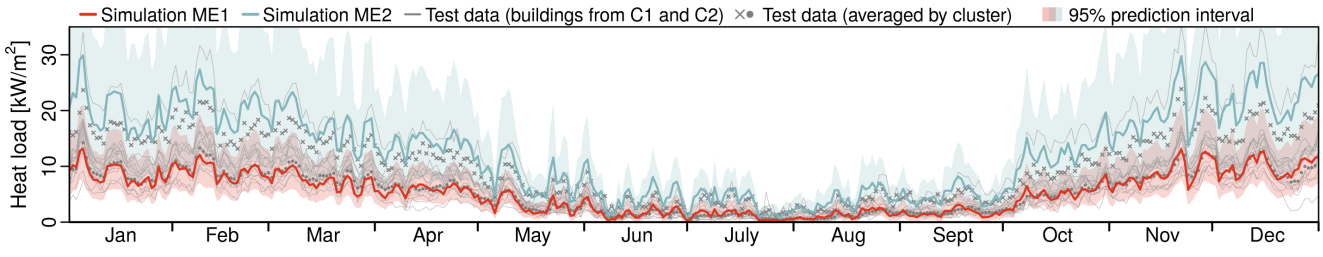

Figure 14: Simulated yearly evolution of the heating load for the two clusters compared to the daily mean of the 15 test buildings.

which model represents each test building, the reliability of both models is computed for each of the 15 buildings. When the measurements of a test building show high reliability with model ME1, it is assumed that the building belongs to C1 and vice-versa. The results show that 13 of the 15 test buildings are better described by ME1. Hence, the test set is split in two: one subset contains 13 buildings to test ME1 and the other subset contains only two buildings to test ME2.

Figure 14 shows one year of simulated heating load using ME1 and ME2. It is seen that the heating load simulated using ME2 is always higher that the trend simulated using ME1 and presents more pronounced fluctuations; similarly, the prediction interval of ME1 is wider. The figure includes measured data from the individual test buildings, as well as their daily averages by cluster. The averaged test data of buildings from C1 (marked with •) falls very close to the simulated mean with ME1, suggesting the model is a good representative of the subcategory. On the other hand, the average of C2 test buildings (marked with ×) falls lower than the ME2 simulation; however, it is important to recall that this average is computed using only two test buildings, which does not allow us to have an accurate heating trend for testing purposes.

Finally, the accuracy of each fitted model is quantified following ASHRAE guidelines 14-2014 [36]. These guidelines propose the NMBE and CVRMSE metrics to evaluate the model performance, and give boundaries for each metric to guarantee a good fit. For each sub-category, the monthly average of its test buildings is computed and compared to the simulated monthly heating load. The results can be seen in Table 4, which confirms model ME1 as a good representative of C1. The results for ME2 are significantly worse due to the low number of test buildings.

		NMBE [%]	CVRMSE [%]
ASHRAE 14-2014		≤ ±5	≤ 15
Model ↓	**Test set ↓**		
ME1	13 buildings (C1)	1.12	6.29
ME2	2 buildings (C2)	-26.30	50.75

Table 4: Comparison of NMBE and CVRMSE metrics of the whole data set, C1 and C2.

5. Conclusion

This work presents a methodology to model the heating load of archetypes of buildings using existing weather and energy meter data. The results from this model can be used to refine segmentation of a population of buildings. First of all, a non-linear model was introduced which captures the weather dependency of buildings. Using this model, reliable results were presented simulating the daily heating load of a single building during the period of one year. The resulting simulation is continuous and adapts to the typical heating regime change from heating season to non-heating season.

To model an entire category of buildings, the model was extended with the addition of random effects; in this work, a population of apartments was modelled. Results showed that the simulated heating load accurately follows the measured trend of the buildings in the training set. The non-linear model structure was able to adapt to the regime changes of the heating load during the year, which cause high variance during colder periods compared to warmer ones. Thus, the model shows a high uncertainty region during winter months which narrows as the heating load approaches zero during the summer. This uncertainty is caused by the random differences between apartments, and quantifying it allowed us to compute the region where 95% of measurements of the heating load will fall. This region was validated using measurements from 15 out-of-sample buildings, capturing 91% of these test data. Thus, given the weather conditions of an arbitrary period, the simulation using ME provides a reliable estimation of the range where the heating load of any apartment might fall during such a period.

The model is based on known physical phenomena and is easy to interpret. The estimated parameters give direct insights into the effects of outdoor temperature, wind speed and solar dependence. In addition, a proxy of the heat loss coefficient can be computed through these parameters. The stochastic nature of the proposed model allowed us to estimate how this thermal performance is distributed for the studied category.

One of the major challenges of working with models that aim to represent urban areas is finding a way to accurately segment the building stock. Working with a large enough data set, the proposed model allows identifying sub-categories based on the estimated random effects, which offers a richer description of the building landscape. This method is purely data driven and does not require having access to qualitative data of the building (such as the geometry or year of construction) to seg-

ment a population of buildings. The model completely characterises the thermal response for a climatic year, and the buildings are directly grouped based on estimated random effects. In addition, if partial qualitative information about the studied set of buildings is available, this method can be used to fill the gaps. In the presented work, it was possible to classify buildings lacking key information, such as their construction year or clear efficiency labelling. The results indicate that this method can also be used to complement and validate segmentation that uses the classic archetype approach.

When working with mixed effects (ME) models, specially with non-linear ME, it is recommended to use a low number of random effects to ensure the computational feasibility. In this work, it was possible to add a random effect for each major parameter since the proposed model has a low order structure. In case of using a more complex model, it will be necessary to evaluate which parameter would be more affected by random effects. Issues can also arise when dealing with long high-frequency data sets; for instance, in the proposed model, the trials to address the significant auto-correlation in the residuals were unsuccessful due to computational limitations.

Segmenting a population of buildings based on data-driven methods requires to be able to interpret the cause behind the newly found categories. In the studied case, the model was interpretable and the differences between sub-categories were easy to identify, which allowed to recognise a sub-category containing mostly low-energy buildings. However, the other sub-category could not be properly validated since its test set was too small and proved not to be representative. This arises the question of how to categorise the buildings that are not part of the training set.

Nevertheless, the results of this work are satisfactory and suggest that mixed effects are an effective modelling framework to develop urban models and adapt to the modelling needs. In this case, pursuing generality, the model is relatively simple as it uses daily values. Still, the results indicate that a mixed effects approach can be applied to more complex applications.

Acknowledgments

This work was done as a part of the Flexbuild project, which provided a clean and complete data set to work with. Furthermore, we wish to acknowledge the FME-ZEN project (Research Council of Norway - Project No. 257660) which has inspired and supported this work.

References

[1] *Urban Development*. https://www.worldbank.org/en/topic/urbandevelopment/overview. Last Updated: Apr 20,2020.

[2] Yongbao Chen, Peng Xu, Jiefan Gu, Ferdinand Schmidt, and Weilin Li. "Measures to improve energy demand flexibility in buildings for demand response (DR): A review". In: *Energy and Buildings* 177 (2018), pp. 125–139.

[3] Usman Ali, Mohammad Haris Shamsi, Cathal Hoare, Eleni Mangina, and James O'Donnell. "Review of urban building energy modeling (UBEM) approaches, methods and tools using qualitative and quantitative analysis". In: *Energy and Buildings* 246 (2021), p. 111073.

[4] Usman Ali, Mohammad Haris Shamsi, Cathal Hoare, Eleni Mangina, and James O'Donnell. "A data-driven approach for multi-scale building archetypes development". In: *Energy and Buildings* 202 (2019), p. 109364.

[5] Jaume Palmer, Christoffer Rasmussen, Rongling Li, Kenneth Leerbeck, Ole Michael Jensen, Kim B. Wittchen, and Henrik Madsen. "Characterisation of thermal energy dynamics of residential buildings with scarce data". English. In: *Energy and Buildings* 230 (2021). ISSN: 0378-7788. DOI: 10.1016/j.enbuild.2020.110530.

[6] Mehmet Aksoezen, Magdalena Daniel, Uta Hassler, and Niklaus Kohler. "Building age as an indicator for energy consumption". In: *Energy and Buildings* 87 (2015), pp. 74–86.

[7] Gabriel Happle, Jimeno A Fonseca, and Arno Schlueter. "A review on occupant behavior in urban building energy models". In: *Energy and Buildings* 174 (2018), pp. 276–292.

[8] Jong-Hwan Ko, Dong-Seok Kong, and Jung-Ho Huh. "Baseline building energy modeling of cluster inverse model by using daily energy consumption in office buildings". In: *Energy and Buildings* 140 (2017), pp. 317–323.

[9] Sebastian Wolf, Jan Kloppenborg Møller, Magnus Alexander Bitsch, John Krogstie, and Henrik Madsen. "A Markov-switching model for building occupant activity estimation". In: *Energy and Buildings* 183 (2019), pp. 672–683.

[10] Hamed Nabizadeh Rafsanjani, Changbum R Ahn, and Jiayu Chen. "Linking building energy consumption with occupants' energy-consuming behaviors in commercial buildings: Non-intrusive occupant load monitoring (NIOLM)". In: *Energy and Buildings* 172 (2018), pp. 317–327.

[11] Graeme Flett and Nick Kelly. "A disaggregated, probabilistic, high resolution method for assessment of domestic occupancy and electrical demand". In: *Energy and Buildings* 140 (2017), pp. 171–187.

[12] Rebecca DerSimonian and Raghu Kacker. "Random-effects model for meta-analysis of clinical trials: An update". In: *Contemporary Clinical Trials* 28.2 (2007), pp. 105–114. ISSN: 1551-7144. DOI: https://doi.org/10.1016/j.cct.2006.04.004. URL: https://www.sciencedirect.com/science/article/pii/S1551714406000486.

[13] Ricardo Forgiarini Rupp, Rune Korsholm Andersen, Jørn Toftum, and Enedir Ghisi. "Occupant behaviour in mixed-mode office buildings in a subtropical climate: Beyond typical models of adaptive actions". In: *Building and Environment* 190 (2021), p. 107541.

[14] Alfonso Capozzoli, Marco Savino Piscitelli, Francesco Neri, Daniele Grassi, and Gianluca Serale. "A novel methodology for energy performance benchmarking of buildings by means of Linear Mixed Effect Model: The case of space and DHW heating of out-patient Healthcare Centres". In: *Applied Energy* 171 (2016), pp. 592–607.

[15] Jaume Palmer, Jan Kloppenborg Møller, Christoffer Rasmussen, Karen Byskov Lindberg, Igor Sartori, and Henrik Madsen. "Simulating heat load profiles in buildings using mixed effects models". In: *Journal of Physics: Conference Series* (Lyngby, Denmark). Web of Science, 2021.

[16] Karen Byskov Lindberg, Steffen J Bakker, and Igor Sartori. "Modelling electric and heat load profiles of non-residential buildings for use in long-term aggregate load forecasts". In: *Utilities Policy* 58 (2019), pp. 63–88.

[17] Carlos Cerezo, Julia Sokol, Saud AlKhaled, Christoph Reinhart, Adil Al-Mumin, and Ali Hajiah. "Comparison of four building archetype characterization methods in urban building energy modeling (UBEM): A residential case study in Kuwait City". In: *Energy and Buildings* 154 (2017), pp. 321–334.

[18] Julia Sokol, Carlos Cerezo Davila, and Christoph F Reinhart. "Validation of a Bayesian-based method for defining residential archetypes in urban building energy models". In: *Energy and Buildings* 134 (2017), pp. 11–24.

[19] Martin Heine Kristensen, Rasmus Elbæk Hedegaard, and Steffen Petersen. "Hierarchical calibration of archetypes for urban building energy modeling". In: *Energy and Buildings* 175 (2018), pp. 219–234.

[20] Ina De Jaeger, Jesus Lago, and Dirk Saelens. "A probabilistic building characterization method for district energy simulations". In: *Energy and Buildings* 230 (2021), p. 110566. ISSN: 0378-7788. DOI: https://doi.org/10.1016/j.enbuild.2020.110566. URL: https://www.sciencedirect.com/science/article/pii/S0378778820333521.

[21] M Gholami, D Torreggiani, P Tassinari, and A Barbaresi. "Narrowing uncertainties in forecasting urban building energy demand through an optimal archetyping method". In: *Renewable and Sustainable Energy Reviews* 148 (2021), p. 111312.

[22] P Nageler, Andreas Koch, Franz Mauthner, Ingo Leusbrock, Thomas Mach, Christoph Hochenauer, and Richard Heimrath. "Comparison of dynamic urban building energy models (UBEM): Sigmoid energy signature and physical modelling approach". In: *Energy and buildings* 179 (2018), pp. 333–343.

[23] Kathleen M. C. Tjørve and Even Tjørve. "The use of Gompertz models in growth analyses, and new Gompertz-model approach: An addition to the Unified-Richards family". In: *PLOS ONE* 12 (June 2017), pp. 1–17. DOI: 10.1371/journal.pone.0178691. URL: https://doi.org/10.1371/journal.pone.0178691.

[24] Henrik Madsen. *Models and methods for predicting wind power*. English. 1996.

[25] Małgorzata O'Grady, Agnieszka A. Lechowska, and Annette M. Harte. "Quantification of heat losses through building envelope thermal bridges influenced by wind velocity using the outdoor infrared thermography technique". In: *Applied Energy* 208 (2017), pp. 1038–1052. ISSN: 0306-2619. DOI: https://doi.org/10.1016/j.apenergy.2017.09.047. URL: https://www.sciencedirect.com/science/article/pii/S0306261917313284.

[26] Kyriaki Foteinaki, Rongling Li, Alfred Heller, Morten Herget Christensen, and Carsten Rode. "Dynamic thermal response of low-energy residential buildings based on in-wall measurements". In: *E3S Web of Conferences*. Vol. 111. EDP Sciences. 2019, p. 04002.

[27] Christoffer Rasmussen, Linde Frölke, Peder Bacher, Henrik Madsen, and Carsten Rode. English. In: *Solar Energy* 195 (2020), pp. 249–258. ISSN: 0038-092X. DOI: 10.1016/j.solener.2019.11.023.

[28] Stig Hammarsten. "A critical appraisal of energy-signature models". In: *Applied Energy* 26.2 (1987), pp. 97–110.

[29] Øystein Rønneseth and Igor Sartori. *Possibilities for Supplying Norwegian Apartment Blocks with 4th Generation District Heating*. Tech. rep. SINTEF, 2018.

[30] Christoffer Rasmussen, Peder Bacher, Davide Calì, Henrik Aalborg Nielsen, and Henrik Madsen. "Method for scalable and automatised thermal building performance documentation and screening". In: *Energies* 13.15 (2020), p. 3866.

[31] Henrik Madsen and Paul Thyregod. *Introduction to general and generalized linear models*. Chapman Hall, 2011.

[32] Henrik Madsen. *Time series analysis*. Chapman Hall, 2008. ISBN: 978-1420059670 0.

[33] *Byggteknisk forskrift (TEK 10)*. Standard. Direktoratet for byggkvalitet, Feb. 2011.

[34] Kasper Kristensen, Brad Bell, Hans Skaug, Arni Magnusson, Casper Berg, Anders Nielsen, Martin MAechler, Theo Michelot, Mollie Brooks, Alex Forrence, Christoffer Moesgaard Albertsen, and Cole Monnahan. *Template Model Builder: A General Random Effect Tool Inspired by 'ADMB'*. 2021.

[35] Leonard Kaufman and Peter J Rousseeuw. *Finding groups in data: an introduction to cluster analysis*. Vol. 344. John Wiley & Sons, 2009.

[36] *Measurement of Energy, Demand, and Water Savings*. Standard. ASHRAE, Dec. 2014.

Technical University of Denmark
Department of Applied Mathematics and Computer Science

Richard Petersens Plads, Building 324
2800 Kgs. Lyngby
Tel.: +45 4525 3031

www.compute.dtu.dk